

Development of Hybrid Machine Learning Models for Assessing the Manufacturability of Designs for Additive Manufacturing Processes

By

Ying Zhang

Doctor of Philosophy

Department of Mechanical Engineering

Faculty of Engineering

McGill University, Montreal

2022 May

A thesis submitted to McGill University in partial fulfillment of the requirements of the degree
of Doctor of Philosophy

© **Ying Zhang**

Abstract

Additive manufacturing (AM), which is also widely known as three-dimensional (3D) printing, has been a new trend in the manufacturing process in recent years. It can produce parts following a generated 3D model by adding layers of materials and fusing them. The main advantage of AM is the ability to enable customization and fabrication of complex geometries such as lattice structures, which are extremely difficult to manufacture in the subtractive manufacturing process. Although AM has been employed in many industrial applications, it is still difficult for beginning users to ensure the success of every print. It requires users to have a deep understanding of AM techniques to fully utilize this technology. The printing may fail owing to many factors such as the poor selection of the build orientation, materials, process settings, and insufficient geometric support for overhangs. It is difficult for non-AM experts to determine whether their designs are printable through a selected AM process, and it is even more difficult for them to make proper modifications without expert guidance before the fabrication. To fill these knowledge gaps, this study investigated the use of machine learning (ML) to assess the manufacturability of designs for AM processes. A web-based automated manufacturability analyzer and recommender for AM was developed as the implementation of the developed hybrid ML models. This tool can be used for the first-level evaluation of designs for novice AM users such as designers to ensure efficiency in terms of time and cost required for AM fabrications.

The major contributions of this thesis are listed as follows:

1. Establishment of a unique database for the laser-based powder bed fusion (LPBF) process and fused deposition modeling (FDM) process.

2. Development of a novel approach on manufacturability analysis of LPBF using hybrid ML models. The models consider both process information and design perspectives.
3. Development of a hybrid sparse convolutional neural network (CNN) to predict manufacturability to increase the efficiency and effectiveness of the ML models.
4. Development of a recommendation system to provide potential modifications to assist users on AM printing.
5. A web-based application of analyzer and recommender was implemented to provide a comprehensive and easy-to-access manufacturability analysis to novice AM users.
6. Demonstration of how data-driven approaches can help on design and manufacturing processes and the framework can be extended to any process where parts can be classified based on visual inspection and basic labeling.

Résumé

La fabrication additive (AM), également connue sous le nom d'impression 3D, est une tendance émergente du processus de fabrication gagnant en popularité. Cette méthode génère des pièces à partir d'un modèle 3D en ajoutant des couches successives de matériaux et en les fusionnant. Les principaux avantages de la AM est la possibilité de personnaliser les pièces et de fabriquer des géométries complexes telles que des structures en treillis qui sont extrêmement difficiles à fabriquer dans le processus de fabrication soustractive. Bien que la AM ait été utilisée dans de nombreuses applications industrielles, elle a une barrière à l'entrée très élevée pour les débutants. Pour tirer pleinement parti de cette technologie, une compréhension approfondie est nécessaire. L'impression 3D peut échouer pour de nombreuses raisons telles qu'une mauvaise sélection de l'orientation de fabrication, des matériaux, des paramètres de processus et un support insuffisant. Il est difficile pour les non-experts en AM de déterminer si leurs conceptions sont imprimables ou non via le processus sélectionné. Il leur est encore plus difficile d'effectuer seuls les modifications appropriées avant la fabrication. Pour combler ces lacunes, une recherche a été réalisée sur l'utilisation d'une méthode d'apprentissage automatique (ML) pour évaluer la fabricabilité des conceptions pour les processus de AM. Un analyseur ainsi qu'un outil de recommandation de fabricabilité automatisés avec une interface Web ont été développés en tant que mise en œuvre des modèles ML hybrides développés. Cet outil peut servir d'évaluation de premier niveau des conceptions pour les utilisateurs AM novices tels que les concepteurs afin de réduire la perte de temps et de coût dans les fabrications AM.

Les contributions majeures de cette thèse sont les suivantes:

1. Une base de données unique pour le processus de fusion laser sur lit de poudre (LPBF) et le processus de modélisation de dépôt par fusion (FDM).
2. Une nouvelle approche sur l'analyse de la fabricabilité du LPBF en utilisant des modèles hybrides ML. Les modèles prennent en compte à la fois les informations de processus et les perspectives de conception.
3. Un réseau de neurones convolutifs (CNN) hybrides clairsemés a été développé pour prédire la fabricabilité afin d'augmenter l'efficacité et l'efficacité des modèles ML.
4. Un système a été développé pour aider les utilisateurs en impression AM en fournissant des recommandations sur les modifications potentielles.
5. Une application Web d'analyseur et de recommandation est mise en œuvre pour fournir une analyse de fabrication complète et facile d'accès aux utilisateurs AM novices.
6. Démonstration de la façon dont l'approche basée sur les données peut aider les processus de conception et de fabrication et le cadre peut être étendu à tout processus où les pièces peuvent être classées sur la base d'une inspection visuelle et d'un étiquetage de base.

Acknowledgments

First and foremost, I would like to take this opportunity to express my sincere thanks to my Ph.D. advisor, Prof. Yaoyao Fiona Zhao for her understanding, support, patience, and inspiration. Her experiences and insights gave me a deep understanding of this research. Her feedback from both academia and industry assured me of the practical values and the direction of this pioneering research. Without her help, this thesis would not be possible.

I would also like to thank Prof. Larry Lessard and Prof. Jovan Nedic for being my committee members. Their suggestions and comments on the projects helped me to think deeply about the study.

I was fortunate to have had the opportunity to work with my labmates at the Additive Design and Manufacturing Lab (ADML): Sheng Yang, Jinghao Li, Nikita Letov, Guoying Dong, Zhibo Luo, Xiaoyi Guan, Yunlong Tang, Mutahar Safdar, Jiarui Xie, Chonghui Zhang, Manual Sage, Pavan Velivela, Dawei Li, Siyuan Sun, Wenbo Min, and others for their help and suggestions for the past few years. They are the source of inspiration, collaboration, and friendship. I would also like to thank the members of the Strategic Network for Holistic Innovation in Additive Manufacturing (HI-AM). Special thanks to Lisa Brock and Baltej Rupal for sharing their experimental data with me.

I thank all my friends at home and abroad for their friendships. They have provided me an enjoyable social atmosphere. I also thank McGill University for providing such a great place for me. I really enjoy the campus life and its academic support.

I would also like to express my gratitude to Natural Science and Engineering Research Council of Canada (NSERC) HI-AM with NSERC Project Number: NETGP 494158 – 16, Collaborative Research and Development (CRD) CRDPJ 520348-17, and McGill Engineering Doctoral Award (MEDA) for the financial support to this research.

Importantly, I would express my love and sincere thanks to my family. Without them, it would not have been possible to receive good education and lead life. First, I thank my parents, Zhengkang Zhang and Weifang Chen, for their support and understanding. I thank them for giving me the gift of life and raising me. I would also like to thank my younger sister, Yi Zhang, for taking care of my parents when I was away. Finally, I thank those who have loved me and whom I have loved.

Ying Zhang

September 22, 2021

Claim of Originality

The author claims the originality of the main ideas and research results reported in this thesis. The major contributions from this thesis are listed as follows:

1. It provides a comprehensive literature review of the manufacturability of the AM process.
2. It establishes a unique database for the laser-based powder bed fusion process and material extrusion process.
3. It presents a novel approach to manufacturability analysis of LPBF using hybrid machine learning (ML) models. The models consider both process information and design perspectives.
4. It develops a hybrid sparse convolutional neural network for predicting manufacturability to increase the efficiency and effectiveness of the ML models.
5. It develops a recommendation system to provide potential modifications to assist users on AM printing.
6. It develops a web-based application of analyzer and recommender to provide a comprehensive understanding and realize easy-to-access manufacturability analysis for novice AM users.
7. It provides an example of how data-driven approaches can help in design and manufacturing processes and the framework can be extended to any process where parts can be classified based on visual inspection and basic labeling.

Some contents of this thesis have been published in some journal and conference articles. The abstracts of these papers are listed in Appendices II and III.

List of Abbreviations

ABS	Acrylonitrile Butadiene Styrene
AM	Additive Manufacturing
CM	Conventional Manufacturing
CNN	Convolutional Neural Network
DACM	Dimensional Analysis Conceptual Modeling
FDM	Fused Deposition Modeling
FNN	Feedforward Neural Network
HKS	Heat Kernel Signature
LDNI	Layered Depth Normal Images
LPBF	Laser-based Powder Bed Fusion
LPS	Liquid-Phase Sintering
MAR-AM	Manufacturability Analyzer and Recommender for AM
MAT	Medial Axis Theorem
ME	Material Extrusion
ML	Machine Learning
NN	Neural Network
OBB	Orientated Bounding Box
PC	Polycarbonate
PEEK	Polyether Ether Ketone
PETG	Polyethylene Terephthalate
PLA	Polylactide

RNN	Recurrent Neural Networks
SEM	Scanning Electron Microscopy
SM	Subtractive Manufacturing

Table of Contents

Abstract.....	II
Résumé.....	IV
Acknowledgments	VI
Claim of Originality	VIII
List of Abbreviations	IX
Table of Contents	XI
List of Figures.....	XVII
List of Tables	XXI
Chapter 1. Introduction and motivations	1
1.1. Additive manufacturing	2
1.1.1. Laser-based powder bed fusion	2
1.1.2. Material extrusion	4
1.2. Manufacturability of AM.....	6
1.3. Why machine learning?	8
1.4. Research objectives.....	9
1.5. Thesis organization	10
Chapter 2. Literature review	12

2.1.	Existing Approaches on Evaluating the Manufacturability of SM	12
2.1.1.	Definition of the manufacturability of SM	13
2.1.2.	Feature-based Approach	14
2.1.3.	Feature-less based Approach	15
2.2.	Major factors on evaluating the manufacturability of AM	16
2.2.1.	Design aspects.....	17
2.2.2.	Process aspects.....	18
2.3.	Existing approaches on evaluating the manufacturability of AM	20
2.3.1.	Design Guidelines/Checklists	21
2.3.2.	Real-time Process Monitoring	26
2.4.	Computational methods in manufacturability analysis.....	28
2.4.1.	Manufacturable feature recognition.....	29
2.4.1.1.	Slicing data-based approach	30
2.4.1.2.	Voxel-based approach.....	32
2.4.1.3.	Mesh-based approach.....	33
2.4.1.4.	3D feature-based approach	34
2.4.2.	Knowledge-based or rule-based approach	35
2.4.3.	Machine learning approach.....	38
2.4.4.	Tested commercial software	40
2.5.	Comparison of manufacturability analysis between SM and AM	40
2.6.	Fundamentals of ML.....	41
2.7.	Chapter summary	47

Chapter 3. Definition of manufacturability of AM and the methodological framework for a manufacturability analyzer and recommender.....	48
3.1. New definition of the manufacturability of AM.....	48
3.2. Proposed manufacturability levels.....	50
3.3. Proposed methodological framework	55
3.4. Basic research assumptions and research focus.....	57
3.5. Chapter summary	58
Chapter 4. Establishment of AM datasets for manufacturability analysis.....	60
4.1. Data acquisition	60
4.1.1. Design of experiments	60
4.1.2. FDM setup	64
4.1.3. LPBF setup.....	65
4.2. Database management system	66
4.3. AM data port.....	74
4.4. Chapter summary	76
Chapter 5. Hybrid machine learning models for manufacturability prediction.....	77
5.1. Voxel-based CNN model.....	77
5.1.1. Proposed ML algorithm and architecture	78
5.1.2. Loss function and evaluation metrics	83
5.1.3. Hyperparameters	84

5.1.4. Input data generation and preprocessing.....	89
5.1.5. Data Labeling.....	92
5.1.6. Results and discussion	94
5.1.6.1. Results of Output 1 Predicting the Printability of the Entire Part.....	94
5.1.6.2. Results of Output 2 Predicting the Printability Map.....	97
5.2. Advanced sparse-based CNN model	102
5.2.1. Framework of the sparse-based CNN model	103
5.2.2. Data generation and preprocessing	105
5.2.3. Network operations on sparse-data structure.....	107
5.2.4. Network structure and learning parameters	109
5.2.5. Results and discussions.....	113
5.2.5.1. Two-Class Manufacturability Classification	113
5.2.5.2. Semantic Manufacturability Segmentation.....	115
5.3. Chapter summary	119
Chapter 6. MAR-AM Recommendation system	121
6.1. ML-assisted manufacturability model for FDM.....	121
6.2. Proposed structure and algorithm of closed-loop recommendation system	124
6.3. Potential variations in the design aspect	127
6.3.1. Build orientation with the least overhang.....	128
6.3.2. Build orientation with the most contacting area to the build plate	129
6.4. Potential variations in material and processing information.....	130
6.5. Chapter summary	132

Chapter 7. Implementation and case studies	134
7.1. Web-based implementation and deployment.....	134
7.1.1. Architecture.....	134
7.1.2. User interfaces	137
7.2. Case studies.....	140
7.2.1. Case 1: Simple customized mechanical parts	141
7.2.2. Case 2: Material-related and process-related demo	144
7.2.3. Case 3: Design-related demo	147
7.2.4. Case 4: Skulls.....	151
7.3. Chapter summary	155
Chapter 8. Conclusions and future research	157
8.1. Conclusions.....	157
8.2. Future research.....	162
References.....	164
APPENDIX I: Investigations of effects on varying processing parameters	176
APPENDIX II: Lists of related publications	179
Published journal papers	179
Journal papers under review or revision	179
Peer-reviewed conference papers	179
APPENDIX III: Abstract of major journal publications.....	180

Journal publication D1	180
Journal publication D2	181
Journal publication D3	182
Journal publication D4	183

List of Figures

Figure 1-1: Schematic of the LPBF process [11].....	3
Figure 1-2: Schematic of the FDM process [28]	5
Figure 1-3: Examples of unsatisfactory printing	7
Figure 2-1: Geometric explanation for machining characteristics: (a) visibility, (b) reachability, (c) accessibility, and (d) setup complexity [37]	14
Figure 2-2: Map of manufacturing difficulties and the associated color scale [38]	16
Figure 2-3: Manufacturability of AM.....	17
Figure 2-4: Principle process parameters in LPBF [1]	19
Figure 2-5: AM worksheet provided by Booth et al. [67]	23
Figure 2-6: Examples of geometric features considered in LPBF: (a) minimum thickness [8], (b) support, (c) part orientation [26], (d) surface [8], and (e) holes (overhangs) [8].....	26
Figure 2-7: LPBF process monitoring setup scheme [68]	28
Figure 2-8: Illustration of computing infeasible features using the LDNI-based offsetting algorithm [93].....	31
Figure 2-9: (a) For the same slice (yellow), when the skeleton is obtained using the thinning process, the protrusion is elongated in the corrected model (gray). (b) Spur pixel removal achieves the intended length by deleting the end-point pixels (marked green). [90]	31
Figure 2-10: Flowchart of the manufacturability analysis tool [86]	32
Figure 2-11: Octree-based voxelization [85]	33
Figure 2-12: Computing E for a single vertex. (a) Input polygon with both the convex hull and the triangulation. (b) $R(x)$ at the first iteration. (c) Disk at the first iteration (d) Disk at the second iteration. (e) Final iteration in this case [94].....	34

Figure 2-13: Flow of feature recognition using HKS [84]	35
Figure 2-14: Structure of the knowledge management system: (a) overall structure, (b) submodel for LPBF [95].....	37
Figure 2-15: ML-assisted manufacturability analysis by Guo et al. [105]	39
Figure 2-16: Graphical representation of feedforward neural network	44
Figure 2-17: Graphical representation of convolutions	46
Figure 3-1: Manufacturability analysis in the design process [145].....	50
Figure 3-2: Example of (a) geometric incompleteness and (b) warping	51
Figure 3-3: Example of (a) pores and (b) cracks [146].....	52
Figure 3-4: Example of (a) SEM images and (b) roughness analysis for printed parts [150]	54
Figure 3-5: Overall framework of MAR-AM.....	56
Figure 4-1: Example benchmarks	62
Figure 4-2: Example designs in the database.....	63
Figure 4-3: Photograph of Ultimaker3 in the laboratory	64
Figure 4-4: Entity relationship diagram of the developed database	67
Figure 4-5: Example tables in the database	73
Figure 4-6: Preliminary design for the AM data port	75
Figure 5-1: Flowchart of the developed system.....	79
Figure 5-2: ML architecture of Model 1 performing the initial analysis.....	80
Figure 5-3: ML architecture of Model 2 performing the printability map analysis.....	82
Figure 5-4: Detailed ML model architecture (Model 1)	87
Figure 5-5: Detailed ML model architecture (Model 2)	88
Figure 5-6: Examples of voxelized geometric 3D model	90

Figure 5-7: Interface of the annotation tool	93
Figure 5-8: Examples of data labeling	93
Figure 5-9: Test cases of the validation set. (a) Diamond lattice structure fabricated from AlSi10Mg using an EOS machine, (b) benchmark with tiny needles, and (c) AlSi10Mg tensile bar printed using Renishaw.....	99
Figure 5-10: Comparison of the predictions obtained using two different materials with varying strut thicknesses	100
Figure 5-11: Prediction of a long overhang bridge.....	102
Figure 5-12: Framework of the ML-assisted manufacturability analysis.....	104
Figure 5-13: Comparison between different voxel sizes for a given design.....	106
Figure 5-14: Examples of data labeling for sparse-based approach	107
Figure 5-15: Graphical explanation of convolution on a sparse matrix.....	108
Figure 5-16: Network structure for two-class manufacturability classification	111
Figure 5-17: Network structure for semantic manufacturability segmentation.....	112
Figure 5-18: Memory cost comparison between the dense and sparse matrices	115
Figure 5-19: Comparison of the (a) original design model, (b) prediction from the two-class manufacturability classification, (c) prediction from the commercial software Materialise Magics, and (d) printed result [185].	118
Figure 5-20: Comparison of the (a) ground truth (labeling), (b) prediction from the semantic manufacturability segmentation, (c) prediction from the commercial software Materialise Magics, and (d) printed result.....	119
Figure 6-1: Graphical view of ML training procedure	123
Figure 6-2: Flowchart of the recommender system	125

Figure 7-1: High-level architecture of the developed webpage.....	135
Figure 7-2: Framework of the developed web-based tool	137
Figure 7-3: User interfaces of the MAR-AM: Main page	138
Figure 7-4: User interfaces of the MAR-AM: Results page	139
Figure 7-5: User interfaces of the MAR-AM: Feedback page	140
Figure 7-6: (a) Prediction of bevel gear (b) printing result of bevel gear.....	142
Figure 7-7: (a) Prediction of hexagonal organizer, (b) printing results of hexagonal organizer for before implementing the suggestion and after implementing it.....	145
Figure 7-8: (a) Prediction of polyhedron model, (b) printing results of polyhedron model.....	147
Figure 7-9: (a) Prediction of art creative, (b) printing results of art creative for both before and after the suggestion	149
Figure 7-10: (a) Prediction of the steam locomotive component, (b) printing results both before and after the suggestion	151
Figure 7-11: (a) Prediction of the skull lamp cover, (b) printing results of the skull lamp cover. The red boxes indicate the problematic areas	153
Figure 7-12: (a) Prediction of the skull bowl, (b) printing results of the skull bowl.....	154

List of Tables

Table 2-1: Recent efforts to evaluate the manufacturability of AM.....	21
Table 2-2: Comparison of the existing computational methods	29
Table 4-1: Most critical geometric features in AM	61
Table 4-2: Attributes and data types of each table at design or preparation stage.....	68
Table 4-3: Attributes and data types of each table at the manufacturing process stage	69
Table 4-4: Attributes and data types of each table at the product level.....	72
Table 5-1: Examples of the material and printing process used for data training	91
Table 5-2. Cross-validation results of the prediction in the initial analysis.....	95
Table 5-3. Effects of voxelization resolution on the computing cost and performance	96
Table 5-4. Cross-validation results of the printability map prediction	98
Table 5-5: Cross-validation results of the two-class manufacturability classification	114
Table 5-6: Cross-validation results of the semantic manufacturability segmentation.....	116
Table 5-7: Comparison of the dense and sparse matrices.....	117
Table 6-1: Selected ML input features for material and processing information	122
Table 6-2: Potential variations for design aspects	128
Table 6-3: Potential variations for process aspects.....	131
Table 7-1: Detailed printing information of the gear.....	141
Table 7-2: More successfully printed case studies	143
Table 7-3: Detailed printing information of the organizer.....	144
Table 7-4: Detailed printing information of the polyhedron model	146
Table 7-5: Detailed printing information of the art creative.....	148
Table 7-6: Detailed printing information of a steam locomotive component.....	150

Table 7-7: Detailed printing information of skulls	152
--	-----

Chapter 1. Introduction and motivations

Additive manufacturing (AM), which is also widely known as three-dimensional (3D) printing, has been a new trend in the manufacturing process in recent years. It involves building parts following a generated 3D model by adding layers of materials and fusing them. The main advantage of AM is the ability to enable customization and fabricate complex geometries such as lattice structures that are extremely difficult to manufacture in subtractive manufacturing (SM). Although AM has been employed in many industrial applications, it is still difficult for beginning users to ensure the success of every print. It requires users to have a deep understanding of the AM techniques to fully utilize this technology. The printing may fail owing to many factors such as the poor selection of the build orientation, materials, process settings, and insufficient geometric support for overhangs [1-8]. Non-AM experts may have difficulty in determining whether their designs are printable through the selected AM process, and it is even more difficult for them to make proper modifications before the fabrication. This thesis is dedicated to addressing these challenges.

In this chapter, the background of AM technology is introduced. Two focused processes, material extrusion (ME) and laser-based powder bed fusion (LPBF) are briefly introduced in Section 1.1. The manufacturability challenges in AM are described and discussed in Section 1.2, which results in the motivation for this study. Section 1.3 explains why machine learning (ML) is used as the major approach to model the manufacturability of AM. The detailed research objectives are stated and explained in Section 1.4. This chapter ends with the organization of the thesis in Section 1.5.

1.1. Additive manufacturing

As introduced by ISO/ASTM standards [9], AM techniques can be divided into seven categories: binder jetting, directed energy deposition, powder bed fusion, sheet lamination, material extrusion, material jetting, and vat photopolymerization. The first four can be used to produce metal products, and the remaining ones primarily focus on polymers. ME process and LPBF are the two focuses of this thesis as they are well known and widely used. The following sub-sections provide more details on each process.

1.1.1. Laser-based powder bed fusion

In the metal LPBF process, a laser beam as a power source melts and fuses the metal powder on each layer according to the given pattern. After one layer is complete, the next layer of metal powder is applied, and the laser is projected. The process continues layer by layer until the products are completely built [10-13]. The schematic of the LPBF process is shown in Figure 1-1. The LPBF process is ultimately about the successful control of heat transferred from an intense laser beam to a powder bed with poor heat conductivity to produce the geometrically precise localized fusion of powder [14]. The fusion mechanisms can be grouped into four groups, which are solid-state sintering, chemically induced binding, liquid-phase sintering (LPS), and full melting [15]. When metal is used, LPS and full melting are the two conventional approaches used to solidify metal powder.

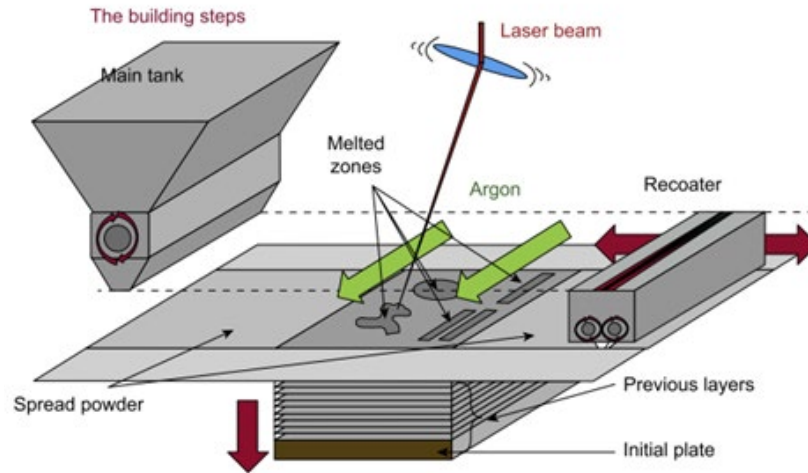


Figure 1-1: Schematic of the LPBF process [11]

Because of its relatively high resolution, numerous metallic powder material options, and potential for manufacturing virtually any shape, the LPBF process is widely used and studied in both academia and industry [13, 16-18]. LPBF is applied in the medical and dental, aerospace, automotive, energy, and tooling industries [16, 18-23]. Compared with conventional manufacturing (CM), the LPBF process is more suitable for prototyping and low production volumes of high complexity parts owing to its advantages in cost, production time, and machinability [17]. In contrast to SM methodologies, it provides more design freedom with the layer-upon-layer material addition approach [13]. As no tooling is required in the LPBF process, designers can consider more complex geometries that are not achievable with CM processes. The increasing market demand for the LPBF process has increased the research efforts in academia [16, 24, 25].

Over the past 20 years, significant research has been conducted in the field of LPBF. Process, materials, designs, applications, and constraints related to LPBF have been investigated extensively and were summarized in a recent survey paper [26]. With the rapid iterative

deployment of LPBF equipment, the process has been updated and improved and is considered to be a mature technology. An increasing number of materials have become available for LPBF processes such as aluminum AlSi10Mg, cobalt chrome MP1, Maraging steel MS1, nickel alloy HX, stainless steel 17-4PH, titanium Ti64ELI, and tungsten W1. [27] With the expansion of materials and equipment, industries attempt to employ LPBF to benefit their current design or manufacturing process in various applications. More recently, the LPBF process has been used to progress from more than only fabricating prototypes to the area of functional end-product fabrication.

1.1.2. Material extrusion

ME is a type of AM process in which a feedstock material (typically a thermoplastic polymer) is forced through a heated nozzle and selectively deposited layer by layer to create a 3D object. The most well-known example is fused deposition modeling (FDM), which is also known as fused filament fabrication. Figure 1-2 demonstrates the schematic of the FDM process [28]. Filaments are used in the printing process. Potential variants of the ME process include different extrusion processes such as the hot extrusion of rods, cold extrusion of slurries, and hot extrusion of pellets.

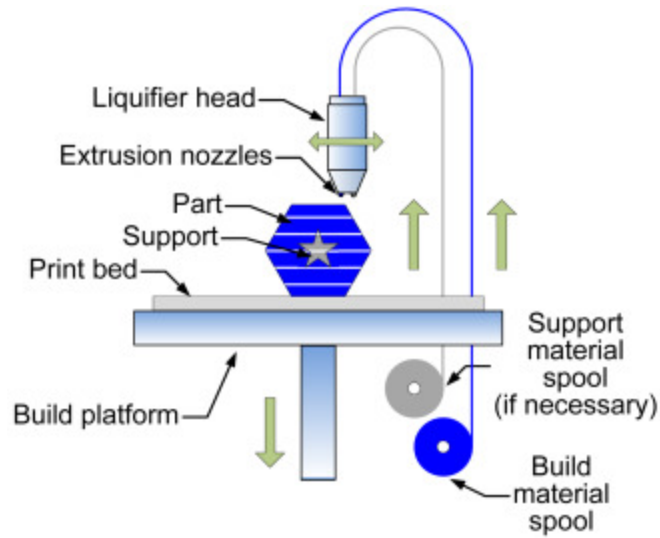


Figure 1-2: Schematic of the FDM process [28]

ME is typically not as fast or accurate as other types of AM technologies. However, ME technology and its compatible materials are widely available and inexpensive. It is the most popular process for hobbyist-grade or desktop-grade 3D printers. ME is often utilized in manufacturing and industrial contexts to create non-functional prototypes or cost-effective design iterations. ME also offers a wide selection of materials, including thermoplastics such as polylactide (PLA), acrylonitrile butadiene styrene (ABS), polycarbonate (PC), nylon, polyether ether ketone (PEEK), and polyethylene terephthalate (PETG); ceramics such as alumina and zirconia; green metal mixtures such as stainless steel, titanium, and Inconel; food pastes; and biological materials.

This research used only the FDM process to validate the developed ML models with the material selection for thermoplastics, which are the most common type in ME.

1.2. Manufacturability of AM

For the CM process, the study on manufacturability can be traced back to World War II [29] owing to the demand to build better weapons. Thereafter, increasing global competition and desire to reduce the time and cost resulted in the increasing awareness of the manufacturing considerations [30]. In the CM process, particularly for the SM process, the product is fabricated by removing the materials from solid blocks. Hence, the products resulting from the SM process are always considered to be dense. The only consideration in manufacturability is the geometric inconsistency and the tool accessibility.

The definition of the manufacturability of AM is vague in the literature. For the AM process, the parts are generally built from materials layer by layer. The density of the part varies. As investigated in the literature, the mechanical and microstructural properties of specimens fabricated via the AM process may vary owing to the different building orientations or process parameters [31]. In the past, investigations using simulations, modeling, materials, and design optimizations of the AM process have been conducted extensively. However, gaps still largely exist in understanding and representing manufacturability. Designers are challenged with the lack of understanding of AM capabilities and the influence of process parameters on the final products [32].

When considering the manufacturability of the AM process, two questions must be answered. The first question is whether the part can be successfully fabricated or not, i.e., whether all the geometry can be successfully built without considering their dimensional and geometric accuracy. Not all geometric features can be fabricated using AM. Many features present printing difficulties such as inclined surfaces, overhangs, holes, and walls. Figure 1-3a depicts an example of incomplete printing through the LPBF process. The bottom area of the objects failed to be

fabricated in this case because of the improper support structure added to the bottom. Designers may think the certain geometry is not printable through LPBF; however, Figure 1-3b shows a similar geometry printed from another printing direction using a different machine. Compared with Figure 1-3a, the lattice part in Figure 1-3b was successfully printed, but the flat top cover was warped and not completely printed. The entire circled area is considered to be not manufacturable. It is difficult for designers who are not experts in AM to determine these potential failures at the early design stage.

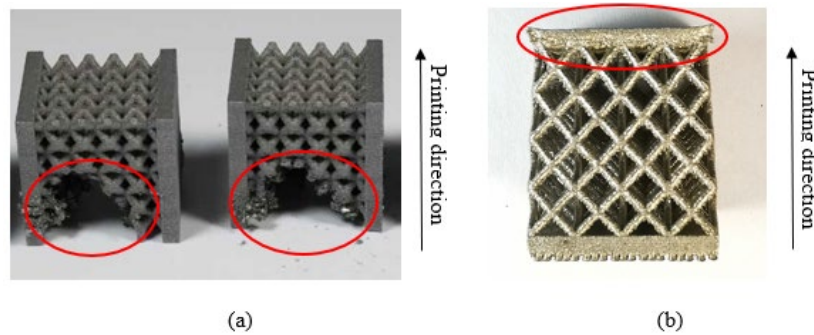


Figure 1-3: Examples of unsatisfactory printing

The second question is whether the fabricated parts are satisfactory to customers' requirements in terms of dimensional accuracy, geometric accuracy, and mechanical properties. These technical requirements are the standards to determine whether the final products satisfy the required qualities [33-35]. For the AM process, the technical requirements can vary based on different applications. In addition, from most studies in the literature, researchers nearly always consider the geometric inconsistencies for the manufacturability analysis of the AM process just as is conducted in the manufacturability analysis of the SM process. However, as discussed earlier, considering only the geometric aspects may not be sufficient for the manufacturability analysis. A clear definition of the manufacturability of the AM process is critically required. A comprehensive manufacturability model is in demand, which motivated this research.

1.3. Why machine learning?

ML is an artificial intelligence subset that offers the ability for machines to learn and improve through experience [36]. ML approaches have been successfully applied in various applications such as virtual personal assistants, email spam and malware filtering, product recommendations, and computer versions. ML can be the most suitable approach to solve problems with two main aspects as outlined in the following:

First, if the problems to be solved are too complex for human capabilities or too complex to be systematically modeled, ML can provide the advantage of time cycle reduction and efficient utilization of resources. Second, the tasks often require adaptivity; thus, traditional approaches such as guidelines or mathematical models have a limitation on the rigidity of adapting changes. Once the guidelines and mathematical models are developed, they remain unchanged. However, with the ML approach whose behaviour is primarily affected by the input data, the model will have the ability to adapt to future variations without any further investigation or code implementation. These benefits support ML as a potential approach for many applications including AM technologies. Unlike the conventional manufacturing process, AM processes have not been standardized yet. There are seven AM techniques depending on the printing methods. Even for the same AM technique, the quality of products fabricated by the different machines varies significantly. The AM process is difficult to generalize owing to its uncertainty and variability. Mastering and modeling the knowledge of the AM process is a complex and extremely difficult task. Furthermore, most studies related to AM research produced a large set of numerical data such as experimental results, simulation results, material, and machine information, and the objective of these studies is to predict the incoming printing process or product quality, which are the

preconditions and the targets of the ML approach. These characteristics make ML a reasonable solution in AM studies.

More importantly, compared to some traditional numerical methods such as simulation and morphological operations, ML is much faster. It may require a few hours of training. However, once the model is defined and trained, the prediction only takes seconds.

1.4. Research objectives

To enable the adoption of AM in real applications, this study investigated the use of ML to analyze the manufacturability of a given design for a selected AM process. This research aimed to develop an automated manufacturability analyzer and recommender for novice AM users (MAR-AM) such as designers at the design stage. It is expected to achieve rapid evaluation before the fabrication on whether the given design is printable with the selected machine settings and material. Moreover, such an analyzer is expected to provide some suggestions for users to increase the printing success rates. More specially, the research objectives of this thesis are summarized as follows:

1. To develop a more appropriate definition of manufacturability to guide designers toward AM design. The definition of the manufacturability of AM is still vague. The characteristics to be satisfied to consider manufacturability are first clarified and defined in this research.
2. To develop an accurate ML model to effectively identify manufacturability challenges. It can be specified in two sub-objectives. The first is to develop an AM (in this thesis, LPBF and FDM are the focus) database. The datasets will be then used for ML training. The

second portion is to develop a general, efficient, and effective ML model to predict AM manufacturability.

3. To develop an automated manufacturability analyzer and recommender for AM. Such an analyzer and recommender can predict the manufacturability of a given design and selected machine and material settings at the design stage. Meanwhile, it can provide suggestions to novice AM users to increase the printing success rate.

1.5. Thesis organization

This thesis consists of eight chapters. Chapter 1 introduces the background of AM technology with a focus on two AM processes: FDM and LPBF. Moreover, the reason for using ML as the solution for manufacturability is stated. The research objectives are addressed based on the research limitations and gaps in the literature. In Chapter 2, the existing studies on manufacturability analysis are discussed, and the fundamentals of ML methods are introduced.

Chapter 3 first introduces the new definition of the manufacturability of AM. It clearly states the level of manufacturability used in this research. Thereafter, the methodological framework of the MAR-AM is described. The framework comprises three major parts: (1) dataset establishment, (2) ML model training, and (3) manufacturability prediction and suggestion, which are explained in detail in Chapters 4, 5, and 6. The basic assumptions and research focus are clearly identified at the end of Chapter 3.

Chapter 4 describes the methods for dataset establishment that are used to train the ML model. The entity-relationship diagram is shown. The experimental setup and design of experiments are explained, as well as the method of data labeling. An AM data port is finally proposed in this chapter to increase public data sharing.

The collected data is sent to either ML model training or manufacturability prediction and suggestion depending on whether it is labeled. Chapter 5 discusses the ML approach and model training on the manufacturability analysis. The voxel-based approach is first discussed to demonstrate the validation of the ML approach. Thereafter, an advanced approach, which involves sparse representation of the ML models, is developed to increase the model performance.

Chapter 6 focuses on the methodology of the recommendation system, which uses the prediction from ML models. With a closed-loop process, suggestions on process parameters or designs are offered. Furthermore, users are invited to provide feedback on the prediction that will be sent to our database to update the ML model regularly.

The proposed framework has been implemented into a web-based application. Case studies have been conducted to validate the proposed approach, and they are described in Chapter 7. Finally, the thesis conclusions and future perspectives and recommendations are provided in Chapter 8.

Chapter 2. Literature review

This chapter provides the fundamentals related to this thesis and a comprehensive review of the existing studies on the manufacturability of AM. Section 2.1 first introduces the existing efforts in evaluating the SM process as a comparison and references to the manufacturability studies of AM. In Section 2.2, the major factors in evaluating the manufacturability of AM are reviewed and discussed. Based on that, the existing approaches on AM manufacturability analysis and non-computational methods are discussed in Section 2.3. The computational methods are listed and discussed in Section 2.4. Section 2.5 compares the existing manufacturability studies on SM and AM. ML is introduced in this thesis to solve the manufacturability challenges. The fundamental of ML is introduced in Section 2.6. Finally, this chapter is summarized.

2.1. Existing Approaches on Evaluating the Manufacturability of SM

In the past, the manufacturability analysis was always conducted by a designer. Designers use their experience to evaluate the manufacturability of their designs. Some guidebooks have been published by the leading professional societies or manufacturers to provide design rules based on a particular manufacturing process. Designers read carefully through these heavy guidebooks to avoid these configurations that may result in poor manufacturability. The quality of the manufacturability analysis is also highly dependent on their working experience. Automated manufacturability analysis was developed to aid designers in manufacturability evaluations. After years of research and development, manufacturability analysis has become an essential part of computer-aided design (CAD)/computer-aided manufacturing (CAM) systems. Commercialized software such as DFMXpress in Solidworks, VAYO, and DFMPPro, have been released for users to evaluate manufacturability. The manufacturability of SM can be defined under four

characteristics: visibility, reachability, accessibility, and setup complexity [37]. Studies with different approaches to evaluating the manufacturability of a selected SM process have been published [30, 38-42]. According to the existing literature reviews, the main strategies for these approaches can be classified into two groups based on the geometric interpretation: feature-based and feature-less-based approaches [37, 42, 43]. More details are provided in the following.

2.1.1. Definition of the manufacturability of SM

Given the design and a selected SM process, the definition of manufacturability in SM is straightforward. It is defined as whether the design is manufacturable in shape, dimensions, tolerances, and surface finishes. The design or features are evaluated on manufacturability with respect to four characteristics: visibility, reachability, accessibility, and setup complexity [37]. Figure 2-1 provides a geometric explanation for each characteristic. Visibility depicts the view from the machine tool to the part. A part has high visibility if the surface area of the entire model can be seen from the view of the machine tool. Reachability indicates the lengths required for the machine tools to reach the surface of the model. A shorter length of the machine tool is preferred. Accessibility measures the ability of a model to be machined without tool collisions. Accessibility is dependent on both the surface geometry and tool size. Setup complexity measures the number of setups required to fabricate a part. When machining a complex geometry, the tool may require to be rotated to access certain features. In existing research publications, accessibility is the most popular evaluation criterion for both the feature-based and feature-less-based approaches.

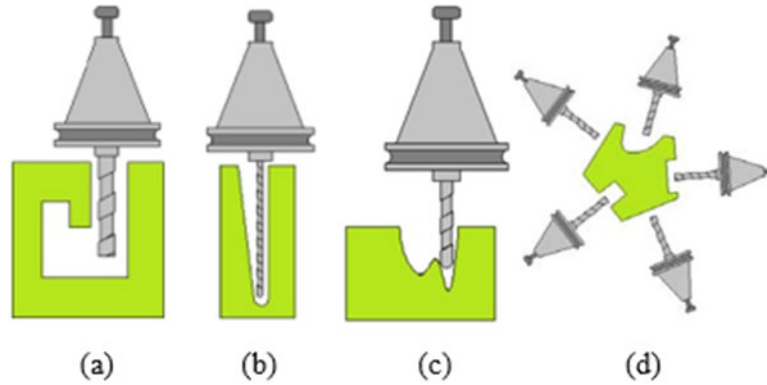


Figure 2-1: Geometric explanation for machining characteristics: (a) visibility, (b) reachability, (c) accessibility, and (d) setup complexity [37]

2.1.2. Feature-based Approach

The general concept of the feature-based approach is to extract the machining features such as holes, pockets, slots, or machinable surfaces from the design features. The extracted features are then used as the input of the manufacturability analysis. The feature-based approach can be further categorized into the three most active approaches, according to Han's review [42]: graph-based, volumetric decomposition, and hint-based approaches. The graph-based approach determines the feature types by translating the given design into multiple graph patterns. The part graphs are analyzed to determine the features [44]. This approach has been successful in recognizing some types of features but has some difficulties when faces are altered owing to feature intersections. For the volumetric decomposition approach [45], the general concept is to decompose the geometric input into volumes and interpret them to the machining features. The decomposition operation can be either convex hull decomposition [46, 47] or cell-based decomposition [48, 49]. The convex hull decomposition is based on geometric Boolean operations, and the cell-based decomposition required that the volume be decomposed into the cells and then composed to generate a volume for a machining feature. The challenge in the volumetric

decomposition approach is that the result features may not match with any predefined feature types after the decomposition. The hint-based approach determines the machining features by following the defined rule that asserts a feature and its associated operation. The most recognized hint-based reasoning algorithms were proposed by Regli for F-Rex [50], Han for an integrated incremental feature finder [51], Brooks for a feature-based machining husk system [52], and Vandenbrande for an object-oriented feature finder [53]. The major problem in the hint-based approach is that interpreting all the machining features is difficult.

2.1.3. Feature-less based Approach

The feature-based approach primarily focuses on detecting manufacturable features in the selected machining process. In contrast, the feature-less approach analyzes the surface representation of the model to determine the manufacturability. It ideally operates with any arbitrary geometries without feature recognition [37]. Moreover, the feature-based approach mostly comprises all the geometric elements as an entity to be a machining feature. However, this constrains the manufacturability analysis. For instance, for multi-axis machining, a portion of the feature can be fabricated in one direction, and then the remaining portion is finished after changing the tool setup orientation. The feature-less approach can solve these challenges that are difficult to solve using the feature-based approach. Li proposed the feature-less-based strategy to determine the manufacturability of a part by slicing geometry files to map machinable ranges [43]. The slices are set orthogonal to the axis of the rotation. The accessibility is estimated using the visibility of the light line on a two-dimensional (2D) slice file. The machining simulation proposed by Jang offers another direction by using the voxel representation in generating collision-free tool paths and determining cutting parameters to increase the fabrication success rate. Kerbrat [38] presented a more advanced approach by decomposing the geometric model into octrees and evaluating the

manufacturability index on each octant (an example shown in Figure 2-2). Compared with the voxel-based and slice-based feature-less approach, the octree-based approach can acquire high accuracy relatively rapidly. His approach also offers the potential for evaluating manufacturability considering both machining and AM.

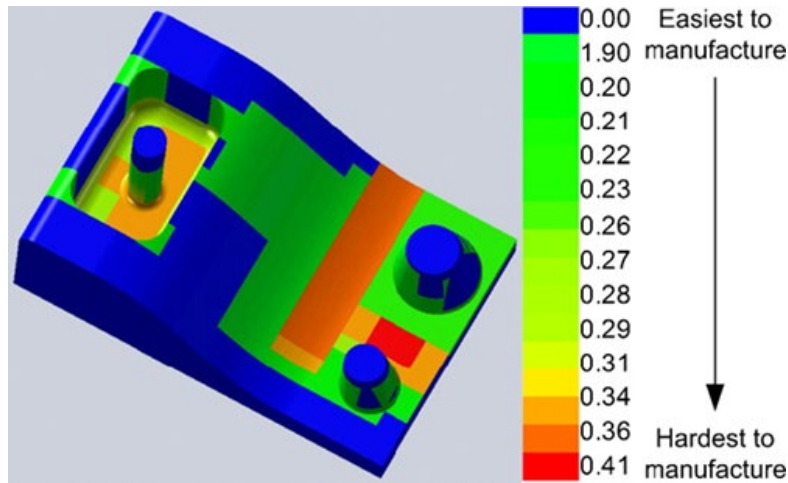


Figure 2-2: Map of manufacturing difficulties and the associated color scale [38]

2.2. Major factors on evaluating the manufacturability of AM

When investigating the manufacturability of the AM process, three key aspects must be considered: design, process, and material (Figure 2-3). Manufacturability is the intersection of these three aspects. Thus, it is necessary to understand all three aspects. Process and material are often correlated to each other and combined as process parameters.

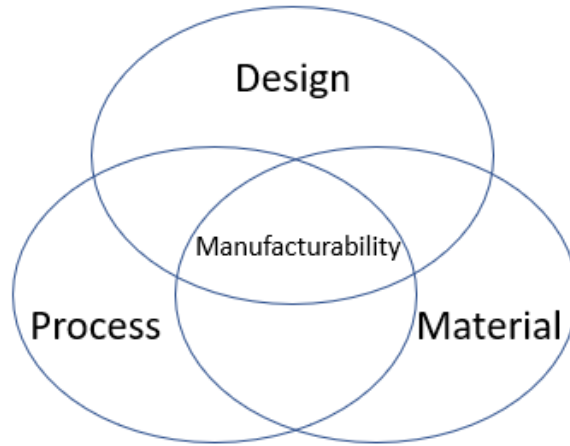


Figure 2-3: Manufacturability of AM

2.2.1. Design aspects

To consider the manufacturability of a manufacturing process, the geometric features that can be fabricated should be considered. In the SM process, the major design geometric features are defined as holes, slots, pockets, etc., which are typically associated with the type of the corresponding tooling required to create these features [42]. However, the design geometric features that the AM process can manufacture are dramatically different from those defined for SM processes. More importantly, a design geometric feature that is manufacturable using one AM machine with a given process parameter setting may not be manufacturable when the machine or process parameters are changed [6]. In Kruth's research [6], the major design geometric features considered in AM were thin walls, overhangs in holes, self-supporting holes, one angled surface, and large radiuses. A few benchmark testing parts were designed to identify the limitations and accuracy of the AM process. For LPBF, Thomas [8] conducted numerous experiments to establish the design guidelines for the LPBF process. The main geometric features considered in this research were object orientation, surface roughness, minimum slot, and wall thickness, parallel edge, angular overhangs, fillet radii, holes, and channels, tapping, and reaming a self-supporting

hole, shrinkage, and stock on the material. Later, Adam [7] investigated the design rules for AM, including LPBF and FDM. The limitations of thickness, orientation, direction, and position of wall feature, as well as the length, inner radius, orientation, and outer radius of the cylinders, were studied. Similar studies were also conducted in industries to identify geometric feature limitations in AM processes. Materialise [54] provides design guides based on their machines for 20 different materials. Taking steel as an example, the main considerations are wall thickness, overhangs, connections, edges and transitions, holes, wireframe structures, hollows, nested objects, hinged and interlinking parts, connection marks, text, and surface details, shrinkage compensation, and dimensional accuracy [55]. Similar guidelines are given by Stratasys [56] in the form of design guides for different AM processes. In the most recent literature, major geometric features considered in the LPBF and FDM processes can be summarized as minimum feature size, overhangs, shrinkage, and object building orientations.

2.2.2. Process aspects

The process parameter is another consideration in the manufacturability analysis. Different AM technologies have different focuses on the process parameters.

For the LPBF process, research shows that more than 130 process parameters influence the process, but only a few of them are critical [1, 57]. These process parameters are grouped into four groups: laser-related, scan-related, powder-related, and temperature-related. The laser-related group consists of laser power, wavelength, spot size, pulse duration, and pulse frequency. The scan-related group comprises scanning speed, scanning spacing, and scanning patterns. The powder-related group contains particle size and distribution, particle shape, powder bed density, layer thickness, and material properties. The temperature-related group contains the powder bed temperature, the powder feeder temperature, and the temperature uniformity. The full list of

process parameters is shown in Figure 2-4. Most of these parameters are strongly interdependent and interacting. For example, steel may require laser power at 150 W for better quality, but for other materials, such as aluminum, the preferred laser power is different [58]. Even for the same material, different particle sizes, shapes, and densities will require different laser powers to achieve the best quality. Other factors such as gas flow also have a significant influence on the quality of the final products [13]. Researchers have conducted many studies [2-4, 59-62] to investigate the interrelationship between process parameters and product qualities.

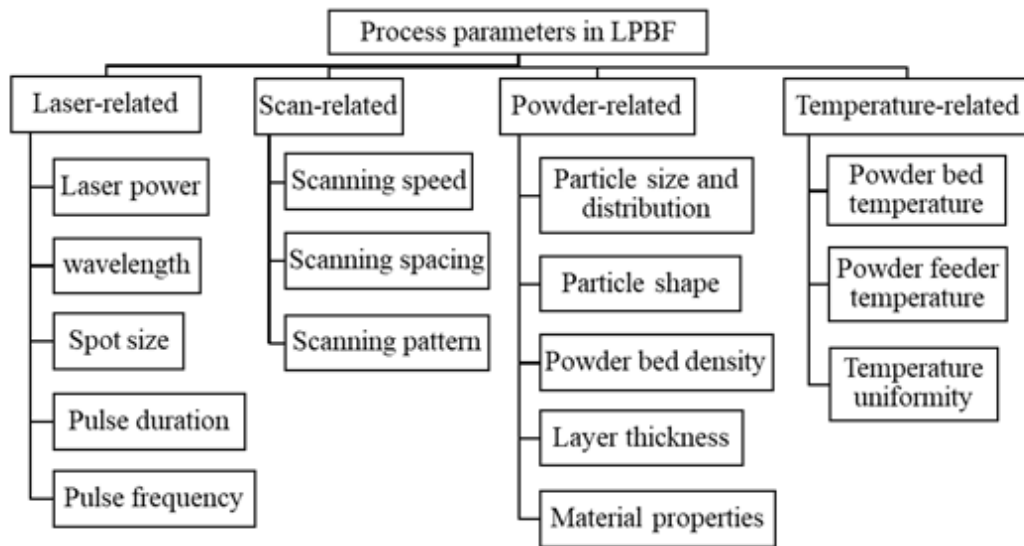


Figure 2-4: Principle process parameters in LPBF [1]

Similar to the LPBF process, the FDM process has hundreds of process parameters. Most of the settings are recommended and settled as default by printer makers. Only a few of them require tuning from users. The most investigated process parameters for FDM are layer thickness, scanning speed, infill percentage and pattern, extrusion temperature, bed temperature, envelope temperature, and build orientation [63, 64]. According to a comprehensive review, layer thickness, infill density, and build orientation have been observed to have a significant influence on the mechanical properties of the final products [64]. Extrusion temperature is also a critical parameter

in the FDM process [63]. FDM has a straight requirement for the range of extrusion temperature for different materials. The extrusion temperature determines the bonding properties of materials, filament material liquidity, and extruded filament width. Envelope temperature has significant effects on the thermal stress inside a part [63]. Increasing thermal stress will result in part warpage. However, not all current FDM printers have an enclosed chamber. The control of the envelope temperature is an advanced option. Bed temperature affects the adhesion between a part and the build plate. The printing part is expected to adhere to the build plate until it is completely built. The bed temperature setting aids with the adhesion. Other options are available to increase the level of adhesion, such as printing a part with a brim and using glue. Scanning speed refers to the speed of nozzle movement, and it is divided into profile and filling scanning speeds. Higher scanning speeds can result in poor printing quality owing to the increase in the mechanical vibration. Lower scanning speeds may cause the hot nozzle to burn a part [64].

2.3. Existing approaches on evaluating the manufacturability of AM

Efforts on manufacturability analysis of the AM process have been conducted by a few researchers. To summarize the studies in the literature, the recent efforts to evaluate the manufacturability of AM are categorized into three groups (Table 2-1): design guidelines/checklists, real-time process monitoring, and computational methods in manufacturability analysis. Many studies have been conducted on real-time process monitoring in AM. In this section, current non-computational approaches in evaluating manufacturability are summarized and discussed. The computational approach is fully explained and discussed in the next section. The general concept of modeling manufacturability is similar for both LPBF and FDM. Therefore, the existing approaches are summarized together in the following sections.

Table 2-1: Recent efforts to evaluate the manufacturability of AM

Approaches		Description	Reference
Design guidelines/checklists		Numerous experiments were conducted to provide a manufacturable range of geometric design features, including minimum thickness, part orientation, surface roughness, chamfers and radius, holes, and overhang. Designers are expected to follow these guidelines or checklists in their designs.	[7, 8, 32, 65-67]
Real-time process monitoring		Using image-based real-time monitoring to detect and predict potential failure and printing quality during the process.	[68-82]
Computational methods in manufacturability analysis	Manufacturing features recognition	Automate the identification of erroneous features that are under the capability of the selected printer. The general concept of this approach is to discretize the 3D model into 2D/2.5D segments to reduce the difficulty of the direct identification of 3D features. According to the types of input data for feature recognition, prior research can be classified as 3D feature-based approach, slicing data-based approach, voxel-based approach, etc.	[83-94]
	Knowledge-based or rule-based approach	Integrate the models of design aspects and the material and process aspects to predict the performances of the AM parts	[95-97]
	ML approach	Use ML as a black box to predict the manufacturability of the given design or in-situ process	[98-107]

2.3.1. Design Guidelines/Checklists

To bridge design to actual manufacturing, both academics and industries seek the answer modeling the manufacturability or manufacturing capabilities. Both industries and academics have

conducted research to represent manufacturability in the form of design guidelines for different AM processes [67, 108, 109]. Numerous experiments have been conducted to provide a manufacturable range of geometric design features including minimum thickness, part orientation, surface roughness, chamfers and radius, holes, and overhang. Designers are expected to follow these guidelines in their design. However, most of the design guidelines for the AM process focus only on the limitations of a single standard design feature, whereas high complexity designs that are specialized by the AM process to produce are rarely studied [110]. Moreover, most of the guidelines assume the users have prior knowledge and design experience with the AM process. This is a disadvantage for novice users.

Booth et al. presented another approach called the design for additive manufacturing worksheet [67]. A worksheet (Figure 2-5) is provided as a checklist for the designer to validate in advance whether their design is manufacturable. For each category, the importance of weight is applied, and the final total score is calculated. The score is grouped into levels of manufacturability. It offers a simple visual list of details that addresses common mistakes in the AM process. Designers can evaluate the suitability of their designs in the AM process based on that checklist. The worksheet approach can provide an initial evaluation of the design, but it may not be applicable for complex designs because the worksheet simplifies the entire design guidelines by offering the most common suggestions. The limitation of both guidelines and worksheet approaches is that they consider only the design aspects. Each printer has some unique characteristics. By varying process parameters, some of the challenging geometric features may still be successfully manufactured. Such examples have been fully demonstrated in the literature where process parameter optimization is conducted to improve manufacturability [10, 59, 111, 112].

Design for Additive Manufacturing

A quick method for reducing the number of printing and prototyping failures, by Joran Booth

Instructions: Mark one for each category for the part you plan to print. Check daggers and stars first, then scores

Mark One	Complexity	Mark One	Functionality	Mark One	Material Removal	Mark One	Unsupported Features	Sum Across Rows	Totals
<input checked="" type="radio"/>	The part is the same shape as common stock materials, or is completely 2D	<input checked="" type="radio"/>	Mating surfaces are bearing surfaces, or are expected to endure for 1000+ of cycles	<input type="radio"/>	The part is smaller than or the same size as the required support structure	<input type="radio"/>	There are long, unsupported features	x5 =	
<input checked="" type="radio"/>	The part is mostly 2D and can be made in a mill or lathe without repositioning it in the clamp	<input checked="" type="radio"/>	Mating surfaces move significantly, experience large forces, or must endure 100-1000 cycles	<input type="radio"/>	There are small gaps that will require support structures	<input type="radio"/>	There are short, unsupported features	x4 =	
<input type="radio"/>	The part can be made in a mill or lathe, but only after repositioning it in the clamp at least once	<input type="radio"/>	Mating surfaces move somewhat, experience moderate forces, or are expected to last 10-100 cycles	<input type="radio"/>	Internal cavities, channels, or holes do not have openings for removing materials	<input type="radio"/>	Overhang features have a sloped support	x3 =	
<input type="radio"/>	The part curvature is complex (splines or arcs) for a machining operation such as a mill or lathe	<input type="radio"/>	Mating surfaces will move minimally, experience low forces, or are intended to endure 2-10 cycles	<input type="radio"/>	Material can be easily removed from internal cavities, channels, or holes	<input type="radio"/>	Overhanging features have a minimum of 45deg support	x2 =	
<input type="radio"/>	There are interior features or surface curvature is too complex to be machined	<input type="radio"/>	Surfaces are purely non-functional or experience virtually no cycles	<input type="radio"/>	There are no internal cavities, channels, or holes	<input type="radio"/>	Part is oriented so there are no overhanging features	x1 =	
Mark One	Thin Features	Mark One	Stress Concentration	Mark One	Tolerances	Mark One	Geometric Exactness		
<input type="radio"/>	Thin features will almost always break	<input type="radio"/>	Interior corners must transition gradually	<input type="radio"/>	Mating parts should not be the same size	<input type="radio"/>	Large, flat areas tend to warp		
<input type="radio"/>	Some walls are less than 1/16" (1.5mm) thick	<input type="radio"/>	Interior corners have no chamfer, fillet, or rib	<input type="radio"/>	Hole or length dimensions are nominal	<input type="radio"/>	The part has large, flat surfaces or has a form that is important to be exact	x5 =	
<input type="radio"/>	Walls are between 1/16" (1.5mm) and 1/8" (3mm) thick	<input type="radio"/>	Interior corners have chamfers, fillets, and/or ribs	<input type="radio"/>	Hole or length tolerances are adjusted for shrinkage or fit	<input type="radio"/>	The part has medium-sized, flat surfaces, or forms that are should be close to exact	x3 =	
<input type="radio"/>	Walls are more than 1/8" (3mm) thick	<input type="radio"/>	Interior corners have generous chamfers, fillets, and/or ribs	<input type="radio"/>	Hole and length tolerances are considered or are not important	<input type="radio"/>	The part has small or no flat surfaces, or forms that need to be exact	x1 =	
				Starred Ratings	Total Score				
				* Consider a different manufacturing process	33-40 Needs redesign				
				† Strongly consider a different manufacturing process	24-32 Consider redesign				
					16-23 Moderate likelihood of success				
					8-15 Higher likelihood of success				
				Overall Total					

Copyright: The Design for Additive Manufacturing Worksheet, by Joran W. Booth, 2015. This work is licensed under the Creative Commons Attribution-NonDerivatives 4.0 International License. To view a copy of this license, visit <http://creativecommons.org/licenses/by-nd/4.0/>.

Figure 2-5: AM worksheet provided by Booth et al. [67]

Based on these design guidelines or checklists, the manufacturable geometric features are summarized with design suggestions. They are primarily grouped into six categories: minimum feature size, support structure, part orientation, surface, hollow interiors, and overhangs (Figure 2-6). In addition, these criteria are the major considerations for feature recognition in the computational methods, which are discussed in Section 2.4.1. More details on the manufacturing features for the AM process are provided in the following:

Minimum feature size: Research shows that minimum manufacturable feature sizes exist in the LPBF process [113]. The minimum gaps between two features or the minimum wall thickness are

two critical examples. Thomas concluded that the minimum gap thickness for LPBF is 0.3 mm, and the minimum wall thickness is $0.4 \text{ mm} \pm 0.02$ [8]. These data are based on the machine and material used in this research. They offer a good reference but may not be applicable to all cases. The values vary slightly on different materials and machines. Kruth et al. [6] examined different LPBF machines with a benchmark to check the process limitations. They demonstrated that each machine has its own limitations in terms of the minimum feature size. Moreover, since materials used in the AM process are not standardized, and each company has its own proprietary information on the powder they provide, it is not comparable in this case.

Support: A support structure is required in most of the AM processes for two main functions: holding the fabricated piece and resisting the thermal stress [114]. However, the support structures significantly reduce the surface finish [8]. Moreover, improper support structures may cause printing failure [114]. Moreover, for the LPBF process, since the support and structural materials are both metals, they are very difficult to remove. Removing the support structure may significantly reduce the surface finish [26, 115-119]. For the FDM process, although some soluble support materials are used, it only supports several material options such as PLA. Not all FDM materials have compatible soluble support materials. Therefore, support structures are expected to be minimized. The use of support is a prominent problem in the AM process.

Part Orientation: There are two aspects to the part orientation. The first is the placement orientation of the entire part. The second is the angles of the features under the placement orientation of the part. If an overhang tilts at an angle less than a certain degree from the build direction, it may be able to be printed without support structures. The threshold of the overhang structure is defined based on different materials and machines. To minimize the support structures, the optimal placement orientation must be determined to minimize the surface that requires support

during printing [8, 26, 65, 66, 115, 118-123]. Most slicer software offer such functions to determine the best placement of the part. The part orientation has been observed to have significant effects on strength and surface finish. Vertically printed parts with the layers oriented perpendicular to load direction have better mechanical properties than horizontally printed parts with the layers parallel to load direction [124]. Part orientation dictates how many support structures are required to fabricate samples, and removing the support structures reduces the surface roughness [121].

Surface: The surfaces of a part can be categorized into top, side, and bottom surfaces. As the characteristics of the LPBF process, the surface of the part is always attached with incompletely melted powders. To achieve a fully dense metal surface, the part will be printed oversize for post-processing. However, for fine features, post-processing may not be applicable. Here, the surface roughness is affected [3, 8]. For non-flat down-facing surfaces, regardless of whether they are printed with or without support structures, the inclined surfaces may have a certain level of surface roughness challenges.

Hollow interiors: A hollow interior is a type of feature that the AM process specializes in fabricating. Frequently, the traditional manufacturing process cannot produce an entire hollow part at once, but the AM process offers this possibility. When the functionality is promised, using a thick wall and hollow interiors significantly reduces printing time and part weight [26, 115, 125].

Overhangs: Relative long overhangs without support are not printable in the AM process. The maximum overhang distance without support varies based on different process parameters. As mentioned earlier, it is recommended for designers to minimize the support structures when the functionality is promised. When applicable, concave and convex radii are alternative design features with self-supporting dimensions [116, 126-129].

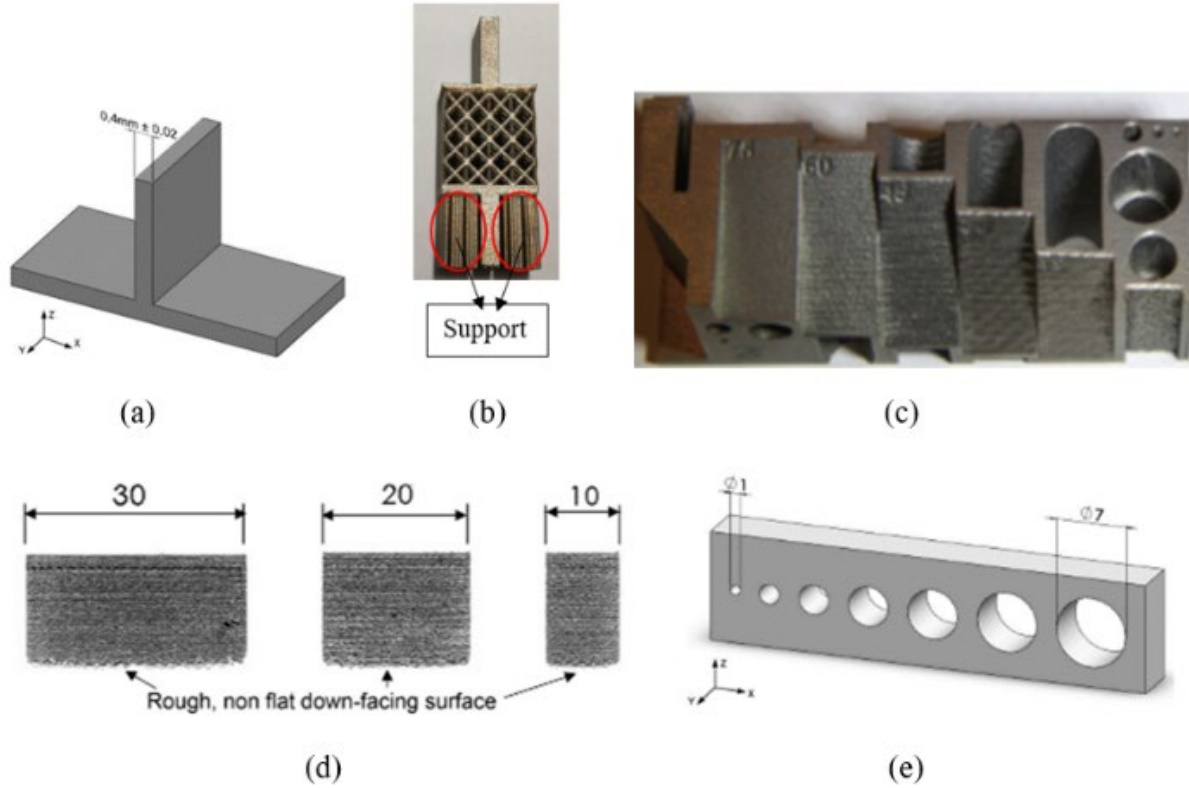


Figure 2-6: Examples of geometric features considered in LPBF: (a) minimum thickness [8], (b) support, (c) part orientation [26], (d) surface [8], and (e) holes (overhangs) [8]

2.3.2. Real-time Process Monitoring

Real-time process monitoring is often used to detect potential failure during printing time. Although the AM was invented decades ago, and many commercial machines are available on the market, process repeatability and stability are still a challenge for the industry's breakthrough. Hence, real-time process monitoring was introduced to improve process stability. It is also considered a real-time manufacturability detection. Image-based real-time monitoring is used to detect and predict potential failure and printing quality during the process. The scheme of the LPBF process monitoring setup is shown in Figure 2-7 as an illustration. Printing failure and unsatisfied printing quality such as surface finish, porosity, tolerance, and tensile stress [68-74]

can be observed and predicted before the printing process is complete to save time and money. Marco [68] conducted a comprehensive review of in-situ monitoring methods in metal powder bed fusions in 2017. In his review, he summarized the most common categories of defects in the LPBF process such as porosity, residual stresses, cracking and delamination, balling, geometric defects, and dimensional accuracy. A map of the main defects and their approaches causes in the literature was provided. The possible sources of defects can be grouped into four categories: equipment, process, build preparation choices, and material powders. The main set-up parameters and settings for the existing studies are also listed in his paper. Recently, research on using ML to assist real-time process monitoring was proposed to aid in predicting the printing quality and possible printing failure [75-82]. The real-time process monitoring can aid in detecting the printing failure ahead of the completion of the printing and reduces the time and cost. It can effectively aid in solving the problem caused by the repeatability and stability of the process or machine. However, it cannot determine manufacturability in the design stage. It is not applicable if the printing failure is due to the geometric design rather than the printing process or machine. More details are discussed observed in Section 2.4.3 when the ML approach is introduced.

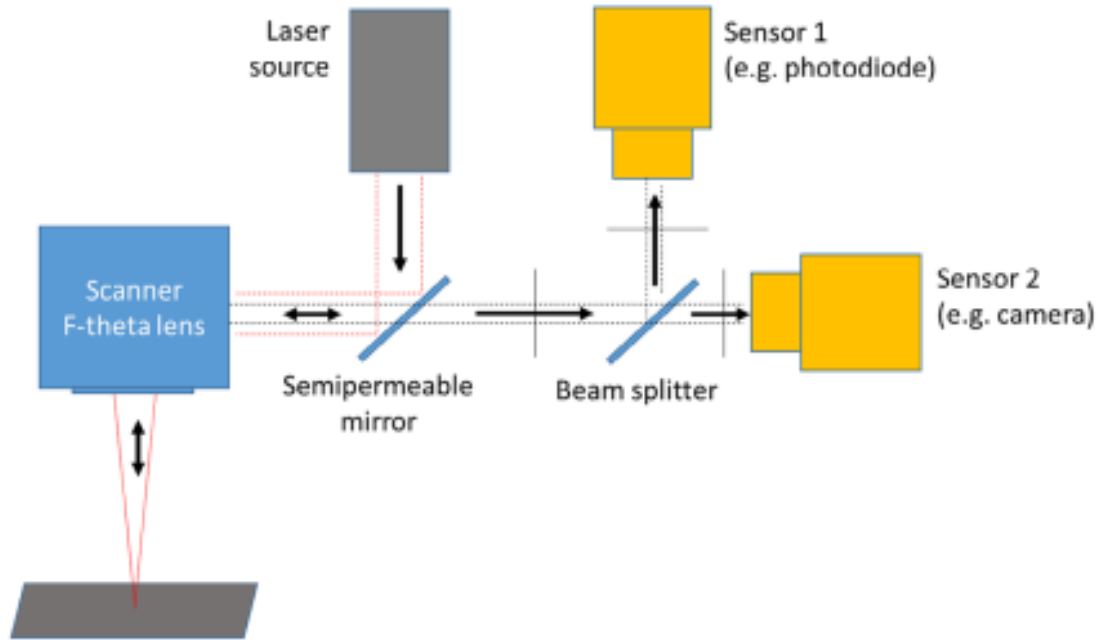


Figure 2-7: LPBF process monitoring setup scheme [68]

2.4. Computational methods in manufacturability analysis

Manufacturability analysis at the design stage is expected to produce suggestions and recommendations for designers to evaluate their design and the selection of the manufacturing process. Automated manufacturability assessment is always sought to assist designers, particularly novice AM users, to fully utilize AM techniques. The manufacturability analysis is expected to be automated with requiring fewer user inputs, comprehensive with considering both design and process aspects, and recommendable with offering reasonable solutions and suggestions to aid users in the fabrication. Table 2-2 compares the related studies are compared based on these requirements. Overall, none of the previous studies provided the demanded manufacturability analysis for novice AM users at the design stage. More details are discussed in the following.

Table 2-2: Comparison of the existing computational methods

		Automated	Comprehensive	Only require novice knowledge	Recommended solutions provided
Manufacturable feature recognition	Slicing-based approach [90]	Yes	No	Yes	Yes
	Voxel-based approach [86]	Yes	No	Yes	Yes
	3D feature-based approach [84]	Yes	No	Yes	Yes
Knowledge-based or rule-based approach	Knowledge management system [95, 96]	No	Yes	No	No
	Ontology-based management system [97]	Yes	Limited	No	Yes
ML approach [98-107]		Yes	Limited	Yes	No

2.4.1. Manufacturable feature recognition

Manufacturing feature recognition is the most popular approach to analyzing manufacturability in AM. This approach automates the identification of erroneous features that are under the capability of the selected printer. The general concept of this approach is to discretize the 3D model into 2D/2.5D segments to reduce the difficulty of directly identifying 3D features. The detected features are then evaluated based on the similar criteria listed in the design guidelines (Section 2.3.1). Moreover, depending on the types of input data for feature recognition, prior research can be classified as 3D feature-based approach [83, 84], slicing data-based approach [93, 94], voxel-based approach [85-90], and others [91, 92].

2.4.1.1. Slicing data-based approach

Chen and Xu [93] proposed a layered depth normal images (LDNI)-based offsetting method for computing thin features in sliced data (Figure 2-8). The tunable offset values are consistent with the manufacturing constraints. Nelaturi et al. [88] applied the medial axis theorem (MAT) to identify the thin features in the sliced model. However, MAT has some challenges with computing corners. In addition, it is sensitive to small noises and artifacts, which results in many unknown branches in the skeleton that require more work to remove. Because of these challenges, it requires extra computation, and thickness maps for intricate shapes are difficult to compute. A more recent advance was realized by the same authors [90] by extracting a “meso-skeleton,” which is the maximal area within each slice where a print head can be positioned during the printing process. It is topologically equivalent to the corresponding slice of the input shape. Their approach enables the topologically important area that is smaller than the single deposition path to be thickened. Build orientation is simultaneously optimized to minimize the modification of the original model. The correction of each slice is realized using pixels (Figure 2-9).

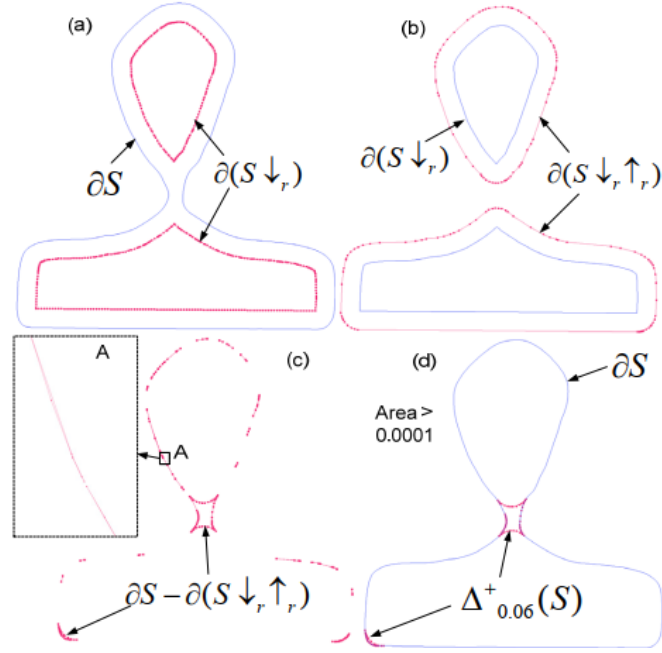


Figure 2-8: Illustration of computing infeasible features using the LDNI-based offsetting algorithm [93]

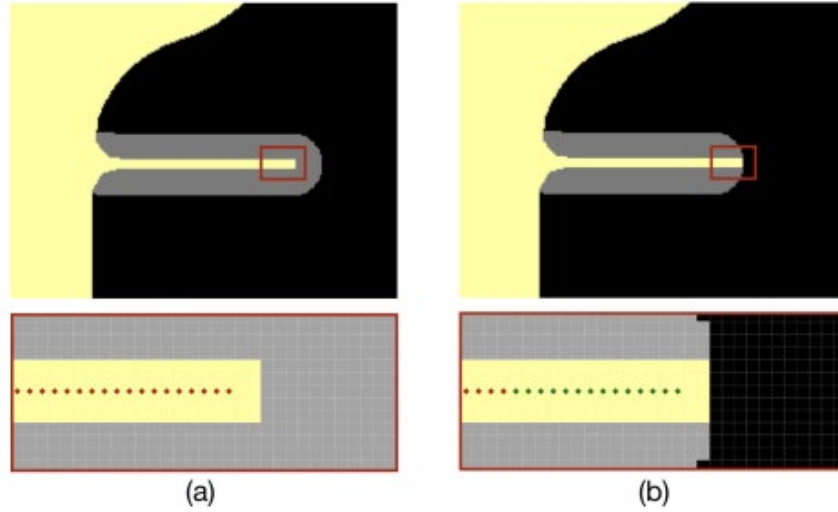


Figure 2-9: (a) For the same slice (yellow), when the skeleton is obtained using the thinning process, the protrusion is elongated in the corrected model (gray). (b) Spur pixel removal achieves the intended length by deleting the end-point pixels (marked green). [90]

2.4.1.2. Voxel-based approach

Tedia [86] proposed an automated manufacturability-analysis tool using voxel-based geometric modeling. The input design, which is a CAD file, is first converted into voxel representation. Thereafter, thin features and undersized negative features are identified. Support material generation, void detection, and build time estimation are also considered. The flowchart of his manufacturability analysis is shown in Figure 2-10. Several case studies have been conducted to validate his work. Results from the support material generation and build time estimation have been compared with commercial software to validate his approach. Although his case study was fabricated through the ME process, which is another type of AM process, the concept is similar in the LPBF process.

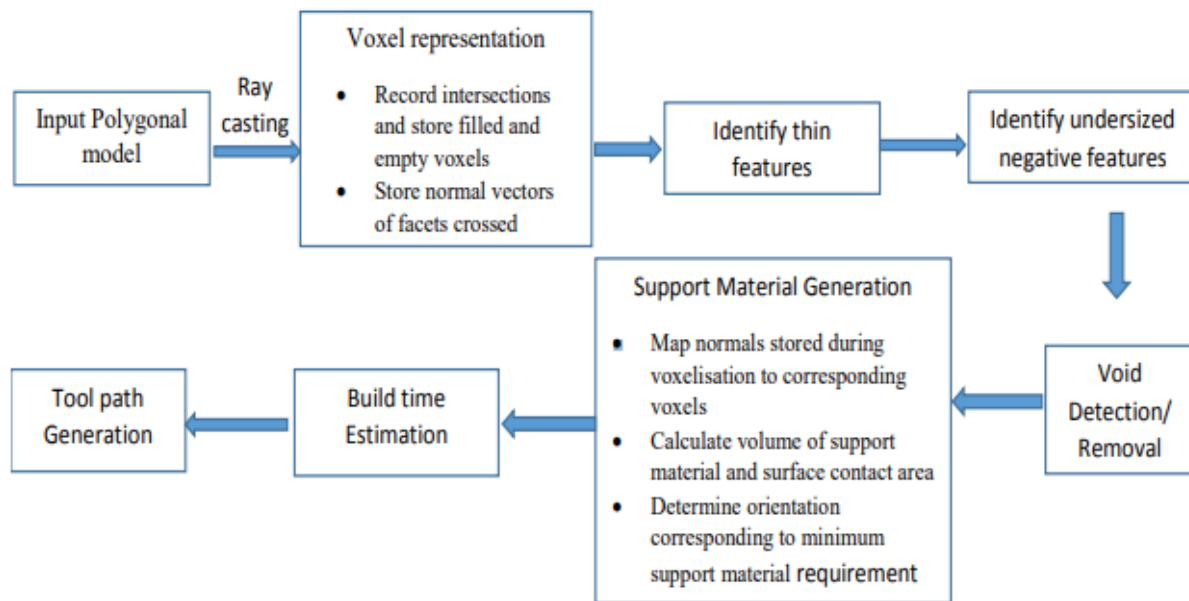


Figure 2-10: Flowchart of the manufacturability analysis tool [86]

A more advanced approach proposed by Kerbrat et al. [85] introduced an octree-based voxelization to decompose a CAD model for hybrid additive and subtractive manufacturing. The

manufacturability index incorporates geometric information (maximum and minimum dimension, geometric accessibility, radii, void volume, etc.), material information (material availability and material properties), and technical specifications (tolerance and surface quality). An example of 2D octree-based voxelization is shown in Figure 2-11. The octants are categorized into three categories: black, white, and grey octants. To construct an octree, the object is first enclosed by the root octant that can completely contain the object in any direction. It is then subdivided into eight sub-octants to obtain the first level of the octree representation. Black octants are those that are completely inside the object. Grey octants depict those that are partially inside and outside the object. White octants are those that are completely outside the object. The subdivision process is performed on grey octants until the desired resolution is achieved. Based on the octree decomposition algorithm, a map of manufacturing complexity is obtained.

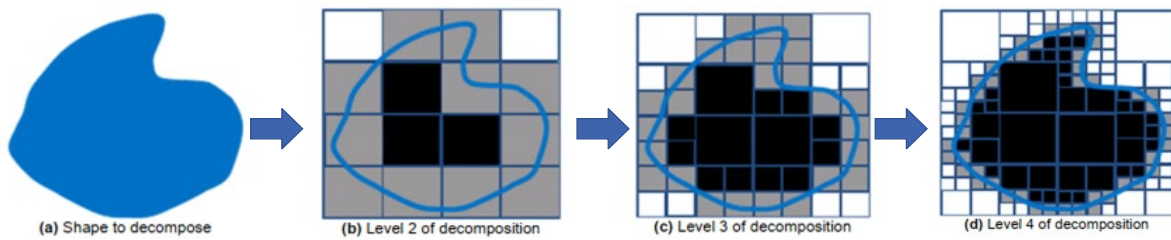


Figure 2-11: Octree-based voxelization [85]

2.4.1.3. Mesh-based approach

Cabiddu and Attene [94] developed a mathematical model called epsilon shapes that can detect and thicken the thin features of both 2D and 3D geometric models. In 2D geometry, the thickness is computed at the local minimum of each vertex using triangulation. In the 3D model, the polygonal model is first meshed using tetrahedrization, and then the local minimum thickness of each vertex is computed to determine global thin features. Generally, the mesh-based approach can be considered as a generalization of the voxel-based approach. A scheme of thickness

computing for a 2D polygon is shown in Figure 2-12. One typical disadvantage of the voxel-based approach is distortion in the voxelization step. In addition, to satisfy the high resolution of industrial printers, a 103 cm cube would require more than a billion voxels.

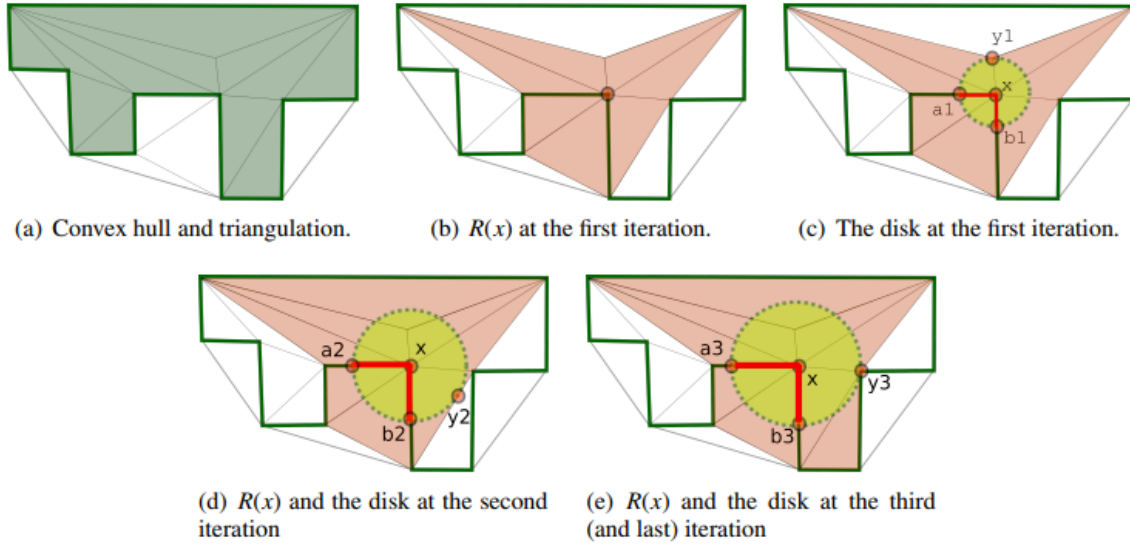


Figure 2-12: Computing E for a single vertex. (a) Input polygon with both the convex hull and the triangulation. (b) $R(x)$ at the first iteration. (c) Disk at the first iteration (d) Disk at the second iteration. (e) Final iteration in this case [94]

2.4.1.4. 3D feature-based approach

Shi et al. [84] first listed infeasible features including unsupported features, minimal features, maximum vertical aspect ratio, minimum clearance, and minimum support-free angle. Heat kernel signature (HKS) is adopted to cluster surfaces based on vertices with triangular meshes as the original input. The basic concept of HKS is to compute the heat losses through time. The heat diffusion rate is considered to be an indicator of topological and geometric entities. The heat diffusion equation is applied to obtain the rate. The rate is represented by the quantity of heat received by a point after a unit. With the heat persistence value and a percentage similarity, the

vertices can be clustered into different sets to predict a mass distribution pattern and prepare the potential shape recognition (Figure 2-13).

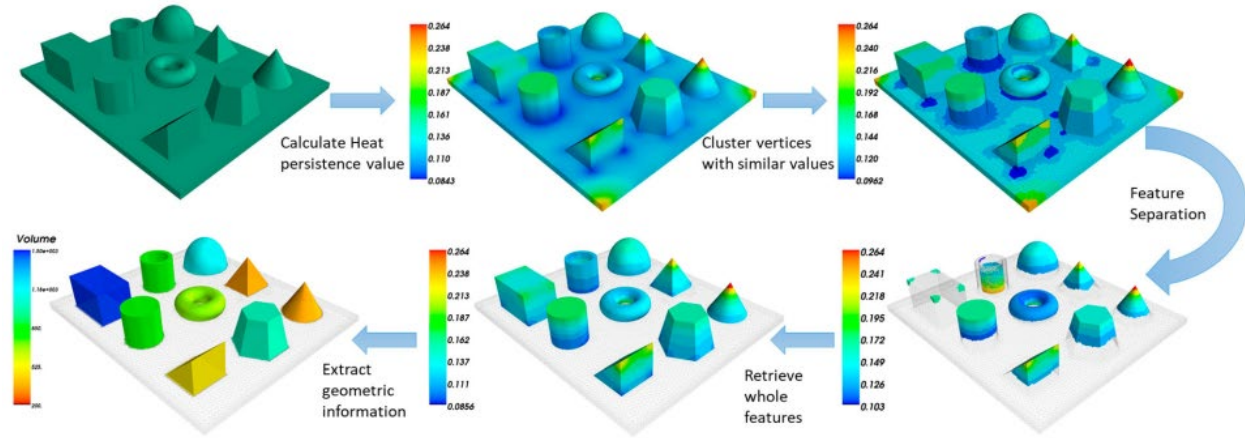


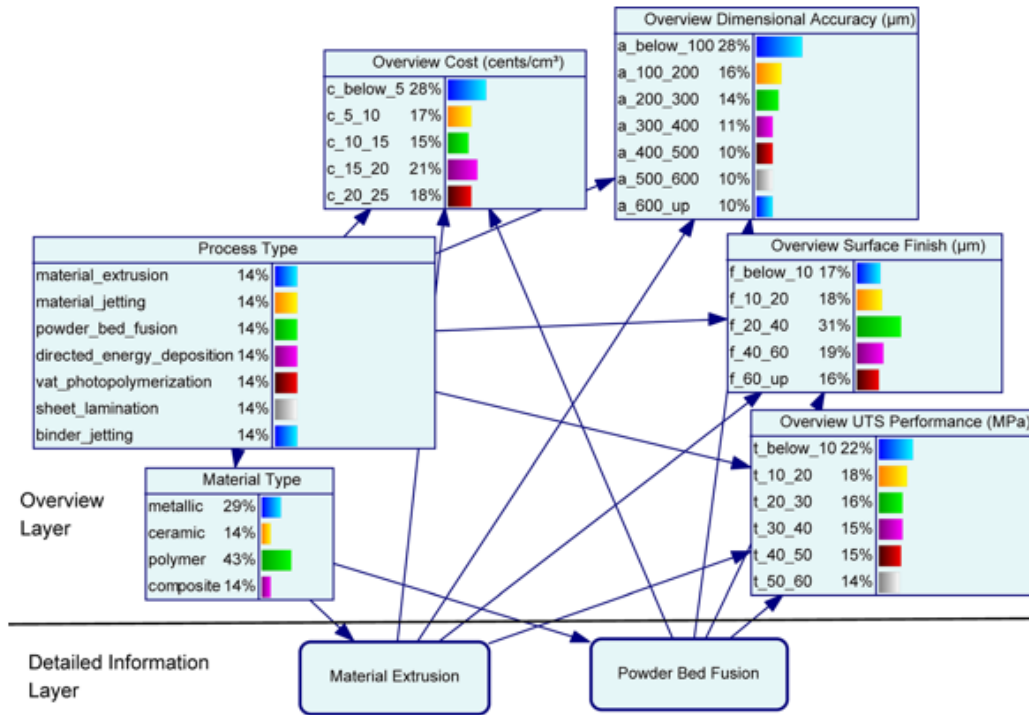
Figure 2-13: Flow of feature recognition using HKS [84]

2.4.2. Knowledge-based or rule-based approach

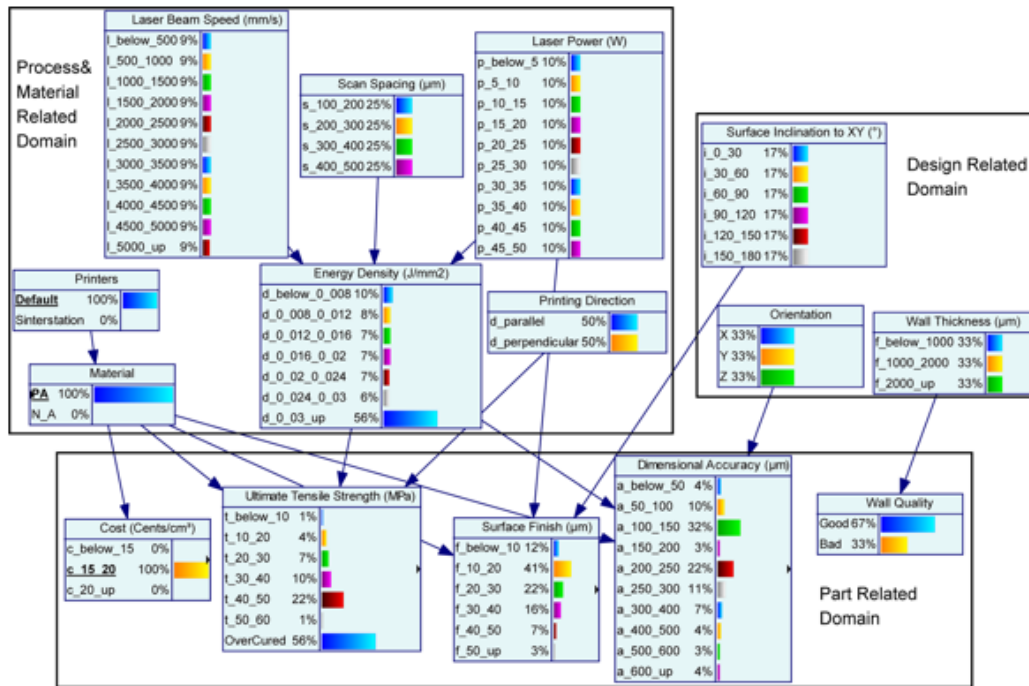
Manufacturing feature recognition primarily considers the effects of the design aspects, but not the process aspects. The performance of the printed part may vary owing to the variation in the machine selections, material selections, and the setting of the process parameters. To fill this gap, researchers such as Hossein et al. [96] integrated the performance of parts and the AM process into a model to predict the performances of the AM parts and improve the design and processes. They proposed the dimensional analysis conceptual modeling (DACM) framework to generate the interrelationship between the performance and process models by producing a set of governing equations.

A similar concept generated by Xu et al. [95] presented a knowledge management system using Bayesian networks. The method was referred to as the Guide-to-Principle-to-Rule approach. The model was set based on AM fundamentals. The structure of the system is presented in Figure

2-14. The knowledge management system was organized into three domains: process, material-related, design-related, and part-related. Each domain was quantified. The manufacturability was modeled numerically from the top level to the detail level. The system can learn conditional probabilities in the model from different sources of information, and inferences can be conducted in both forward and backward directions. Users are expected to use this management system to determine the best AM process that can be used before the actual fabrication. Moreover, the estimated dimensional accuracy, mechanical properties, and surface finish are given in a range. Note that in contrast to other computational approaches that primarily focus on feature recognition, Xu's approach attempts to model the relationships among the process, design, and products. This approach provides a general tool to explore the relationship among the process, design, and product qualities of the AM process, but it was not intended for a precise prediction on the manufacturability of a given design. It offers a well-modeled knowledge management system on the AM process, and it is intuitive for users to understand the manufacturing process. However, when applied to the specific design, uncertainties from different printing strategies and printers are not considered. It can aid the designer in understanding the AM process better, but users still require some knowledge to decide on whether their designs are manufacturable.



(a)



(b)

Figure 2-14: Structure of the knowledge management system: (a) overall structure, (b) submodel for

LPBF [95]

A more recent and comprehensive method proposed by Kim et al. [97] offers an ontology-based knowledge management system. The rules are developed to recognize manufacturable features and analyze manufacturability. Moreover, their approach offers redesign suggestions to designers to improve the printing success rate. However, their approach requires designers to understand the information structure of the ontology and lacks the support of machine and material selections.

2.4.3. Machine learning approach

Recently, the ML approach has been a new trend for solving industrial problems [130]. Studies in design and manufacturing are also attempting to utilize the benefits of ML [131, 132]. Several novel computational methods that apply ML to predict the manufacturability of the given design through AM process have been proposed. Such applications include the prediction of visual defects, surface roughness, microstructure, and machining features [98, 99]. The current approaches to applying ML in AM manufacturability analysis can be categorized into two major categories: real-time detection and analysis at the design stage.

Real-time detection has two main approaches. The first one is to use layer-wise images from the in-situ sensor as input features to predict the defects. The prediction of the defects can be an image or a simple yes or no value. Representative studies include those on detecting flaws [100] and porosity defects [101] during the LPBF process, detecting warping [133] during the FDM process, and a quality control study by Liu et al. [102]. The second approach is to use the process information such as temperature, layer thickness, and scanning speed as the inputs to predict some characteristics such as roughness, tolerance, and printability. Such studies include the research proposed by Li et al. [103] to predict surface roughness with a set of input features in time and frequency domain, and a similar approach by Cerda-Avila et al. [104] to predict the structural

performance with the input features such as layer thickness, infill pattern, and build orientation. However, as mentioned in Section 2.3.2, the real-time detection approach cannot determine the manufacturability at the design stage. It is not applicable if printing failure occurs due to geometric design instead of the printing process or machine.

The analysis at the design stage has two main approaches. The first is the use of 3D models as inputs to predict a single value such as printability, which is a yes or no question. The most common method is voxelization. For instance, Guo et al. [105] proposed a deep-learning-based framework for assessing the manufacturability of cellular structures in the LPBF process (Figure 2-15). The voxelization of the design model was used as the input to predict manufacturability. An auto encoder-generative adversarial network was developed as the classification model. The results demonstrated the capability of the model for manufacturability analysis even with a small amount of data. A similar concept was conducted by Mycroft et al. [106]. Their study proposed a predictive model that could estimate the printability of a given artifact before the actual fabrication is conducted. A voxel map was used as one of the geometrical descriptors.

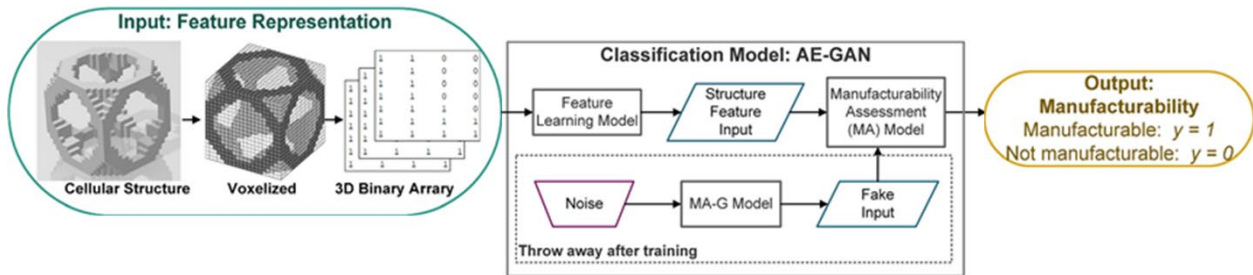


Figure 2-15: ML-assisted manufacturability analysis by Guo et al. [105]

The second approach is to analyze the critical feature parameters of the design model (e.g., lattice type, strut diameters for the lattice structure) to predict the single values such as printability, ultimate strength, and elastic modulus. Representative research includes the study by Hassanin et

al. [107]. In their study, the strut length, strut diameter, and strut orientation angle were selected as the input features to the ML model to predict the properties of the printed cellular structures. A deep neural network was developed, and their results outperformed the statistical design of the experimental approach.

In summary, most studies on manufacturability analysis in the ML approach fall into real-time detection. Some ML approaches assist manufacturability analysis at the design stage. However, none of them provide suggestions and recommendations to designers on the changes they can implement to make the design printable. Moreover, none of them provide a comprehensive analysis with the consideration of both design and process aspects.

2.4.4. Tested commercial software

While preprocess software exists, such as Magics, Netfab, and online 3D printing service providers such as Sculpteo, Shapeways, 3D hub, and 3DXpert, they are focused on examining the validity of STL files and reparation of meshes and offering the functionality of slicing, toolpath planning, infill pattern, Boolean operations, and support structure generation. More recently, some software provide options for optimizing the build orientation and the support for a part. Some of them offer the function of recognizing and examining small features that are under the resolution threshold, such as thin walls; however, they are specific for a type of printer, and other types of difficult-to-manufacture features are not included as void and minimum clearance.

2.5. Comparison of manufacturability analysis between SM and AM

For the manufacturability analysis in the SM process, the approaches are summarized into two categories: feature- and feature-less-based approaches. The geometric algorithms are similar in both approaches and are slice-based, volume-based, or hint-based. The difference is that, for the

feature-based approach, the focus is on identifying the machining features such as holes, extrusion, and planes. For the feature-less-based approach, the major investigation is to evaluate the four machining characteristics, which are visibility, reachability, accessibility, and setup complexity, directly on the geometries; thus, there are no feature extractions. The manufacturability analysis of the AM process primarily focuses on the feature-based approach. Very few studies have been conducted on the feature-less approach. The geometric algorithms for analyzing the shape are similar to the SM process; however, the target features in the AM process are different from the features in the SM process. The AM process focuses on features such as minimum thickness and overhang. In addition, it has no defined manufacturing characteristics such as in the SM process. The manufacturability analysis is based on the constraints on these target features. For instance, the minimum gap thickness for LPBF is 0.3 mm, and the minimum wall thickness is $0.4 \text{ mm} \pm 0.02$ [8]. Moreover, the SM process removes the volume from the raw materials; hence, the quality of the same machining process should be nearly the same. However, for the AM process, the printing quality with different selections of the AM machines might differ. It states that, when considering the manufacturability of the AM process, in addition to the geometries of the design, the process settings and material selections should be considered. To comprehensively model the manufacturability model of AM with the coupled relationships among process, material, design, and final product qualities, this thesis introduces the ML approach to solve the challenges.

2.6. Fundamentals of ML

ML systems automatically learn trends from data that enable them to make generalizations about instances they have not encountered before. ML lies at the intersection of computer science and statistics and has been applied to a wide variety of problems in which human intuition is insufficient. Supervised, unsupervised, and reinforcement learning are three major categories in

ML studies [36, 134]. This thesis focuses on supervised learning. Supervised learning uses labeled input data and creates a model to generalize on unlabeled data of the same format. Supervised learning can also be further categorized into regression and classification problems. Regression means that the output of the model will be continuous values. An example of a “real-time” regression problem is predicting the stock price. With the historic pricing data, the developed regression model can predict the price of the stock in the near future. Statistical classification is the most mature and widespread application of ML. Classifiers typically input a vector of feature values and assign them to a discrete class. This is often accomplished using decision boundaries to divide the input/feature space into regions, each representing a class, and observing where new data lies. A typical classification problem is to recognize spam emails. By learning the characteristics of what forms spam email, the classifier can be used to filter new incoming emails. In this paper, manufacturability analysis is considered a classification problem to determine whether the entire part or each voxel of the part can be fabricated.

Many ML algorithms have been investigated in the literature [36, 134]. The most common algorithms are decision trees, support vector machines, naïve Bayes, random forests, neural networks (NNs), etc. NNs, including classic feedforward neural network (FNN), and convolutional neural network (CNN), are the main algorithms applied in this thesis. The FNN is fully investigated because of two main reasons. First, the FNN does not require any restrictions on the input data. It does not have any assumption on the inputs or inputs distribution, and suitability for any case. Second, the FNN has a good capability to learn and model nonlinear and complex relationships between inputs and outputs, which suits the research objective very well. The universal theorem states that a single hidden layer neural network with a linear output unit can approximate any continuous function arbitrarily well when given sufficient hidden units [134]. Moreover, the FNN

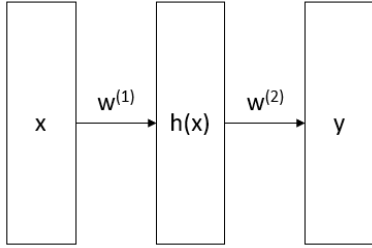
can approximate any continuous function, but this does not mean there is a learning algorithm that can determine the necessary parameter values. The learning algorithm may never reach the correct parameters. Moreover, the number of hidden units required increases exponentially as the complexity of the problem increases. Thus, FNN can be very time-consuming. However, owing to its capability to learn complex models, it is still considered a very effective algorithm, and many types of research have been conducted to improve its capability and reduce its computation cost. The concept of the FNN is defined as follows:

$$a(x) = w^{(1)}x + b \quad \text{Eq. 2-1}$$

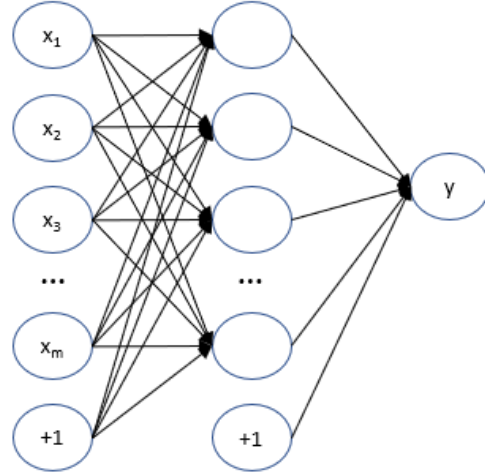
$$h(x) = g(a(x)) \quad \text{Eq. 2-2}$$

$$y = f(x) = O(w^{(2)}h(x) + b^{(2)}) \quad \text{Eq. 2-3}$$

where x is the input feature, $w^{(1)}$, $w^{(2)}$, $b^{(1)}$, and $b^{(2)}$ are the FNN parameters, $a(x)$ is the hidden-layer pre-activation function, $h(x)$ is the hidden-layer activation, $g()$ is the hidden-layer activation function, $O()$ is the output activation function, and y is the output. The graphical representation is shown in Figure 2-16.



(a) General representation of the FNN



(b) Detail representation of the FNN

Figure 2-16: Graphical representation of the FNN

Note that, here x , $h(x)$, and y are the general representation of the input, hidden, and output layers, respectively. For the detailed representation, each layer consists of several neurons. The number of input features defines the size of x , and $+1$ indicates the bias for the current layer. The number of hidden layers, number of neurons, and function of g and O are the hyperparameters in the FNN. These hyperparameters should be tuned and tested to determine the best model performance. The hidden layer activation function $g(\cdot)$ should include some nonlinear activation functions such as tanh, sigmoid, and rectified linear unit (ReLU) to enable the entire process to model a nonlinear relationship. The sigmoid and tanh activation functions are the most common activation functions for the hidden layers, and they were selected for this research. For the output layer, the activation function $O(\cdot)$ can be set based on the objective of the model. An identity function can be used for the regression problem. A sigmoid function can be selected for a two-class classification problem, and a SoftMax function can be used for a multi-class classification problem.

The objective of training an FNN model is to determine all the corresponding coefficients, w , and b , to minimize the loss function, which varies among models. The loss function is computed as the difference between the prediction and ground truth:

$$E = \frac{1}{2} \sum_{i=1}^P \|y_i - t_i\|^2 \quad \text{Eq. 2-4}$$

where y_i is the output of the network for the i -th input, t_i is the actual output, and P is the number of examples. The selection of the loss function depends on the objective of the model. Popular loss functions include hinge loss, binary cross-entropy, mean absolute error, and categorical cross-entropy. The loss function can also be self-defined. To attain the minimum of the error function, several learning algorithms are detailed in the literature, such as stochastic gradient descent and quasi-Newton methods [134]. The process of minimizing the loss cost in the model's prediction and computing all the corresponding coefficients is called backpropagation [135].

Since the neurons for every layer in the FNN are fully connected, which produces numerous coefficients, the FNN can be very time-consuming for a complicated problem, particularly for multi-dimensional inputs such as images or 3D objects. CNN is frequently used to address such challenges. In the convolutional layers, a set of “filters” are applied to a subset of the input variables at a time and swept over the entire input; therefore, only nearby inputs are connected, which results in significantly fewer weights than in the fully connected layer. The convolution operation calculates the sum of the element-wise multiplication between the input matrix and filter matrix; thus, it performs a many-to-one relationship. Figure 2-17 shows an example of convolutions: If the input is an 8×8 matrix and the filter is a 2×2 matrix, The stride for the filter map is 2, which results in a 4×4 output matrix. Similar to the fully connected layer, the learning process will propagate forward and back to update the weight matrix in every epoch to

minimize the loss function. The operation is still linear; therefore, the activation function will also be applied in most cases.

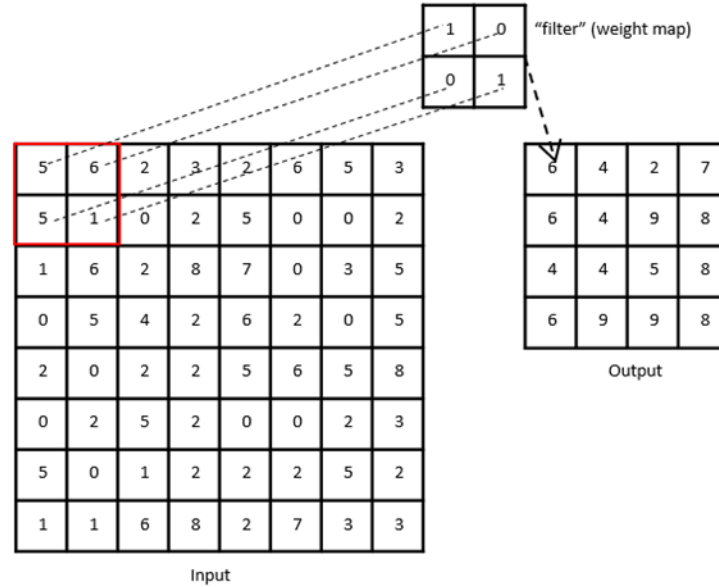


Figure 2-17: Graphical representation of convolutions

When considering the AM process, the manufacturability of one point is related to the surrounding points in the current and previous layers. The manufacturability of a certain point is related to surrounding points but only slightly for the further points. Thus, it is reasonable to apply CNNs in the manufacturability analysis.

Other key ML operations include transpose convolution, pooling, and dropout. Transpose convolution is the opposite of the convolutional operation, and it is also popularly known as deconvolution [136, 137]. It operates in the backward direction of the convolution and performs a one-to-many relationship. For the convolutional operation, the output is always downsizing, but for the transpose convolution, a higher resolution output will be ultimately obtained. Pooling is the operation of downsampling the input variables by summarizing the presence of features in each patch [138, 139]. There are two common types of pooling operations. One is average pooling,

which summarizes the average presence of the patch. The other is the max pooling, which utilizes the most activated presence of the input patch. Dropout is an efficient method of preventing overfitting in the ML [140]. It refers to dropping a certain percentage of the neurons in the FNN.

2.7. Chapter summary

This chapter reviews the background and existing studies related to the research objectives. Major effects on evaluating the manufacturability of AM and the previous manufacturability studies have been reviewed and discussed. The manufacturability of SM is also summarized to compare with the manufacturability studies in AM. ML is the methodology selected to solve the remaining problems. The fundamentals of ML have been depicted in this chapter.

After reviewing previous studies, the major challenges are listed here:

1. No proper or clear definition of the manufacturability of the AM process exists.
The manufacturability of the AM must be defined and quantified first.
2. No suitable model exists to comprehensively represent manufacturability that considers design features, process parameters, machine, and material selections, and end part qualities at the design stage.
3. The major approach for the computational method offers a simple geometry check for the design. It provides the recommended orientation and support structure for the current design. However, in addition to the thin features and overhangs, it lacks the ability to suggest to the designer whether their design features are manufacturable. Moreover, it lacks the recommendation on the process aspects.

Chapter 3. Definition of manufacturability of AM and the methodological framework for a manufacturability analyzer and recommender

The comprehensive reviews in Chapter 2 indicate that the definition of the manufacturability of AM is still unclear. The definition should be first identified before the investigation. Another challenge is quantifying manufacturability. Therefore, in Sections 3.1 and 3.2, the new definition of the manufacturability of AM and manufacturability levels are introduced to clarify the statement. The review in Chapter 2 also highlights the need for manufacturability analysis research that considers both design and process aspects. Most previous studies considered only a single aspect, either design or process. Moreover, providing only the prediction of the manufacturability is insufficient for novice AM users. Recommendations and suggestions should be provided to increase the printing success rate. To fill these gaps, Section 3.3 proposes a methodological framework, providing a structure for the manufacturability analyzer and recommender for AM (MAR-AM). Thereafter, Section 3.4 discusses research assumptions and lays out the research focus. Finally, the chapter is summarized.

3.1. New definition of the manufacturability of AM

As mentioned in Chapter 1, the definition of the manufacturability of the AM process is vague. Depending on different applications, the required quality of the printed parts typically varies. From Chapter 2, it is clear that manufacturability must consider the effects from each stage of the general AM workflow including design, fabrication, and post-processing. For post-processing, whether the fabricated parts can bear the force from the post-processing can also be a challenge. The printed parts can be fractured during post-processing. In the fabrication process, stability could be a critical problem during the printing process. Even after the part is successfully

built, whether it satisfies the product's requirement can be another problem. Therefore, no general definition of the manufacturability of AM has existed. However, a proper definition of AM manufacturability was a necessary first step in this research. Without it, setting the research scope would be difficult. At the design stage, manufacturability has a clearer definition, referring to the design characteristics that indicate the difficulty or ease of the design from a manufacturing perspective [141]. When considering the design process, Figure 3-1 shows the role of manufacturability analysis in the design process. Engineering analysis involves determining whether the current design and materials can satisfy performance requirements. Manufacturability analysis ensures that the part can be properly fabricated based on identified design, materials, and manufacturing processes. The focus of manufacturability analysis is to determine whether the specific design with the defined material can be fabricated in the desired shape using a selected machine with the fixed process parameters. In the literature, common physical AM features reported are dimensions, porosity, and density [142]. Cracks and pores are some of the terms frequently used to determine the behaviour of the products [142, 143]. Generally, materials with a lower amount of cracks and pores have higher tensile strength, Young's modulus, strain-to-failure, and fatigue strength [144]. Generally, if the product is a fully dense metal part, it is defined as a qualified part for functionality in the manufacturability analysis. Hence, this thesis defines the manufacturability of the AM at the design stage to consist two aspects:

- **Geometric inconsistency** between the design model and the built model, which includes shape and dimensional error; whether the geometric features of the design can be built.
- **Functional inconsistency** between the design model and the built model, which includes the manufacturing defects and heterogeneity in properties; whether the quantity of part density satisfies the standard.

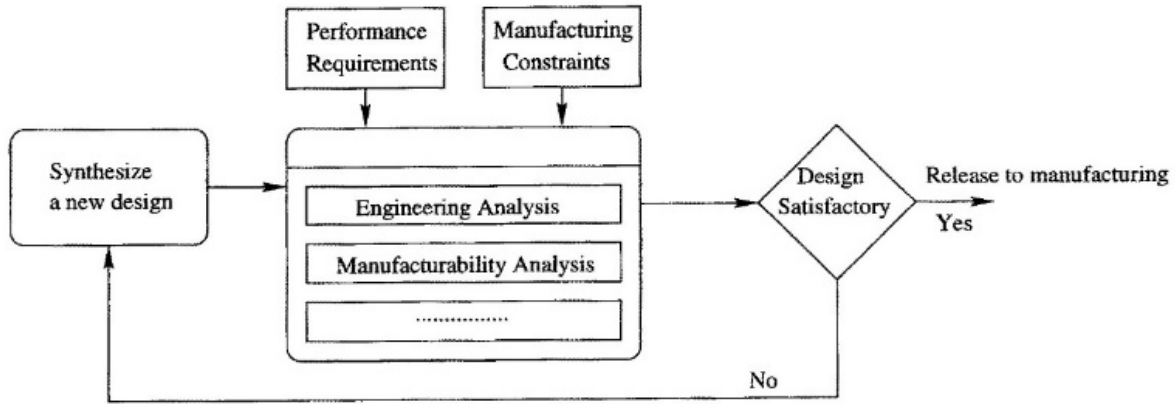


Figure 3-1: Manufacturability analysis in the design process [145]

This definition can be used to guide future research on the manufacturability of the AM process. The fabricated part that satisfies both defined aspects is considered to be manufacturable. In this thesis, AM manufacturability is further elaborated to consist of three levels.

3.2. Proposed manufacturability levels

Based on the definition of AM manufacturability that consists of two aspects, three manufacturability levels are proposed as follows:

Manufacturability Level 1: The printed part should be free of visual defects such as geometric incompleteness and warping (Figure 3-2).

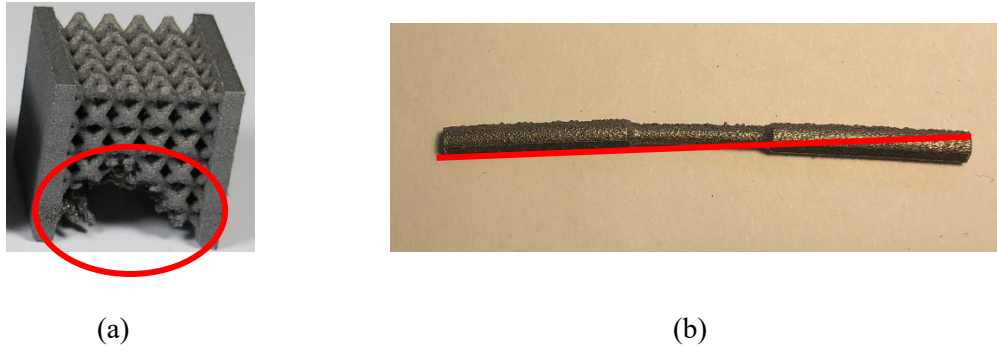
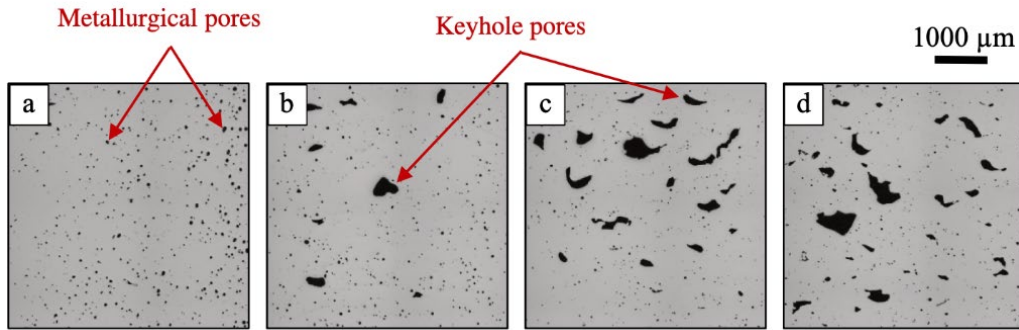
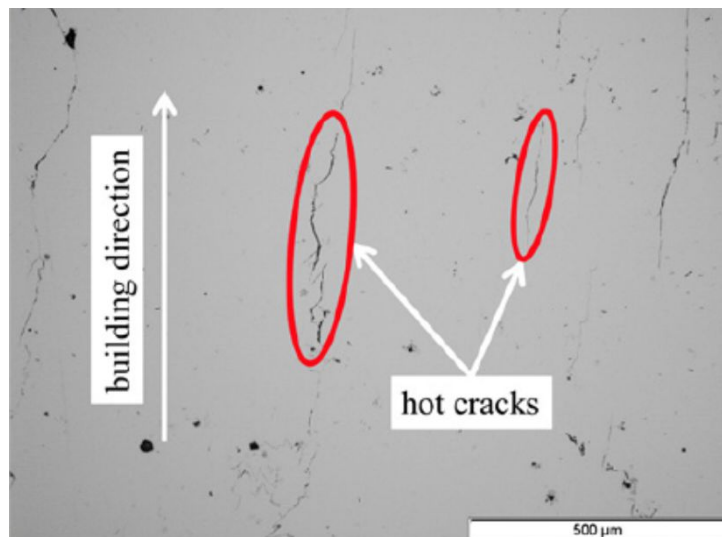


Figure 3-2: Example of (a) geometric incompleteness and (b) warping

Manufacturability Level 2: At the second level, the printed part should first satisfy all the requirements from Level 1. Subsequently, the part should be ensured to be a dense part. The quantity of the density and porosity and cracks should be obtained at this level. Chee et al. [142] explained the details of the metrology measurement methods on measuring these characteristics. The printed part is considered to achieve Level 2 when it satisfies the requirements of the quantity of the density and porosity and cracks (Figure 3-3). Note that not all AM techniques must consider level 2 depending on the process techniques. As the LPBF process uses either a laser or electron beam to melt and fuse the material powder, it is important to ensure the quality of the melting and fusing process. The density of the part is utilized to measure the quality of the fabrication process. However, for the FDM process, whether the density of the part is not critical as the filament material is extruded by the nozzle and bonded together owing to the stickiness of the melted material. In addition, FDM has the option to select different infill percentages. To decrease the printing time and save the material cost, the default setting from the printer makers is 20%. As FDM is always used to print non-functional prototypes or non-functional end-products, it is acceptable to have partially infilled printed parts. As the consequence, FDM products are considered to skip Level 2 in the manufacturability analysis.



(a)



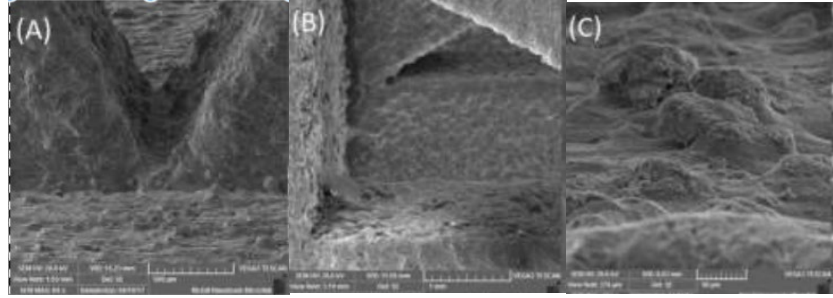
(b)

Figure 3-3: Example of (a) pores and (b) cracks [146]

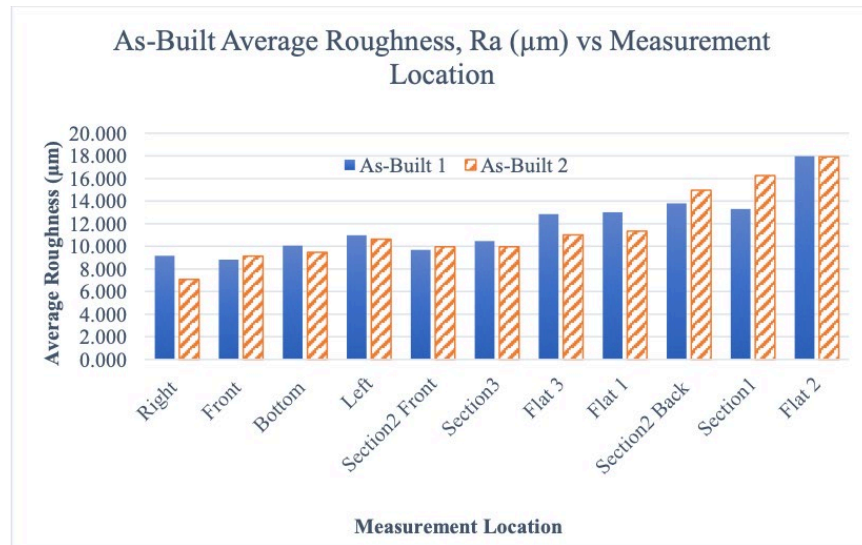
Note that for LPBF, which is a powder-based process, the produced parts have a lower density than the parts produced using SM from bulk materials owing to pores within the parts. Therefore, a 100% relative density is not expected for the LPBF parts [147]. Most recent studies demonstrated that the average relative density of the parts fabricated via LPBF processes can reach above 98% [147]. For some certain materials and machines, it can even be above 99.5% [147-149]. For the manufacturability analysis at the design stage, the relative density is expected to reach the

average of the literature records, which is currently above 98.5%. This value can be adjusted according to the different materials and mature levels of the current LPBF systems.

Manufacturability Level 3: At this level, the printed part should first satisfy all the requirements from Levels 1 and 2. Subsequently, it is compared with the original design to calculate the dimensional error. The printed part is evaluated based on the customer requirements to determine whether it satisfies Level 3. The requirement can be specified on certain dimensions such as hole tolerance, roughness, straightness, and side dimension. Figure 3-4 shows examples of scanning electron microscopy (SEM) results and a table that lists the measured roughness at selected points [150]. Another requirement can be the overall dimensional error. It can be calculated by comparing the dimensional profile of the printed part to the design file.



(a)



(b)

Figure 3-4: Example of (a) SEM images and (b) roughness analysis for printed parts [150]

Finally, the printed part can be defined as manufacturable through the AM process when it satisfies all the requirements of Level 3. The manufacturability analysis can be separated into stages based on the manufacturability levels to achieve the objective step by step. This thesis proposes and develops manufacturability analysis methods for Manufacturability Level 1.

3.3. Proposed methodological framework

To achieve the research objective, this section proposes the ML-assisted manufacturability analysis and recommendation (MAR-AM) system is proposed. As introduced in the previous section, Manufacturability Level 1 ensures that the printed part is free of visual defects. Figure 3-5 shows the overall framework of MAR-AM, which comprises three main parts: (1) dataset establishment, (2) ML model training, and (3) manufacturability prediction and suggestion.

For dataset establishment, this research gathered and generated training data for the developed ML models. The training data were collected from three sources. The first one was experimental data collected from experiments, research labs, and collaborative industry. The second source was the literature review. Based on the existing experiments published in the articles or data port, data was extracted in the desired input format to train the ML model. After the entire predictive system is released to the public, any user with access to the entire predictive system can provide new data to train the ML model continuously as the third source of the database and improve its accuracy. The collected data will be sent to either ML model training or manufacturability prediction and suggestion depending on whether it is labeled. More details on dataset establishment are provided in Chapter 4.

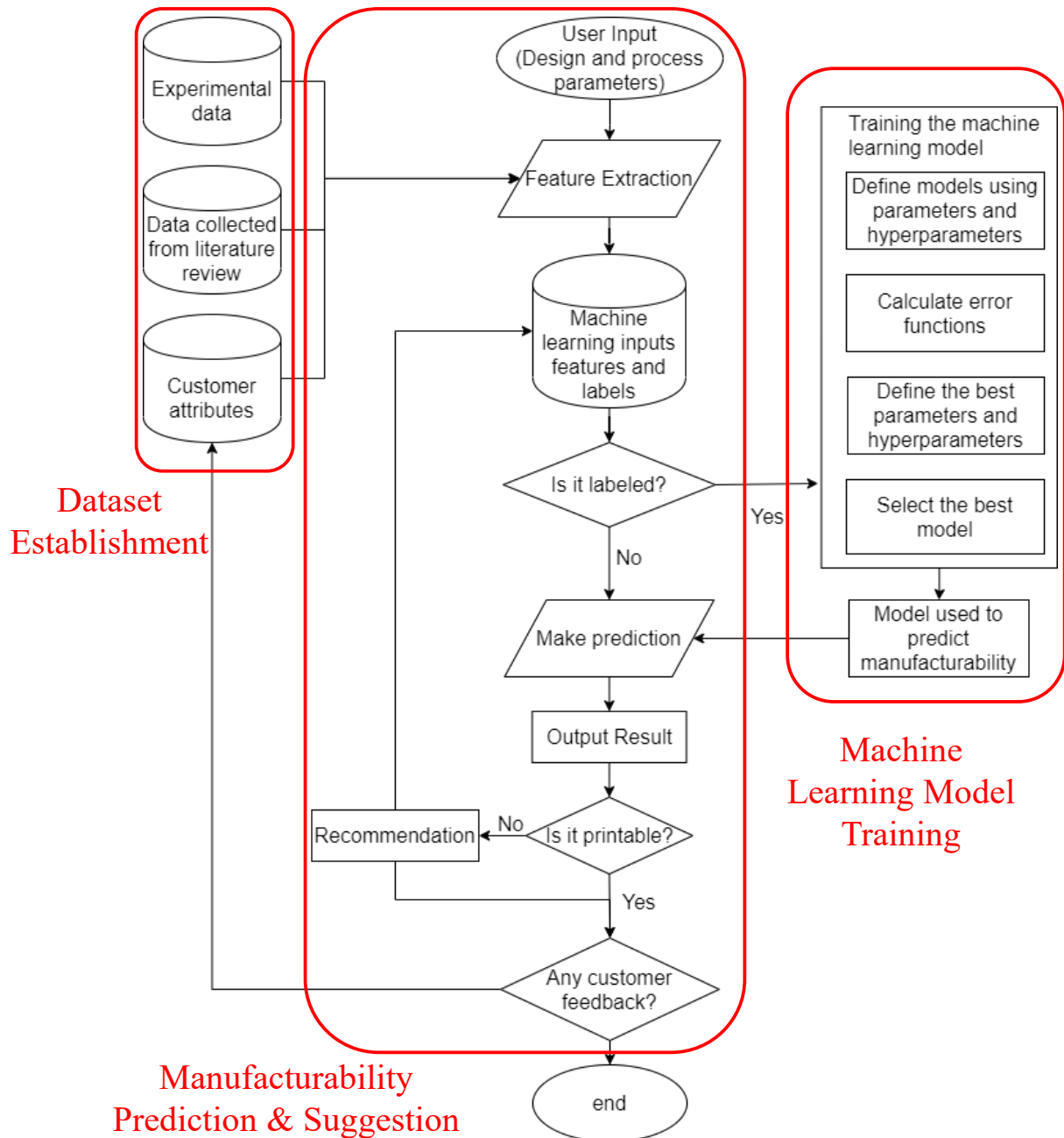


Figure 3-5: Overall framework of MAR-AM

For ML model training, this research developed a general, efficient, and effective ML model to predict visual defects. The first step is the preprocessing of the data to extract the demanded features. In the preprocessing, both the design file and process information are

converted into the required input variables to be trained for the ML model. Additionally, the ground truths of the targets to be predicted are labeled in the required format in this step. The input variables and labels are directed into the ML model to develop the predictive model of visual defects. The architecture of the ML model involves identifying the learning algorithms and all the hyperparameters associated with the selected algorithms. The loss functions are optimized to tune the model to identify the ideal parameters and hyperparameters based on the selected algorithm. Finally, the models are compared with different learning algorithms and parameters, and the best model is selected as the predictive model for the manufacturability analysis. More details are provided in Chapter 5.

For manufacturability prediction and suggestion, the prediction is given based on the trained and well-defined ML model. When a new unidentified instance is incoming, the prediction is made to determine whether the given design is printable. If it is not printable, the file will be sent to the recommendation system. With a closed-loop process, suggestions on process parameters or designs are offered. Furthermore, users are invited to provide feedback on the prediction, which will be sent to our database to update the ML model. Finally, the entire MAR-AM was implemented into a web application. More details can be observed in Chapter 6 and Chapter 7.

3.4. Basic research assumptions and research focus

The proposed framework provides a general approach to modeling the manufacturability of AM and offers a platform to assist novice AM users to evaluate the manufacturability of their designs with the selected manufacturing process at the design stage. The following are the research assumptions to set the research scope and clarify the research objectives.

- The selected commercial AM printers are considered to be reliable and reproducible. The variations and uncertainties during the printing process are not considered at the design stage.
- The humidity and room temperature might affect the printing process. However, these special cases are not considered.
- For the FDM process, we focus only on the most common polymers, and for the LPBF process, we focus only on the most common metals. Other potential materials or process variations are not considered in this thesis.

Moreover, as mentioned in previous chapters, this thesis focuses on FDM and LPBF processes, and Manufacturability level 1 is the main consideration. More specifically in the research objectives, the following challenges are addressed in the remainder of the thesis:

- Create a database for AM to properly manage all the collected data. It should be easy to use in the developed ML models.
- Develop a general, efficient, and effective ML model **at the design stage** to analyze **Manufacturability Level 1** of the given designs through the LPBF or FDM process.
- Develop a recommendation system to assist novice AM users in increasing the printing success rate.

3.5. Chapter summary

In this chapter, a clear definition of the manufacturability of AM is provided as well as three manufacturability levels. This thesis focuses on Manufacturability Level 1, which is free of visual defects. Based on that, the framework of the MAR-AM, which provides an overview of the developed system, is introduced. This analyzing and recommendation system is expected to predict

the manufacturability of a given design with the selected process settings. Moreover, based on the prediction, MAR-AM is proposed to provide recommendations to users to increase the printing success rate. Finally, the research assumptions and research focuses are summarized to focus the research scope on several more specific research questions, which result in the remaining contents of this thesis.

Chapter 4. Establishment of AM datasets for manufacturability analysis

The dataset is an extremely important aspect of ML research. The quality and quantity of the dataset can directly affect the performance of ML models. ML models can be only as good as the quality of the datasets. High-quality training datasets with labels for supervised and semi-supervised learning are considerably difficult and expensive to produce. Most existing well-developed datasets are for decision making, vision recognition or detection, and biological data. No well-defined AM data exists, and data sharing is extremely limited in AM domains. Section 4.1 introduces how data for ML models were collected in this research. The AM database management system for these collected data is established in Section 4.2 to better organize them. To increase data sharing and data access, Section 4.3 provides an AM port, followed by a summary.




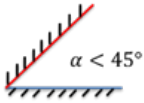
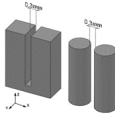
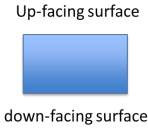
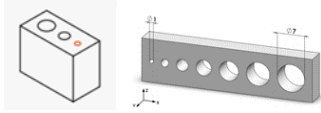
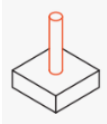



4.1. Data acquisition

For the training of the ML model, the data was sought to be established with the consideration of high accuracy, reliability, consistency, completeness, and diversity. The data in this research was proposed to be obtained from three main resources: reported literature, experiments, and user contribution. For the current database, data was primarily obtained from experiments and contributions from academic collaboration. As introduced earlier, FDM and LPBF were the two focuses of this research. The following sections will depict the details on data collection for each AM process.

4.1.1. Design of experiments

Based on the literature, the most critical geometric features are listed in Table 4-1. These features must be included in the dataset. Various designs with various critical features must be collected in the developed database.

Table 4-1: Most critical geometric features in AM

Category	Graphical illustration	Category	Graphical illustration
Wall thickness		Overhangs	
Minimum features		Angled surface	
Clearances		Down and up faces	
Holes		Islands	
Extreme points		Corners	
Chamfers & fillets			

With the consideration of all the critical features, benchmarks were first selected. Some examples are shown in Figure 4-1. They include complex benchmarks such as in Figure 4-1a and multiple simple benchmarks such as in Figure 4-1b.

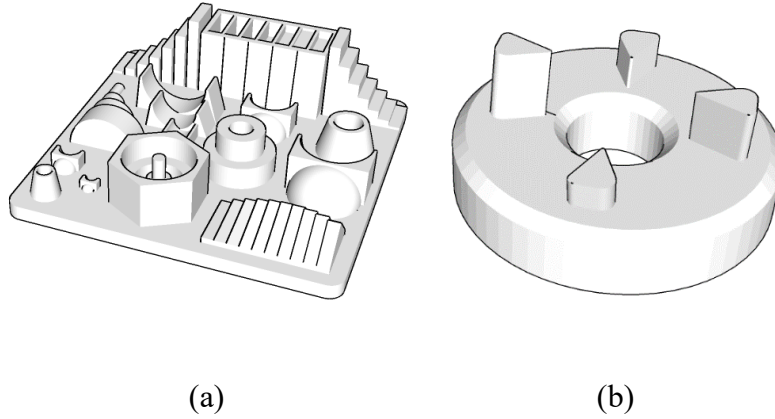


Figure 4-1: Example benchmarks

Including only benchmarks with single geometric features is insufficient. Therefore, more complex geometries with multiple critical features were also selected. The designs were selected from personal design and the open-source repository, Thingi10K, which is a dataset of 3D-printing models [151]. The designs were filtered to have high genus numbers. The genus of a part indicates the number of holes. For instance, a sphere has a genus number as 0, and a torus has a genus number as 1. They were selected because these parts are more suitable for AM process compared with the traditional manufacturing process. In addition to the part with high genus numbers, some customized mechanical parts and model figures portraying humans or other living creatures were also printed as they are the most popular applications in AM prints. Example designs are shown in Figure 4-2. A total of 133 designs were used. All the designs are ensured to be dissimilar to each other in order to increase the variation. Even for the same category, the designs are ensured to have enough variations between each other.

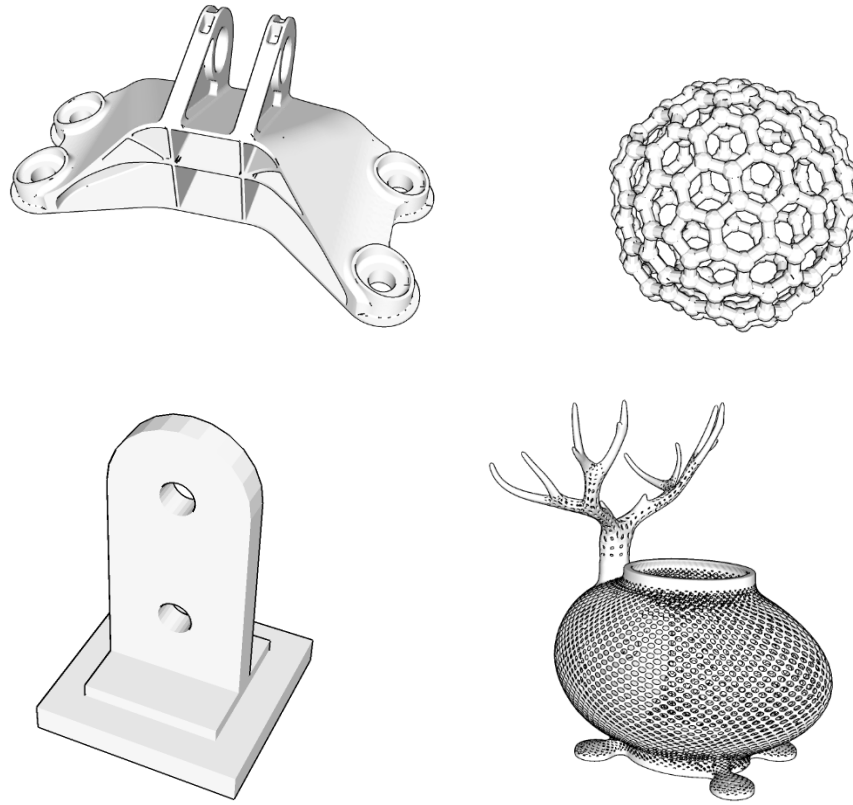


Figure 4-2: Example designs in the database

In addition to the design variations, various process settings were expected to be collected as well. As the starting point, only the most critical process parameters were varied and collected. Different materials were also used. Note that the Taguchi method was not used as a design of experiments method. The Taguchi method assumes that the individual or main effects of the independent variables on performance parameters are separable. Under this assumption, the model assumes that there are no cross-product effects among the individual factors. However, the process parameters in AM are correlated, thus breaking the assumption of the Taguchi method. Therefore, the data was expected to be collected with all the possible variations.

4.1.2. FDM setup

For FDM, Ultimaker 3 (Figure 4-3) was used to print the selected designs with various process settings and materials. Before the fabrication, selected designs were planned for printing with different build orientations, materials such as PLA, ABS, nylon, and PC, and machine settings such as layer thickness, printing speed, adhesion selection, nozzle temperature, and bed temperature. These parameters were selected according to the literature review in Chapter 2 and the ease of the control. Those parameters are shown in their slicing software as default settings and users can easily control those parameters.

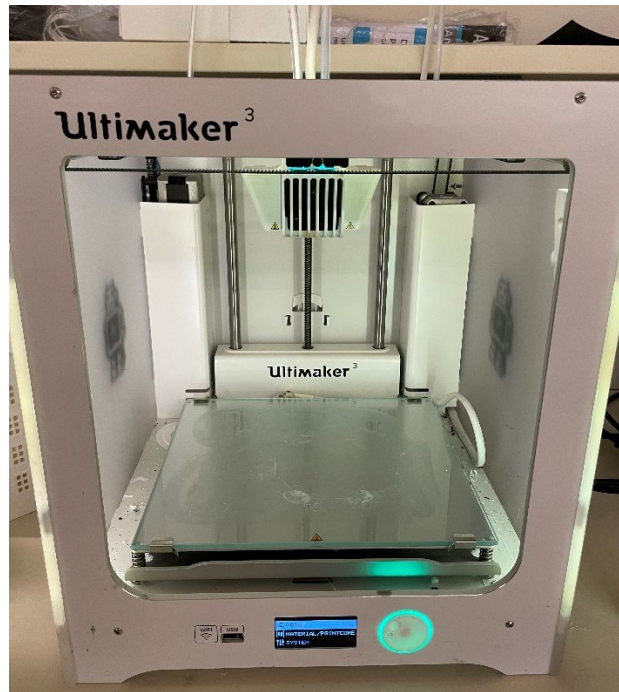


Figure 4-3: Photograph of Ultimaker3 in the laboratory

After the printing, expert inputs were required to determine the manufacturability of the printed parts. To ensure data integrity, AM experts with experience in both AM manufacturing and design voted to assess the manufacturability of the printed part. They will make the agreement on whether the part satisfies the requirement of manufacturability level 1. If the printed part was

free of visual defects, the result would be marked as yes for manufacturable. If the printed part was observed to have any geometric incompleteness or warping challenges, the result would be marked as no for non-manufacturable, and the area of the failure would be labeled. The detailed labeling process is described in Chapter 5 when the ML algorithms are introduced.

Up to the time of this report, 491 printed FDM samples were collected. An increasing number of samples are being printed to expand the database.

4.1.3. LPBF setup

For LPBF, a significant portion of data was donated from other researchers in the laboratory and collaborative partners outside of the laboratory. The data included lattice structures, benchmarking, special designs, and simple geometries such as cubes, cylinders, channels, tensile bars, slots, and thin walls with various materials, process parameters, and LPBF machines.

In addition to the data donated from laboratory and collaborative partners, some experiments were conducted to obtain the LPBF data. The samples were printed with a Renishaw AM 250. The selected designs were from the list used in FDM printing. They were filtered to select the most suitable for LPBF as determined by AM experts. A total of 52 designs were selected to be printed using four materials, different building orientations, and different settings of laser power, printing speed, and hatch space. This experiment is still being planned and data has not been collected into the current database.

Note that, for both FDM and LPBF, the building orientation and supports are considered to be a part of the design. The entire design file is stored with the selected building orientation and proper supports. There is no specific requirement for the dataset. All the printed parts fabricated by any AM machine can be updated to the dataset.

Up to the time of this report, 246 printed LPBF samples have been collected. More samples are being printed to expand the database.

4.2. Database management system

All the data were stored based on the entity-relationship model. Figure 4-4 shows the structure of the database. Based on the AM process chain, the proposed database can be grouped into three entity clusters: design, manufacturing process, and product. To satisfy the demand of the current research, the database is restricted to the most important entities such as keys that aid in managing the database and decisive AM parameters that have been used in ML models. Some details of AM process may be ignored at the current stage. The database will be expanded continuously in the future. The relational database was the type of database used in this research. It provides access to data points that are related to one another. A rational database means the data tables are connected logically. As shown in Figure 4-4, not only are the attributes listed but the actions are clearly defined, which enables applications to manipulate the data and structures of the database.

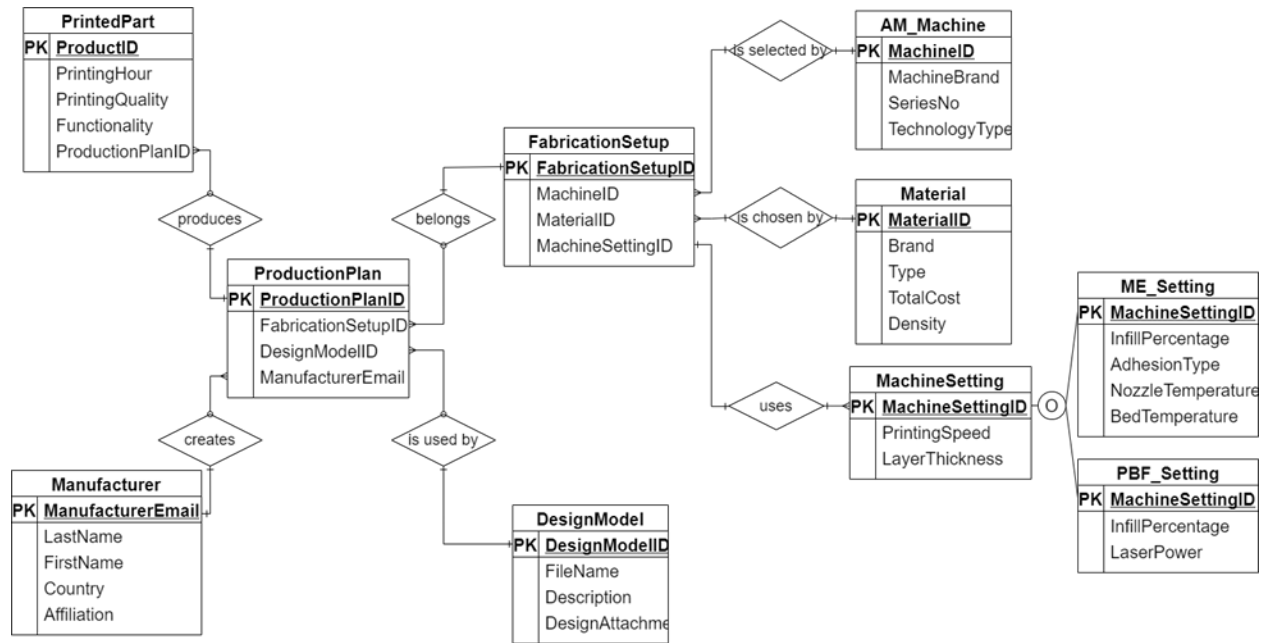


Figure 4-4: Entity relationship diagram of the developed database

The aim of the AM database is to facilitate easy navigation of the data, increase data-sharing, and reduce seamless storage. The purpose is to follow the distinct steps of the AM process. Each step of the process requires unique sets of data. Without a database, it is difficult to follow and manage. The non-relational database alternative is the current standard. However, in the AM process, most entities are closely related. It is difficult for users to search for the exact information they seek. Moreover, the non-relational database requires a higher skill level of AM knowledge to install and maintain the database. Although the design files are often unstructured, they are always converted into binaries when they are used in the AM process. Therefore, a relational database was considered reasonable.

At the design or preparation stage, three tables were created: manufacturer, production plan, and design model. Table 4-2 shows the attributes and data types of each table; thus, each record included the information of manufacturer email, last name, first name, country, affiliation,

production plan ID, and fabrication setup ID. For each table, the bold and underlined attribute denotes the unique ID (a primary key), which is used to identify each record. It cannot contain null values and every record must have a primary key value for each table. Italic attributes indicate a foreigner key. The foreigner key is also the primary key in another table, which provides a link between two tables. For instance, “ManufacturerEmail” is set to be the primary key in the “Manufacturer” table, and it is the foreigner key in the “ProductionPlan” table, which connects two tables.

Table 4-2: Attributes and data types of each table at the design or preparation stage

Manufacturer		
Attributes	Datatype	Description
<u>ManufacturerEmail</u>	VARCHAR (50)	Manufacturer’s email address, which can be used as the personal account ID and as contact information.
LastName	VARCHAR (50)	Last name of the manufacturer.
FirstName	VARCHAR (50)	First name of the manufacturer.
Country	VARCHAR (25)	Country of the manufacturer.
Affiliation	VARCHAR	Academic or industrial organization.

ProductionPlan		
Attributes	Datatype	Description
<u>ProductionPlanID</u>	AUTOINCREMENT	Unique ID for the test/production plan/experiment.
<i>FabricationSetupID</i>	INT	Foreigner ID here to link fabrication setup to the production plan.
<i>DesignModelID</i>	INT	Foreigner ID here to link the design model to the production plan.

<i>ManufacturerEmail</i>	VARCHAR (50)	Foreign ID here to the link manufacturer and the production plan.
--------------------------	--------------	---

DesignModel		
Attributes	Datatype	Description
<u>DesignModelID</u>	AUTOINCREMENT	Unique ID to track the design file.
FileName	VARCHAR (50)	Filename for the design file.
Description	VARCHAR (255)	Brief description of the printed design.
DesignAttachment	BINARY	Attachment of the design file.

The manufacturing stage comprises six tables (Table 4-3): fabrication setup, AM machine, machine setting, material, ME setting, and PBF setting. ME and PBF are used here instead of FDM and LPBF as the big picture for the AM technology types. However, as stated in Section 3.4, this thesis only focuses on LPBF and FDM. Only the data for LPBF and FDM have been obtained in the developed database.

Table 4-3: Attributes and data types of each table at the manufacturing process stage

FabricationSetup		
Attributes	Datatype	Description
<u>FabricationSetupID</u>	AUTOINCREMENT	Unique ID to track the settings for machines and materials.
<i>MachineID</i>	INT	Foreigner ID here to link AM machine to the fabrication setup.
<i>MaterialID</i>	INT	Foreigner ID here to link material to the fabrication setup.
<i>MachineSettingID</i>	INT	Foreigner ID to link machine setting to the fabrication setup.

AM_Machine		
Attributes	Datatype	Description
<u>MachineID</u>	AUTOINCREMENT	Unique ID of the 3D printer (machine) used for the building.
MachineBrand	VARCHAR (50)	Brand of the 3D printer.
SeriesNo	NUMBER	Series number of the printer.
TechnologyType	VARCHAR (50)	Type of AM techniques (defined by the ASTM standard): PBF, ME, etc. (currently only for PBF and ME).

MachineSetting		
Attributes	Datatype	Description
<u>MachineSettingID</u>	AUTOINCREMENT	Unique ID of the machine settings used for this build.
PrintingSpeed	Number	Printing speed used for this build.
LayerThickness	Number	Layer thickness that used for this build.

Material		
Attributes	Datatype	Description
<u>MaterialID</u>	AUTOINCREMENT	Unique ID of the used material for this build.
Brand	VARCHAR (50)	Brand of the used material.
Type	VARCHAR (50)	Material type.
TotalCost	CURRENCY(USD)	Unit price for the material.
Density	Number	Density of the material.

MEsetting		
Attributes	Datatype	Description

<u>MachineSettingID</u>	AUTOINCREMENT	Unique ID of the machine settings used for this build.
Infill percentage	Number	Specific setting for ME indicating the “fullness” of the inside of a part.
AdhesionType	VARCHAR (50)	Specific setting for ME indicating the adhesion type used to increase the ability of printed material to adhere to the build plate including skirt, brim, and raft.
NozzleTemperature	Number	Specific setting for ME indicating the nozzle temperature to melt the material.
BedTemperature	Number	Specific setting for ME indicating the temperature for the build plate.

PBFsetting		
Attributes	Datatype	Description
<u>MachineSettingID</u>	AUTOINCREMENT	Unique ID of the machine settings used for this build.
Infill percentage	Number	Specific setting for PBF indicating the “fullness” of the inside of a part.
LaserPower	Number	Specific setting for PBF indicating the power of the laser used to melt the material powder.
HatchSpace	Number	Specific setting for PBF indicating the separation between two consecutive laser beams.

The product level has only one table (Table 4-4) at the current status to record the printing performance of the design. The quality of the printed part has been recorded as yes or no, indicating

if the design is printable or not based on Manufacturability Level 1. Further product-related properties such as dimensional accuracy, surface roughness, and mechanical properties can be included in the future if required.

Table 4-4: Attributes and data types of each table at the product level

PrintedPart		
Attributes	Datatype	Description
<u>ProductID</u>	AUTOINCREMENT	Unique ID for the printed part (final production).
PrintingHour	TIME	Number of printing hours.
PrintingQuality	Y/N	Whether the quality of the printed part passes the evaluations of the manufacturer in geometric completeness.
Functionality	Y/N	Whether the quality of the printed part passes the evaluations of the manufacturer in density and dimensional accuracy.
<i>ProductionPlanID</i>	INT	Foreigner ID to link production plan to the printed part.

Figure 4-5 shows some example records that have been established in the database. For instance, the general machine setting information is saved in the entity set “MachineSetting.” It has three entities: “MachineSettingID,” “PrintingSpeed,” and “LayerThickness.” “MachineSettingID” is a unique ID to identify each setup. As the printing speed and layer thickness can be collected for both ME and PBF processes, they are recorded in the upper level to avoid repetition. More detailed settings for different AM technique types are stored in lower levels such as “ME_Setting” or “PBF_Setting.”

MachineSettingID	PrintingSpeed	LayerThickness
1	80	0.15
2	80	0.1
3	60	0.15
4	60	0.1
...

ProductID	PrintingHour	Fail?	ProductionPlanID
1	9293	No	7
2	61769	No	8
3	5061	No	9
4	14798	Yes	10
5	12918	Yes	11
...

ProductionPlanID	ManufacturerEmail	FabricationSetupID	PartID
3	ying.zhang8@mail.mcgill.ca	1	4
4	ying.zhang8@mail.mcgill.ca	2	6
5	ying.zhang8@mail.mcgill.ca	2	5
6	ying.zhang8@mail.mcgill.ca	1	7
...

PartID	FileID	Description	DesignAttachment
1	103354	biology;bone;human_skull;teeth;tomography	1
2	106831	customizer;parametric;snowflake	1
3	108147	decoration;heart;house;LED	1
4	39247	household;owl;jar;pot;honeycomb	1
...

Figure 4-5: Example tables in the database

To satisfy the demand of the current research, the database is restricted to the most important entities including keys that aid in managing the database and decisive AM parameters that have been used in ML models. Some details of AM process may be ignored at the current stage. It can be expanded in future research. This approach provides a well-organized data structure to store and manage AM data. However, it is limited in data searching and sharing. It is more appropriate for institutes, industries, or organizations to internally store and manage data. A public and easily accessible data repository is also expected to spread the existing data and advance the ML application in AM. Therefore, in addition to the AM database management system, this thesis proposes an AM data port is proposed. The details are provided in the following section.

4.3. AM data port

No public standard dataset on AM studies is available in the literature. Most existing databases or datasets are private and difficult to access. The existing databases are neither designed for AM nor more suitable for an organization to manage its internal data. No simple data port has been designed for sharing and accessing AM data publicly. A data port for AM is required, and it is expected to be simple, easy-access, and systematic so that datasets from different studies can be collected. Researchers can save time on collecting and sharing data, which in turn encourages connection and collaboration between researchers. Moreover, some small datasets can be combined to generate a larger and richer dataset that can be beneficial for all AM researchers.

Hence, based on the best understanding of the author, a simple data port is proposed here and ready for data uploading and query. This data port is expected to be web-based and shared with the public. Everyone is welcome to provide their open data or download and reuse the data. For each dataset, the donator must fill five required fields and five optional fields. The required fields include AM technique type, raw input data type, application/targets, whether the data is

labeled, and a zip file for the data. The optional fields include raw output data type, reference source, contact information, machine type, and material type. Machine type and material type include the brand and series information for selected machines and materials. This information can be observed in the “more details” panel. The preliminary design for the AM data port is shown in Figure 4-6. On the left of the page, users have the option to filter the database to what they seek based on “AM technique type,” “applications/target,” “raw data type,” and “labeled or not?”. This simple and informative AM data port is aimed to increase data sharing in the AM community and accelerate the ease of data gathering. This data port will not recommend any data handling process or ML algorithm to users. Raw datasets are provided, and users have unlimited freedom to process the data. The data is expected to be used in various research.

Welcome to AM data port

Home Share your data

AM technique type

☒ PBF

☐ ME

☐ BJ

☐ Photopolymerization

☐ MJ

☐ SL

☐ DED

Application/Target

☐ Design-related

☐ Process-related

☒ Product-related

Raw data type

☐ Tabular

☒ Graphics

☐ 3D data

☐ Spectrum data

Labelled or not?

☒ Yes

☐ No

No	AM technique type	Application/Target	Raw data type	Labelled or not?	
1	PBF	product-related; visual defects	graphic	Yes	More details
2	PBF	product-related; visual defects	graphic	Yes	More details
3	PBF	product-related; visual defects	graphic	Yes	More details
4	PBF	product-related; visual defects	graphic	Yes	More details
5	PBF	product-related; visual defects	graphic	Yes	More details
6	PBF	product-related; visual defects	graphic	Yes	More details
7	PBF	product-related; visual defects	graphic	Yes	More details
8	PBF	product-related; visual defects	graphic	Yes	More details

Figure 4-6: Preliminary design for the AM data port

4.4. Chapter summary

This chapter first describes how experimental FDM and LPBF data are conducted and collected on both selections of the design and process variations. Various designs focusing on wall thickness, minimum features, clearances, holes, extreme points, chamfers and fillets, overhangs, angled surfaces, down and up faces, islands, and corners have been printed through the selected AM machines with different materials and machine settings. These experimental samples were collected to establish the dataset for training the ML models that will be introduced in the next chapter.

For systematic management of these collected data, the database management system is developed and introduced. It aids in better organizing and accessing the data. In addition to the database management system, this research observed that an AM data port is in demand to increase the data sharing and data searching for ML in AM applications. Therefore, a public and easily accessible web data port is proposed at the end of this chapter.

Chapter 5. Hybrid machine learning models for manufacturability prediction

In this chapter, a detailed explanation of the development of hybrid ML models for manufacturability prediction is provided. The voxel-based approach is first introduced, followed by an advanced sparse-based approach. The developed hybrid ML models demonstrated promising performance compared with the existing commercial software. Moreover, the models consider both design and process information to predict Manufacturability Level 1, which is the potential visual defects of the given design through the selected AM process and settings. In the remainder of this chapter, the initial voxel-based approach is fully described in Section 5.1, and the advanced sparse-based approach is introduced and compared in Section 5.2. Finally, this chapter is summarized.

5.1. Voxel-based CNN model

The proposed model was inspired by the application of ML in biomedical engineering, wherein several well-developed ML models efficiently detect and locate brain tumors [152-155]. Additionally, certain studies have identified the CNN as a promising approach in 3D model analysis [156-158]. The ML model in this study is developed specifically for the AM process. Although voxelization and CNNs are used to manage the 3D objects in this model, the ML architecture differs from that of the existing models. Moreover, the model combines the input variables with the design, material, and printing process, which is a combination of 3D objects, text, and values. To the best of the author's knowledge, this has not been investigated thus far.

Moreover, supervised learning is selected in this thesis as the starting point of the ML approach. Compared with the other two types of ML, unsupervised and reinforcement learning, supervised learning has been used more widely, demonstrating its feasibility and effectiveness in

AM applications. In recent years, supervised learning has exhibited a high success rate in AM applications such as candidate selections [159], surrogate models in design optimization and simulation [160-162], and predictions on the quality of fabricated components [80, 103, 163]. Supervised learning learns from labeled training data to predict unforeseen data. It obtains the benefits of existing experience, whereas unsupervised learning relies on algorithms to determine structured patterns [164]. Furthermore, reinforcement learning requires more data and more computations to achieve a prediction. This technique is preferred to achieve long-term results [165]. Since the proposed approach is part of a closed-loop manufacturability analysis system, the effectiveness of the ML model is important for subsequent research on design modification recommendations. For this thesis, the prediction (output of the ML model) can be clearly classified and labeled. Beginning to develop the model with supervised learning is easy and beneficial. More details are given in the following content.

5.1.1. Proposed ML algorithm and architecture

Figure 5-1 depicts the flowchart of the developed system to predict the manufacturability of a given design using the AM process. The developed system has two potential outputs. The first output is a single metric generated from Model 1, which is a simple yes or no answer. It indicates whether the entire design can be printed completely using the selected LPBF machine. If the part is not printable, it is redirected to Model 2, wherein the potential failure areas are predicted. If the part is predicted as printable, it can be sent for printing or further evaluations on Manufacturability Levels 2 and 3. The two groups of input variables for the ML model are the design parameters and material and printing process information. The design parameters are represented in a 3D matrix that indicates the occupancy of each voxel. The material and printing process information, which includes machine settings and details of the materials for the printing process, are represented as

text or values. Section 5.1.4 explains the data generation in detail. Output 1 is a single-dimension yes or no result, whereas Output 2 is the printability map with a dimension identical to that of the input data. As the manufacturability analysis system is separated into two ML models, Model 2 analyzes only the non-printable designs, increasing the efficiency of the analysis process.

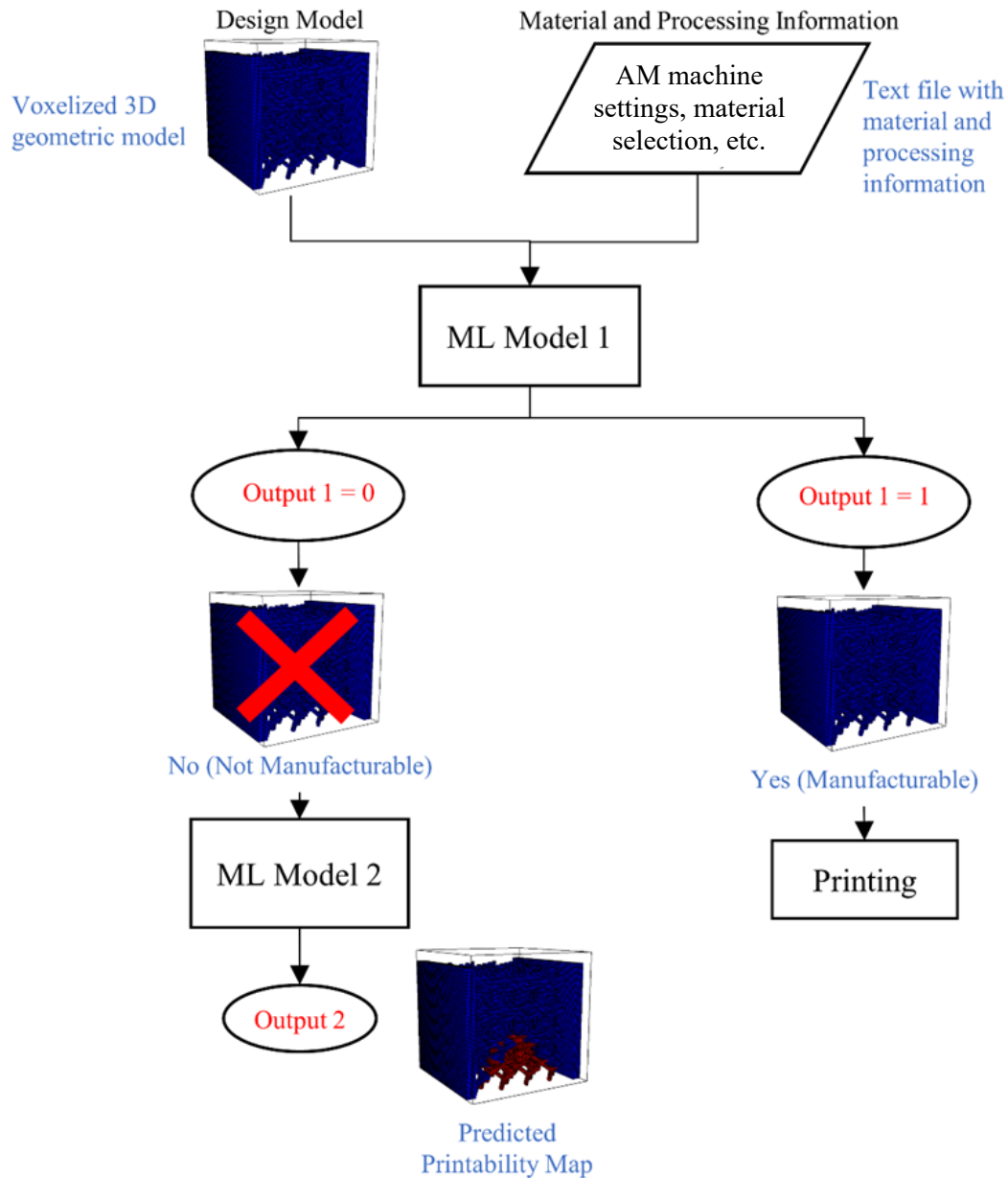


Figure 5-1: Flowchart of the developed system

Figure 5-2 presents the ML architecture of Model 1, wherein the initial prediction of whether the entire part is printable occurs. In the material and printing process, each neuron in one layer is fully connected to the neurons in another layer through the activation function based on the principle of the FNN; these are referred to as dense layers. The frequently used convolution and pooling in the general CNN are applied to the design representations. The final convolutional layer of the design is multi-dimensional, and it is flattened and concatenated to the 1D model of the material and printing process information to generate the joint model of the design and process. Subsequently, several dense layers are applied to the joint model, and each neuron in the final layer is fully connected to predict the value of Output 1.

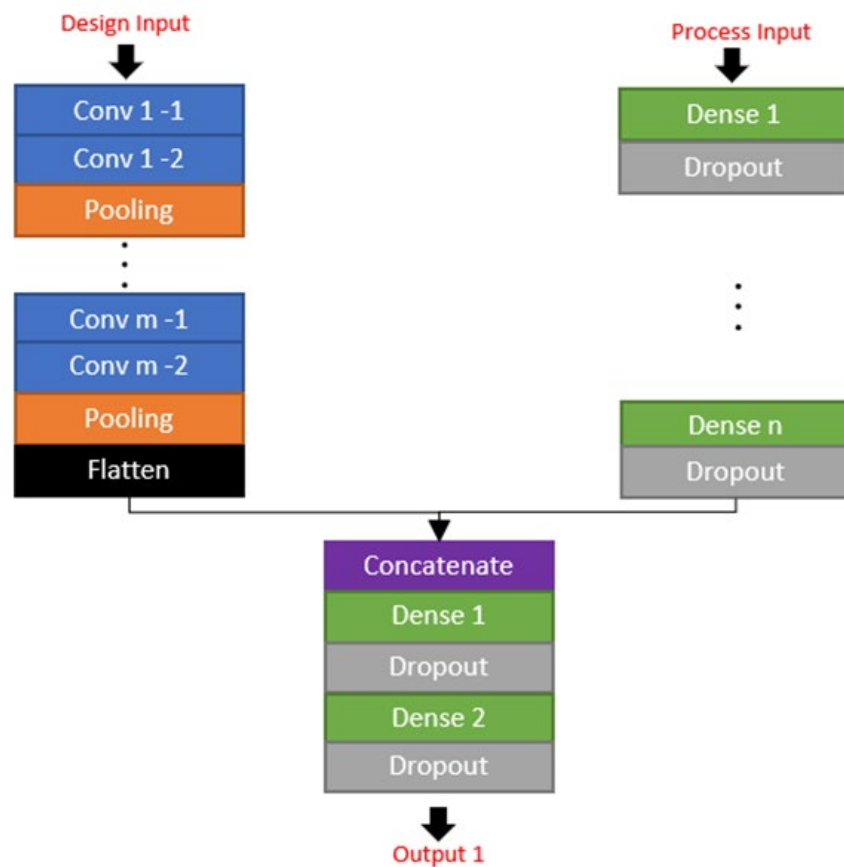


Figure 5-2: ML architecture of Model 1 performing the initial analysis

Figure 5-3 depicts the ML architecture of Model 2, wherein the potential failure areas are predicted. The initial steps in predicting Output 2 are similar to those of Model 1. However, the combination of the NN layers of the design and processing information generates a reshaped multi-dimensional layer. Therefore, a transpose convolutional layer is added to the reshaped layer for upsampling the inputs. Subsequently, the transpose convolutional layers are concatenated with the previous convolutional layers, guiding the learning process. Finally, the model is transferred to other convolutional layers to predict Output 2. The number of transpose convolutional layers equals that of the previous convolutional layers. Moreover, the number of layers in each ML operation constitutes the hyperparameters, which can be tuned to achieve the best performance in the ML method. The proposed architectures are inspired by commonly used models, such as U-Net and VGG16 [152, 166]. However, unlike the architectures in these models, a modified architecture integrating the CNN for 3D objects and the classic FNN for text and numerical parameters is developed here.

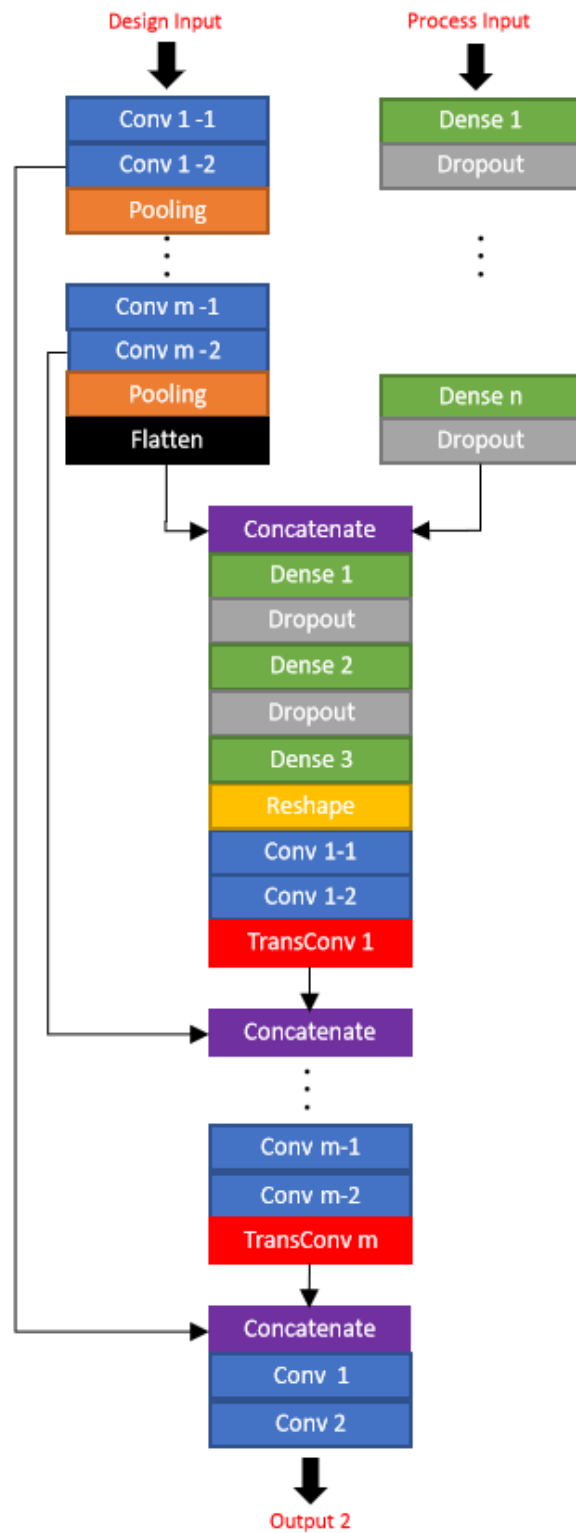


Figure 5-3: ML architecture of Model 2 performing the printability map analysis

5.1.2. Loss function and evaluation metrics

The loss function in the first ML model uses a binary cross-entropy, calculated using Eq. 5-1.

$$\text{Cross Entropy} = -(p \cdot \log(\hat{p}) + (1 - p) \cdot \log(1 - \hat{p})) \quad \text{Eq. 5-1}$$

where p and \hat{p} represent the ground truth in the training sample and the prediction, respectively.

The evaluation metric is based on the accuracy of the prediction.

$$\text{Accuracy} = \frac{TP + TN}{TP + FP + TN + FN} \quad \text{Eq. 5-2}$$

where TP is the true positive, wherein both the prediction and actual output are YES; TN is the true negative, wherein both the prediction and actual output are NO; FP is the false positive, wherein the prediction is YES, but the actual output is NO; and FN is the false negative, wherein the prediction is NO, but the actual output is YES.

The second ML model uses the weighted dice coefficient loss function. The general dice coefficient loss can be calculated using Eq. 5-3 [167].

$$\text{Dice coefficient loss} = -\frac{2TP}{2TP + FP + FN} = -\frac{2p \cdot \hat{p}}{p + \hat{p}} \quad \text{Eq. 5-3}$$

Typically, the dice coefficient loss is the sum of each class involved in the task. In this thesis, it is the sum of three classes, namely the empty, printable, and non-printable voxels. However, the empty and printable voxels in the dataset are more in number than the non-printable voxels. In this scenario, class imbalance occurs, which can be solved using Eq. 5-4.

$$\text{Loss} = \alpha DC_1 + \beta DC_2 + (1 - \alpha - \beta) DC_3 \quad \text{Eq. 5-4}$$

where α and β are the weight coefficients, and DC_i indicates the dice coefficient of each class. In this paper, α and β are set to 0.1 to request the loss function to pay more attention to the non-

printable voxels. The printable and empty voxels are considered to be equally weighted. No significant variations are observed in the model performance until the sum of α and β attain a value larger than 0.3. Beyond this, the performance decreases steeply, particularly in the non-printable voxels. α and β cannot be 0; otherwise, the model ceases the learning process. The intersection over union (IoU), which describes the similarity between any two validation samples, is used as the evaluation metric in the second model. The IoU is calculated using Eq. 5-5 [168]:

$$IoU = \frac{TP}{TP + FP + FN} \quad \text{Eq. 5-5}$$

To present the results clearly, the IoU of each class is calculated together with the mean IoU . All the ML model weights are updated by minimizing the loss function, and the iteration is completed when the convergence of the loss function occurs.

5.1.3. Hyperparameters

Hyperparameters in ML must be manually set before activating the model. Based on the recommendations from other similar models developed and the results obtained from the experiments in the literature, the hyperparameters are set to attain the minimum loss and maximum model performance. The general structure is reconstructed based on the frequently used VGG16 and 3D U-Net models that analyze 2D or 3D images [152, 166]. Initially, the hyperparameters are set considering the general guidelines and then tuned to identify the best performance based on the loss function and evaluation metrics. The details of the hyperparameters and how they are determined can be briefly summarized as follows.

- Activation functions: ReLU, the frequently used activation function that can achieve the best model performance, is adopted in the proposed ML model [169, 170]. The output layer

uses the sigmoid function to predict whether the entire part is printable, whereas the printability map is predicted using the SoftMax function.

- Learning rate: The learning rates in both models are set to $1e-5$ to balance the learning speed and model performance. Lower learning rates may slow down the learning process, and higher learning rates may prevent the convergence of the functions.
- Kernel size: Typically, the values of kernel size vary from $1 \times 1 \times 1$, $3 \times 3 \times 3$, $5 \times 5 \times 5$, to $7 \times 7 \times 7$. As the input dimension of the proposed design model is $128 \times 128 \times 128$, a $3 \times 3 \times 3$ kernel size is selected for each layer.
- Number of filters: The number of filters is always recommended to begin from the range of [32, 64, 128] and can be increased in the deeper layers. However, the proposed model begins with 16 filters owing to the large input dimension, and the number can vary at each layer.
- Stride size: All convolutional layers maintain a stride of 1.
- Padding: Padding is set to be the same in convolutional layers.
- Number of layers: For every ML operation such as convolutions and dense layers, the number of layers varies from 1 to 6. Although deeper layers may slightly enhance the model performance, the learning speed and computational capability are significantly affected.
- Number of neurons in the dense layer: The number of neurons varies between 64 and 512.
- Dropout rate: The dropout rate is set to 0.5 to reduce overfitting and improve the generalization error.

Figures 5-4 and 5-5 depict the detailed model architectures. After the initial values are set, the hyperparameters are manually tuned to attain the best model performance based on the existing dataset and computational power.

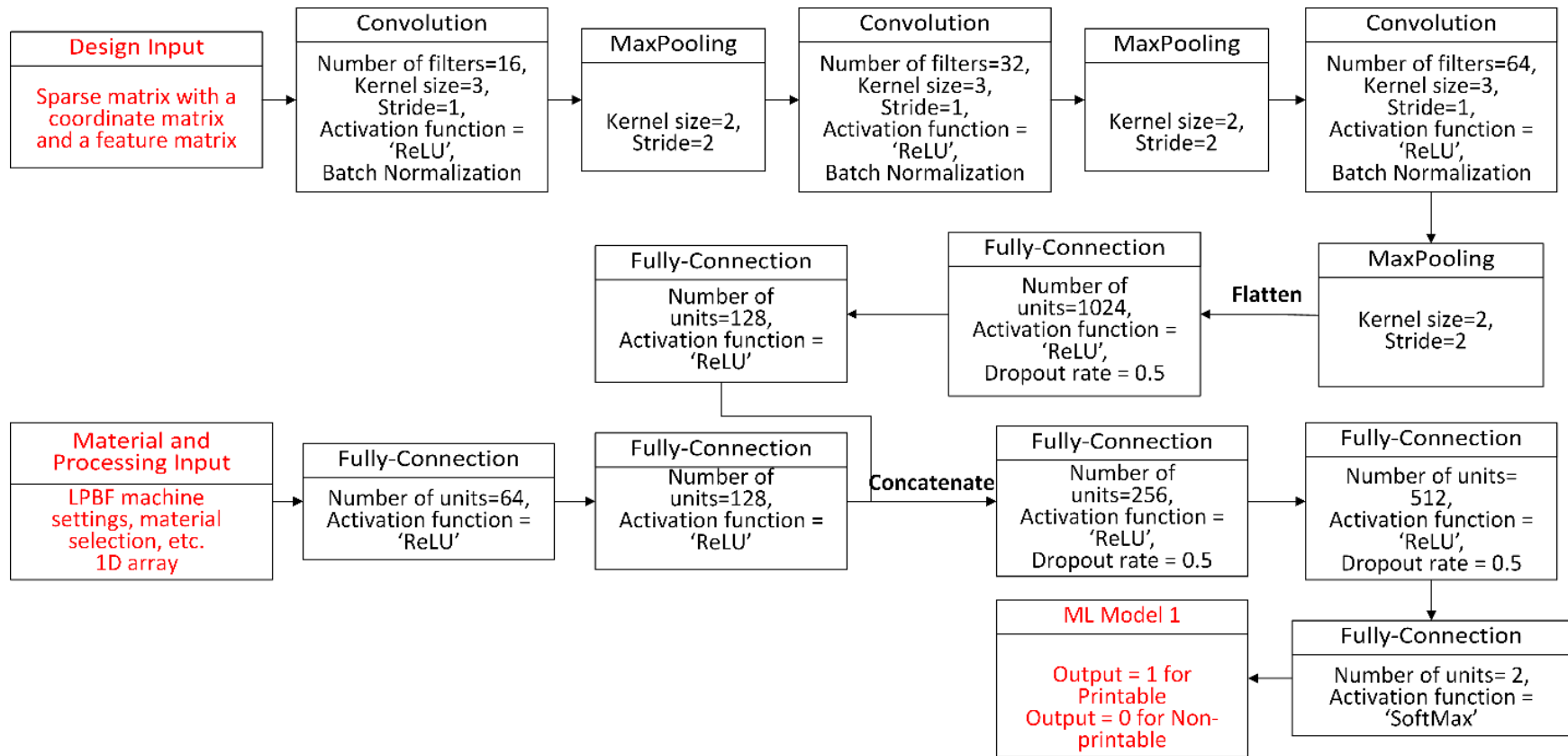


Figure 5-4: Detailed ML model architecture (Model 1)

5.1.4. Input data generation and preprocessing

The training data used in this approach are obtained from the LPBF process introduced in Section 4.1.2. All the designs are voxelized using binvox, a well-developed voxelizer [171] with a size of $128 \times 128 \times 128$. Considering the resolution of the LPBF process and the general building chamber size, $512 \times 512 \times 512$ is the ideal voxelization size of the geometric design to analyze the manufacturability. However, to maintain a balance in the computational cost, time consumption, and geometric resolution, the selected voxelizer has a size of $128 \times 128 \times 128$. $512 \times 512 \times 512$ is out of the capability of the current computer setup. In total, 196 samples are selected in the training data, wherein 49 samples constituted the validation set. The output values of 1 and 0 imply that the voxel is occupied and empty, respectively. Figure 5-6 shows some examples of voxelized geometric 3D models.

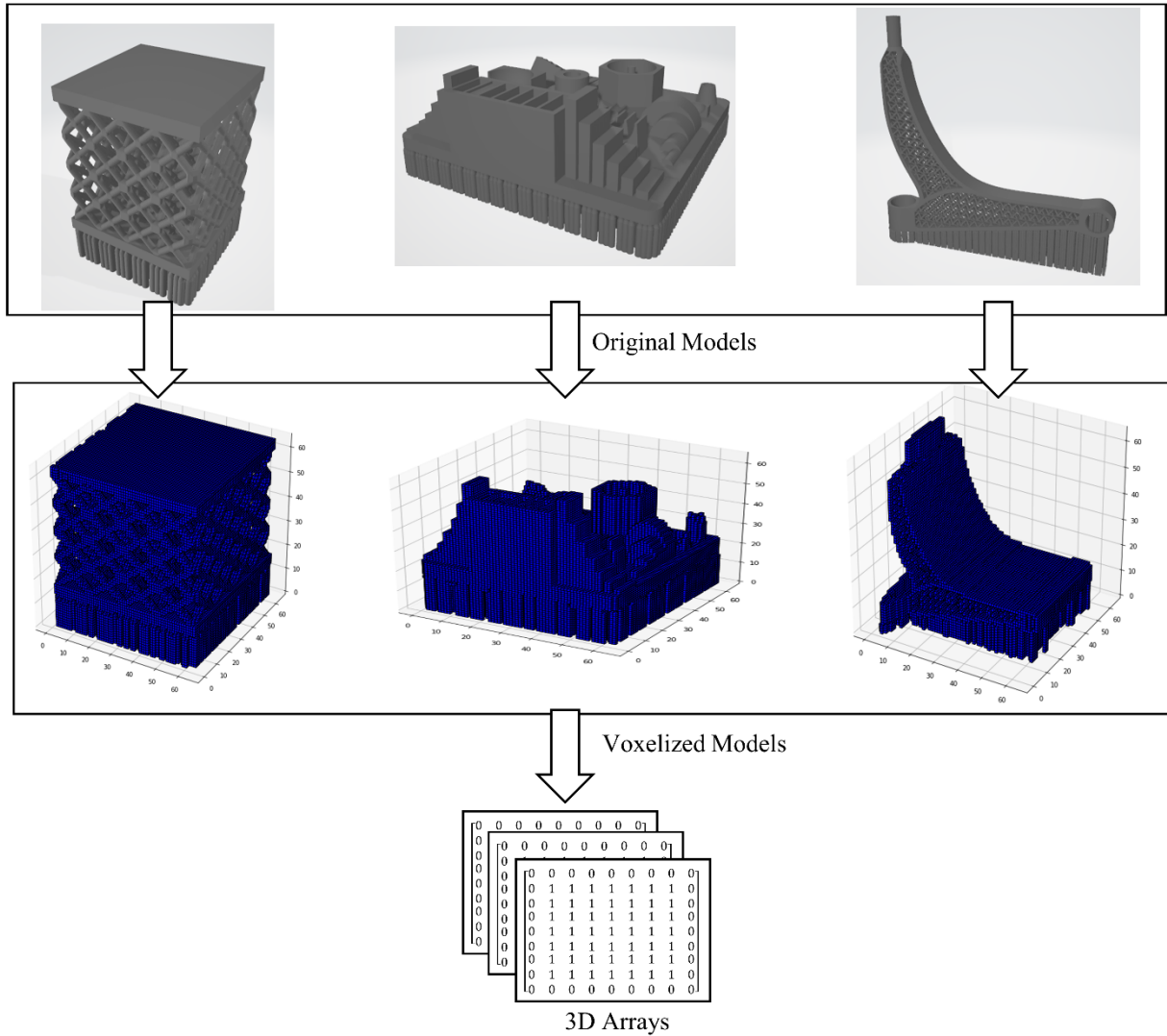


Figure 5-6: Examples of voxelized geometric 3D model

Table 5-1 presents some examples of the different materials and printing processes used for data training. These features were selected owing to the available data and existing studies of major factors on evaluating the manufacturability, which are explained in Section 2.2. Moreover, those selected process parameters are easily understood for novice AM users. They do not need extra time to understand those parameters and those parameters can be easily modified in the machine settings or in their slicing software. Scale is a parameter associated only with the design

aspect and not the manufacturing process; it refers to the size of a part. The scale is considered as a reference because the ML model fails to recognize the overall size of the given object owing to the identical voxelized geometries that maintain uniformity in the input dimension. As the samples in the existing dataset were printed using the default settings of the LPBF printers based on the material selection, the process parameters, such as laser power, printing speed, and hatching space were not considered in this study. However, when the dataset is expanded in the future, certain data samples may be printed using customized settings, wherein all the critical process parameters must be considered. This will not affect the developed ML architecture, as more input variables from the process parameters can be included to improve the model performance.

Table 5-1: Examples of the material and printing process used for data training

No.	Sample name	Material type	Material brand	Material density in loose form (g/cc)	Machine brand	Machine type	Scale
1	v_Inco	Inconel 625	EOS	8.4	EOS	M270	33.46
2	c_Inco	Inconel 625	EOS	8.4	EOS	M270	29.20
3	x_Steel	Maraging steel	EOS	8	EOS	M270	31.33
4	bm_001	AlSi10Mg	EOS	2.67	EOS	M270	52.5
5	channels_01	AlSi10Mg	Renishaw	2.68	Renishaw	AM 400	15
6	Tensile_01	AlSi10Mg	Renishaw	2.68	Renishaw	AM 400	74.12
7	201904_12	SS 316L	Renishaw	7.99	Renishaw	AM 250	106.35
				.			
				.			

5.1.5. Data Labeling

To generate the ground truth for the ML models, the corresponding printed result to the given design is obtained. If the design is successfully printed with associated processing information, and the printed result does not have visual defects, the ground truth is given a value of 1 as printable for the initial prediction. If the design is not printable, the truth is given a value of 0 as non-printable. Moreover, if the design is not printable, the printability map will be generated. The original voxelized models are sent to an annotation tool to label the non-printable voxels. An example of the annotation tool is shown in Figure 5-7. The tool was developed based on VoxCad [172]. The non-printed voxels were manually labeled with red layer by layer according to the printed result. Subsequently, the labeled results are transferred to the dense matrix. Each voxel in the design representation is labeled, wherein 1, 0, and 2 imply that the voxel is printable, empty, and not printable, respectively. Figure 5-8 shows an example of data labeling.

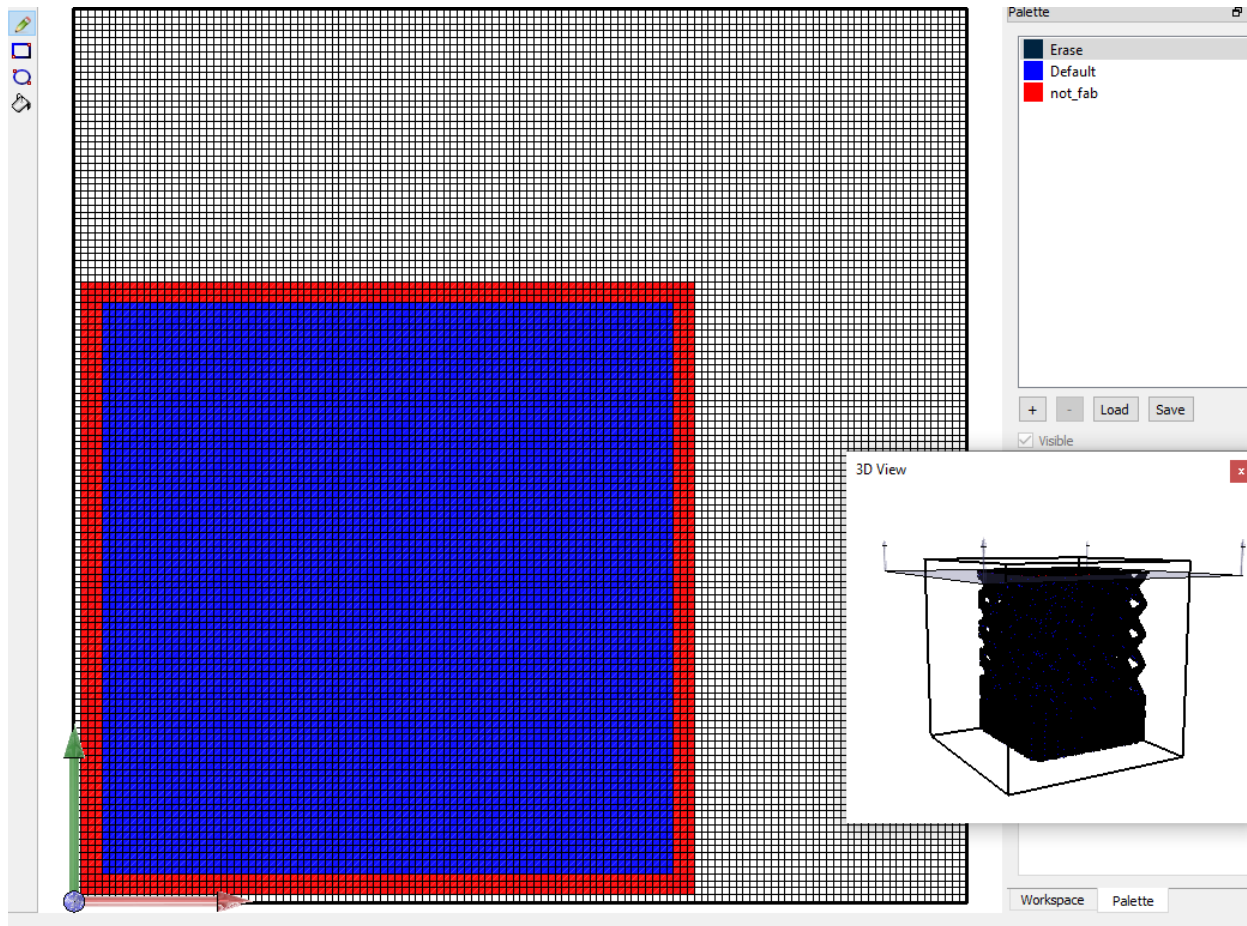


Figure 5-7: Interface of the annotation tool

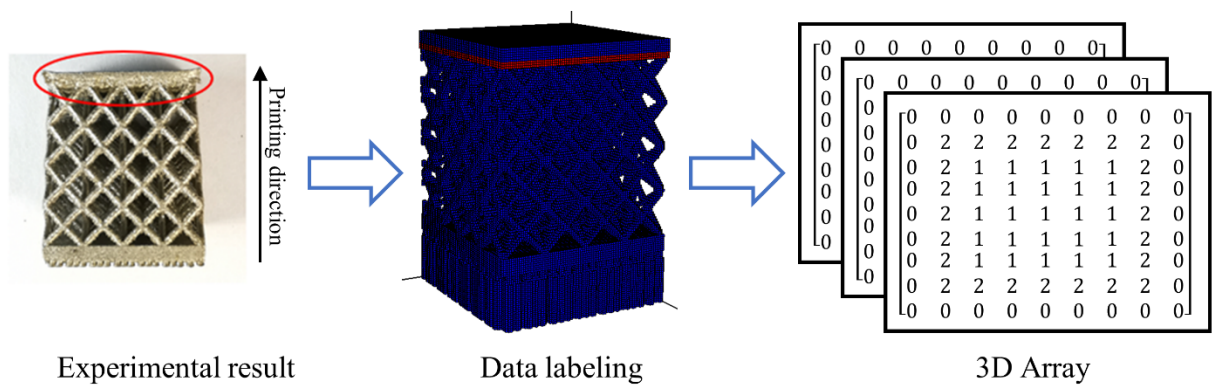


Figure 5-8: Examples of data labeling

5.1.6. Results and discussion

Sections 5.1.5.1 and 5.1.5.2 demonstrate and discuss the validations of the ML Models 1 and 2 results, respectively. The proposed models were verified by evaluating the trained models using the validation dataset with the defined evaluation metrics listed in Section 5.1.2. The developed ML models were implemented using Python on an NVIDIA GeForce RTX 2080 Ti. The TensorFlow, Keras, and Scikit-learn libraries [173] were used in the implementation.

5.1.6.1. Results of Output 1 Predicting the Printability of the Entire Part

The entire dataset was randomly split into training and validation datasets in the ratio of 4:1 to calculate Output 1. To decrease the variations among samples, five-fold cross-validations were performed, and the results are listed in Table 5-2. The average accuracy was approximately 0.8408. We consider this result to be satisfactory at the current state owing to the following reasons. First, no standardized dataset exists to measure the accuracy of different ML models. Thus, in the reported studies such as [105, 174, 175], the accuracy of the ML model was discussed in dramatically different ways. Second, examining the accuracy in Table 8 of [175], the testing accuracy reported for two different scenarios was 84% and 38%, respectively. Thus, the result from this approach was considered satisfactory. Additionally, the result for each iteration did not exhibit major fluctuations, verifying the stability and repeatability of the developed ML model.

Table 5-2. Cross-validation results of the prediction in the initial analysis

Iteration	Accuracy
1	0.8367
2	0.8367
3	0.8776
4	0.8367
5	0.8163
Average	0.8408

When the training dataset was applied to a model that considers only the design aspect, the average accuracy in predicting the manufacturability of the part decreased to 0.7805. This implied that the effects of excluding the material and printing process model are not significant as the training dataset is not sufficiently large. Moreover, the ratios of the failure samples, which are primarily caused by the material and printing process, are low. However, the impact can be significant with a larger dataset, reducing the accuracy further.

The effects of the voxelization size on the computing cost and performance were also investigated for this model. As mentioned in Section 5.1.4., the maximum size reached in this approach was $128 \times 128 \times 128$ owing to the restrictions in computational capability and time. The maximum memory was attained when the model is trained at $128 \times 128 \times 128$ resolution. Table 5-3 summarizes the comparison between different voxel sizes tested using the same ML architecture, hyperparameters, and computational hardware. The results indicated that, despite the longer running time, the accuracy is high at a higher voxelization resolution. At a lower resolution, the performance of the ML model is affected owing to the loss of certain features in the voxelization process. Therefore, higher voxelization resolution to execute the model learning is highly

encouraged, which is the key motivation for the sparse-based approach. It is fully explained in Section 5.2.

Table 5-3. Effects of voxelization resolution on the computing cost and performance

Voxel size	Accuracy	Training time (s)
128×128×128	0.8408	8480
64×64×64	0.7503	1000
32×32×32	0.6341	240

Furthermore, the model was also run with a smaller dataset comprising fewer training samples than the original test. Only 190 samples were selected in the smaller-dataset training rather than the original 245 datasets. The samples were split into training and validation datasets at a ratio of 4:1, identical to the original test. The average accuracy obtained was 0.7436, which was lower than the result presented in Table 2. This demonstrated a potential statement that with more and more data, the prediction accuracy will be better.

The ideal method to identify the size of data is to generate a learning curve for the model performance on datasets [176]. The required number of data sizes can be obtained when the learning curve reaches the saturation point. To make it simple, some common rules from the ML community can be used to identify the ideal size of the dataset. These rules are generally a factor of certain characteristics of the prediction problem. For example, some researchers indicated that the data size must be at least 50 to 1000 times the number of prediction classes [177]. Another rule states that the data size must be at least 10 to 100 times the number of the features [178, 179]. The most common method is to include at least 10 times the number of weights in the network if neural network models are used [180, 181]. However, a later study [176] indicated that a factor of 10 is

insufficient, and they concluded that the data size must be at least 27 to 31 times the number of weights in the network. Although the data size may also vary on the different applications, these common rules can provide a general concept of how many samples are sufficient for their studies.

The training datasets in most existing ML applications of AM are less than 100 [174], and their results prove that small datasets can make reasonable predictions. With more data inputs in the future, the coefficient of the proposed hybrid ML model can be updated to obtain enhanced results.

5.1.6.2. Results of Output 2 Predicting the Printability Map

Cross-validations were also conducted for Output 2. As mentioned in Section 5.1.2., the prediction was evaluated based on the IoU calculations (Table 5-4). The mean IoU calculated was a reasonable value of 0.7951. As indicated in Table 5-4, the model performed excellently in the empty voxels, whereas the performance in the non-printable voxels was slightly weaker. However, it is important to note that the goal of this research was to provide early indicators of potential manufacturability challenges for designers or AM process engineers before fabrication. The benefit of such an early indicator is that the designer or AM process engineer could modify some design geometries or process parameters to guarantee a successful fabrication. There is insufficient research in the literature to provide a printability map through an ML model as a method of indicating potential printing challenges. The result demonstrates the feasibility of such a printability map that can be successfully generated via the joint ML model with decent accuracy.

Table 5-4. Cross-validation results of the printability map prediction

Iteration	IoU_mean	IoU_empty	IoU_print	IoU_non_print
1	0.7866	0.9854	0.8006	0.5737
2	0.7821	0.9899	0.7777	0.5787
3	0.8092	0.9869	0.8355	0.6052
4	0.7918	0.9873	0.7465	0.6416
5	0.8056	0.9860	0.8353	0.5954
Average	0.7951	0.9871	0.7991	0.5989

Figure 5-9 shows three examples depicting the results of the printability map. The top row depicts the ground truth of the samples, labeled based on the experiments. The second row indicates the prediction of the ML model, and the final row is the prediction obtained from the commercial software. Figure 5-9(a) depicts a diamond lattice structure fabricated from AlSi10Mg using an EOS machine. Figure 5-9(b) illustrates a benchmark wherein the needles on the plate are extremely small, and the printer fails to print the precise shapes. Figure 5-9(c) shows an AlSi10Mg tensile bar printed using Renishaw; it suffered from severe warping on the sides. The green and orange regions in Figure 5-9 indicate the printable area and the area with a potential risk of failures, respectively. The prediction obtained from the proposed ML model exhibited competitive results compared with that of the commercial software. Although certain differences existed between the ground truth of the printability map and the prediction of the proposed ML model, the results exhibited the trend of the potential failure areas. Therefore, they can be considered acceptable in predicting part manufacturability.

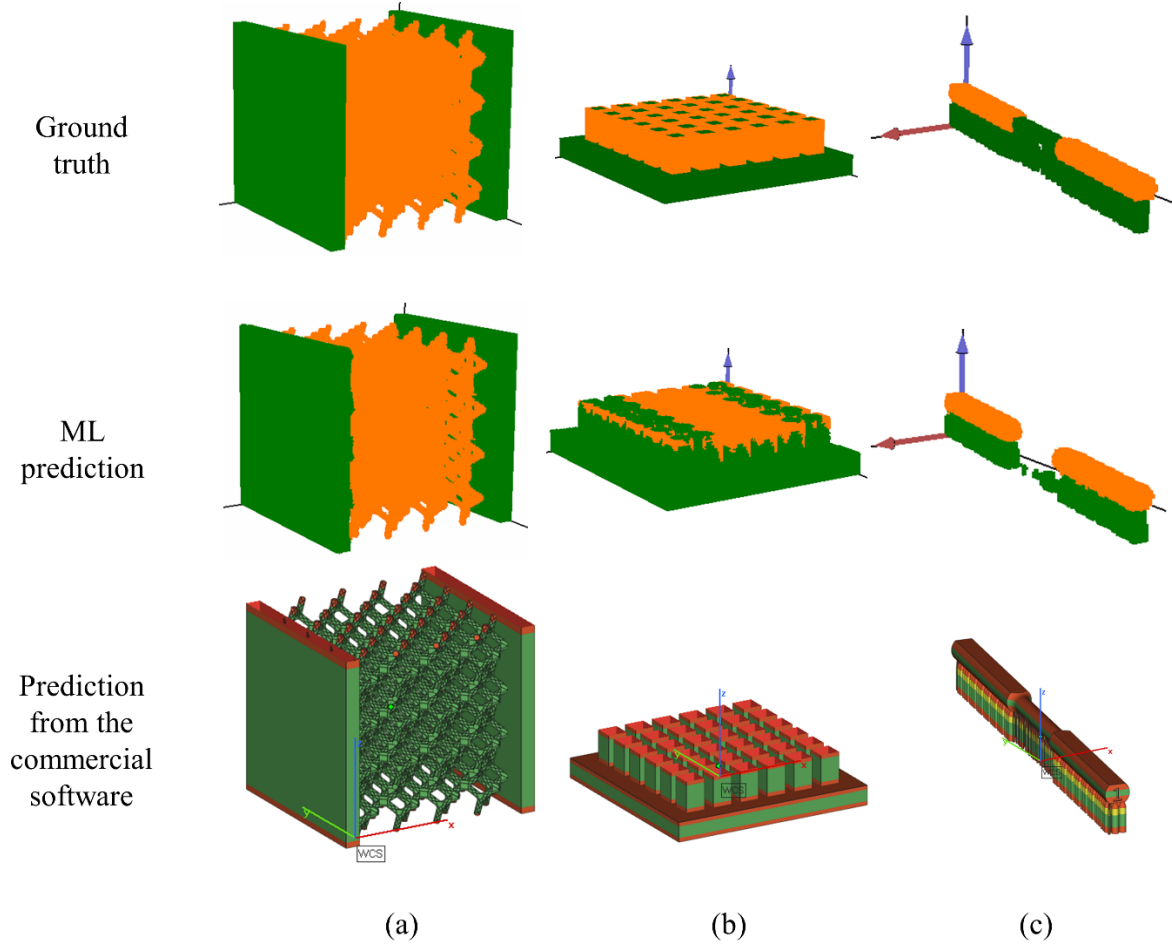


Figure 5-9: Test cases of the validation set. (a) Diamond lattice structure fabricated from AlSi10Mg using an EOS machine, (b) benchmark with tiny needles, and (c) AlSi10Mg tensile bar printed using Renishaw.

Figure 5-10 compares the predictions obtained using two different materials with varying strut thicknesses. The green and orange regions indicate the printable and failure areas, respectively. They were printed using the default machine settings for the selected material. The best process parameters were identified to print the selected material tested by the printer maker. As indicated in the figure, the proposed model provided outstanding results owing to the significant number of lattice structures used in the dataset. This demonstrated that with more data included in

the database, the model performance can be enhanced. Moreover, Figures 5-10(b) and 5-10(c) indicate a green layer at the bottom of the lattice structures. This layer was not labeled in the ground truth data because when the final printed part was obtained, the initial layers may be ignored and eliminated from the building plate. However, these layers were predicted by the proposed ML model as the initial layers can be printed successfully, and the subsequent layers may fail owing to the overhang constraints in the LPBF process.

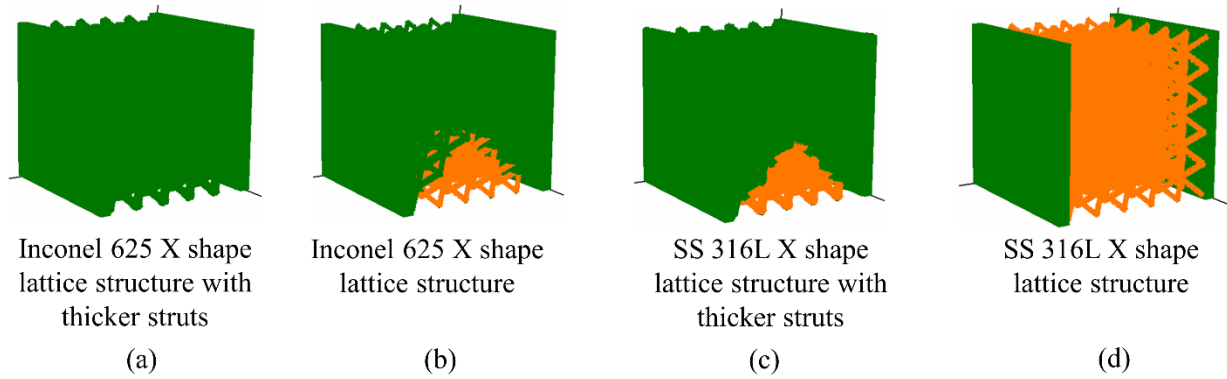


Figure 5-10: Comparison of the predictions obtained using two different materials with varying strut thicknesses

The ML architecture used to predict the printability map was inspired by 3D U-Net, which is frequently used in medical image detection. A similar approach is adapted here with a modified ML architecture, wherein the process and design models are combined. Moreover, the loss function is specifically developed for the manufacturability analysis in the LPBF process. The ML method requires multiple hyperparameters that must be determined before training the model. Owing to the limitations of the dataset, the hyperparameters used in this study are not the ideal values for the prediction in the manufacturability analysis. However, the values were selected considering the existing dataset under the current computational power, as described in Section

5.1.3. As more data are collected in the future, the values of the hyperparameters will be continuously tuned and improved iteratively.

Precise labeling of the dataset is essential in manufacturability analysis. Currently, all the datasets are labeled manually based on the printed part. However, precise labeling of every voxel cannot be achieved as the ground truths of the samples can be subjective owing to the manual detection. Although the printed part can be scanned using computed tomography to obtain a more accurate labeling result, it can be time-consuming and is not cost-effective. Therefore, even for industrial purposes, the parts are not scanned to obtain dimensional accuracy unless their printability is determined. Despite the subjectiveness of manual labeling, it facilitates an initial verification for the designers. Thus, the evaluating criteria in this study were to verify whether the part can be printed completely. In this regard, manual labeling is acceptable, and the results obtained from the prediction notify the designers of the potential design failures. The part is determined to be printable if it is suitable for the subsequent stages, such as dimensional accuracy evaluation or mechanical performance test.

Figure 5-11 depicts the ML prediction of a long-overhang bridge, which is not shown in the dataset. It was a bridge with an 80 mm overhang, and it was printed without any support. ML Model 1 predicted the bridge as not printable, and ML Model 2 provided a predicted failure area (Figure 5-11). The blue and red regions indicate the printable and failure areas, respectively. Several existing studies have proven that the long overhang bridge cannot be completely printed without support structures [128, 182, 183]. Although the prediction may not be identical to the experimental results, it depicts the trends of the potential failure. Moreover, when the bridge was laid down, it was considered by ML Model 1 to be printable.

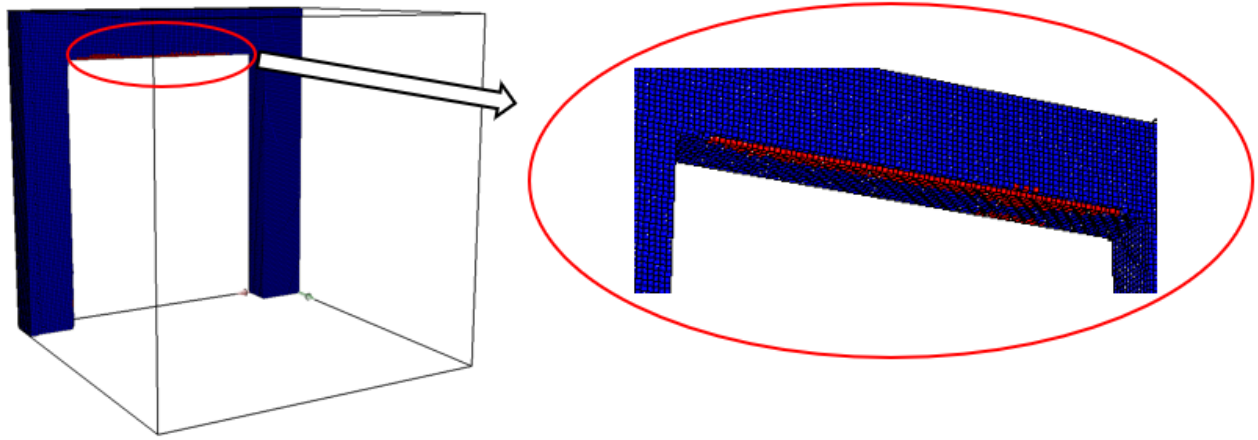


Figure 5-11: Prediction of a long overhang bridge

5.2. Advanced sparse-based CNN model

The voxel-based CNN demonstrated in Section 5.1 was investigated as a potential solution for design shape analysis. This approach is limited by the computational capability available, and only the lower resolution was performed. However, a low resolution is insufficient for precisely analyzing the AM process. Some detailed features may be omitted through the voxelization process. Moreover, as shown in Section 5.1.6.1, a higher voxelization resolution has a better performance. Therefore, to solve this problem, a more efficient CNN is proposed in this chapter. Design data is stored in a sparse matrix for CNN operations to train only the occupied voxels. It combines with the process data to make the prediction of manufacturability. By performing the generalized convolutions, the computational costs decrease significantly compared with the voxel-based CNN, which offers the advantage of performing with high resolutions. The approach was validated in terms of effectiveness and efficiency on the manufacturability prediction for the LPBF process. More details are provided in the following.

5.2.1. Framework of the sparse-based CNN model

Figure 5-12 shows the general framework of the sparse-based CNN model. Instead of using a voxelized 3D geometric model directly as the design input to the ML models, the voxelized 3D geometric model is preprocessed into a sparse matrix, which is combined with a coordinate matrix and feature matrix. Only the occupied voxels are stored in the sparse matrix, and the ML operation is applied only in the sparse matrix, which significantly decreases the computational cost and improves the performance of the models. The integration of the input features for design and material and processing information is first sent to a two-class manufacturability classifier to determine whether the given design is manufacturable with the given material and processing information. If it is printable, the given design is ready for printing. If it is not printable, the input features are sent to a semantic manufacturability segmentation step to determine which voxels are not printable to provide a printability map to designers. With the printability map, the potential failure area can be visualized to aid designers in future design improvement.

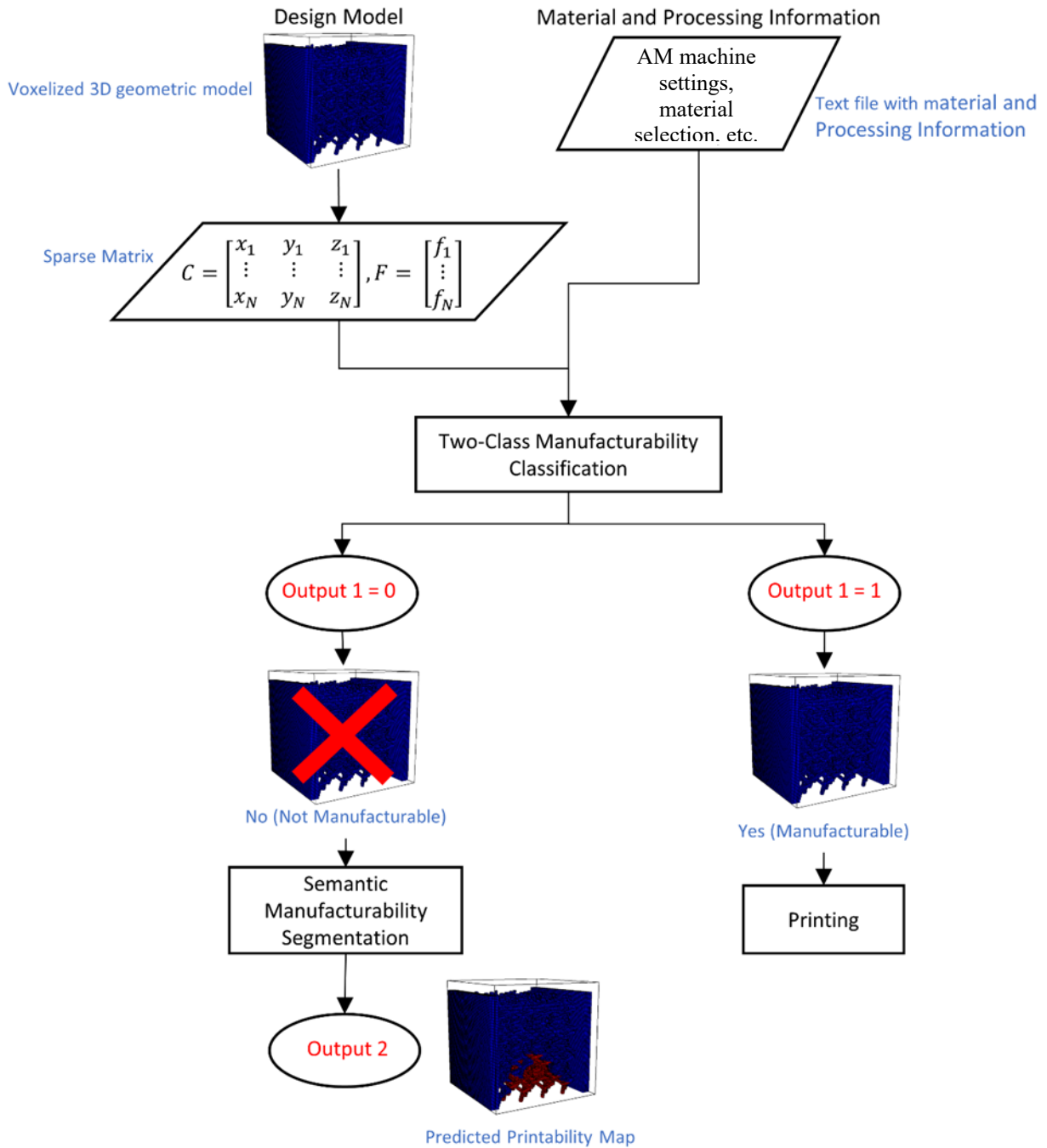


Figure 5-12: Framework of the ML-assisted manufacturability analysis

5.2.2. Data generation and preprocessing

As introduced in Section 5.1.4, the first step to preprocessing the design models is to voxelize the STL files using Binvox [171]. After parsing, the result of the voxelization is turned into a 3D matrix. The value 1 indicates occupied voxels, which are the main body of the designs, and 0 indicates the non-occupied voxels, which are the background. For most existing studies, the voxelization resolution is low. Higher voxelization resolutions cost more computational power, which results in a slow training process, and it may run out of computational capability. When observing the 3D design matrix, most of the elements in the design matrix are zero, which results in a super sparse matrix. Particularly for the high-resolution voxelized matrix, the sparsity is even higher. Figure 5-13 shows an example comparison between different voxel sizes for the same design model. For a conventional CNN, the operation is applied to every element in the matrix. However, it is not necessary to apply the operations to all the zero elements, particularly the zero-elements that are far from the main body of the design. The redundancy wastes the computational memory and slows down the training process. To solve these challenges and improve the performance, the design matrix is preprocessed and stored into a sparse matrix, and ML operations are only applied to these occupied voxels, which is explained in Section 5.2.4. The sparse matrix is stored as the combination of a coordinate matrix (C) and a feature matrix (F), which can be represented as follows:

$$C = \begin{bmatrix} x_1 & y_1 & z_1 \\ \vdots & \vdots & \vdots \\ x_N & y_N & z_N \end{bmatrix}, \quad F = \begin{bmatrix} f_1 \\ \vdots \\ f_N \end{bmatrix} \quad \text{Eq. 5-6}$$

where x_i , y_i , and z_i are the coordinates, N is the number of the non-zero elements, and f_i is the associated feature values. For the input data in this thesis, feature values are uniform, which is 1 indicating occupied voxels.

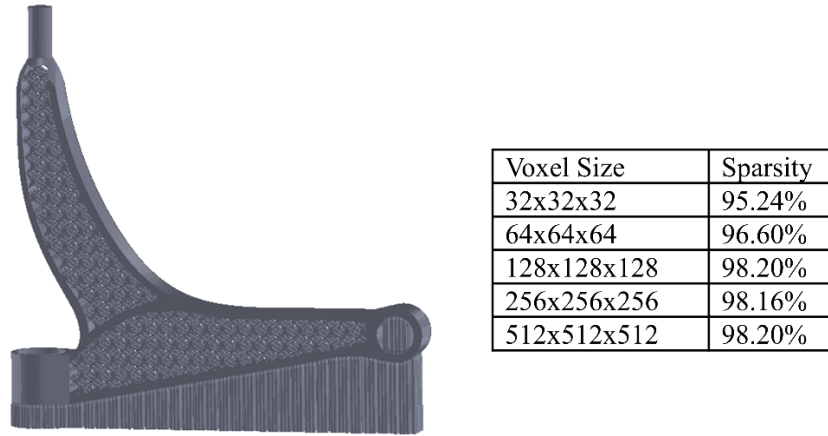


Figure 5-13: Comparison between different voxel sizes for a given design

The same strategy is used from the voxel-based approach to preprocessing the material and processing information data. One-hot encoding is applied to convert the categorical text variables into numerical variables to be provided to the ML model to perform a better prediction. Such material and processing information includes material types and brands, material density in loose form, and machine brand and type.

The data labeling process for the sparse-based approach first follows the same procedure described in Section 5.1.5. Subsequently, the results of the voxelization are transferred to the sparse matrix with coordinates and features as in Eq. 5-6. Note that the coordinate matrix should be the same as the one in the input. For the feature values in the ground truth, 1 denotes the printable voxels, and 0 denotes the non-printable voxels. Figure 5-14 shows an example of the labeling process.

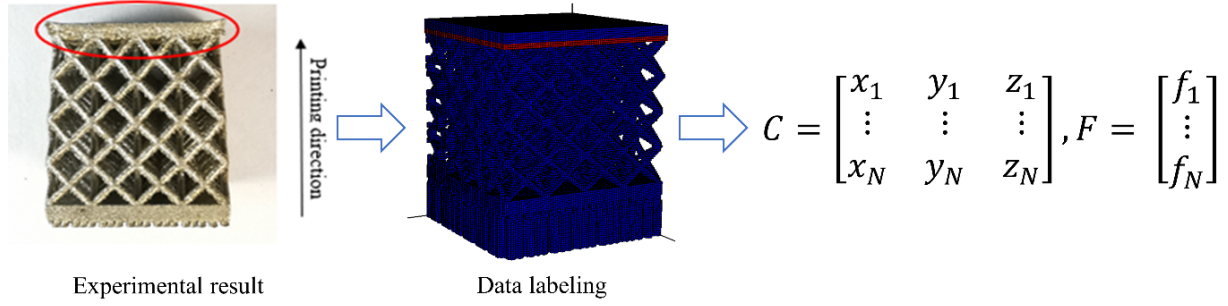


Figure 5-14: Examples of data labeling for sparse-based approach

5.2.3. Network operations on sparse-data structure

The convolution is the most important operation in CNNs. For the conventional convolution operation, it is frequently used for images or 3D objects that are multi-dimensional. In the conventional convolutional layers, a set of “filters” is applied to a subset of the input variables at a time and swept over the entire input; thus, only nearby inputs are connected, which results in significantly fewer weights than the fully connected layer. The convolution operation calculates the sum of the element-wise multiplication between the input matrix and filter matrix; therefore, it performs a many-to-one relationship. Although it costs much less than the fully connected layer, it is still a very expensive operation in deep convolutional networks. In our generalized convolution, the operation only applies to the occupied voxels such that it requires much less computational power than the standard convolution operations. It can be represented as the following equation:

$$O^{(n)}_{i,j,k} = \sum W^{(n)} I^{(n)}_{(i,j,k)}, \quad (i,j,k) \in C \quad \text{Eq. 5-7}$$

where $O^{(n)}_{i,j,k}$ is the n-th channel of the output value on voxel (i, j, k) . $W^{(n)}$ represents the weights of the operation, which is the filter described above. $I^{(n)}_{(i,j,k)}$ represents the n-th channel of the input features on voxel (i, j, k) . C is the coordinate matrix generated in Section 5.2.2. To better

illustrate the generalized operation, Figure 5-15 shows a graphical explanation. It provides a comparison between the standard convolution operation and the generalized convolution operation. On the left-hand side, the standard convolution operation swept over the entire input; however, for the convolution on the sparse matrix, it only sweeps over the occupied elements. When calculating the output value on the selected elements, it first obtains the values from all the neighbors for the selected elements based on the stored coordinates. Subsequently, the “filters” are applied to the pattern, which consists of the selected point and surrounding neighbors to compute the output.

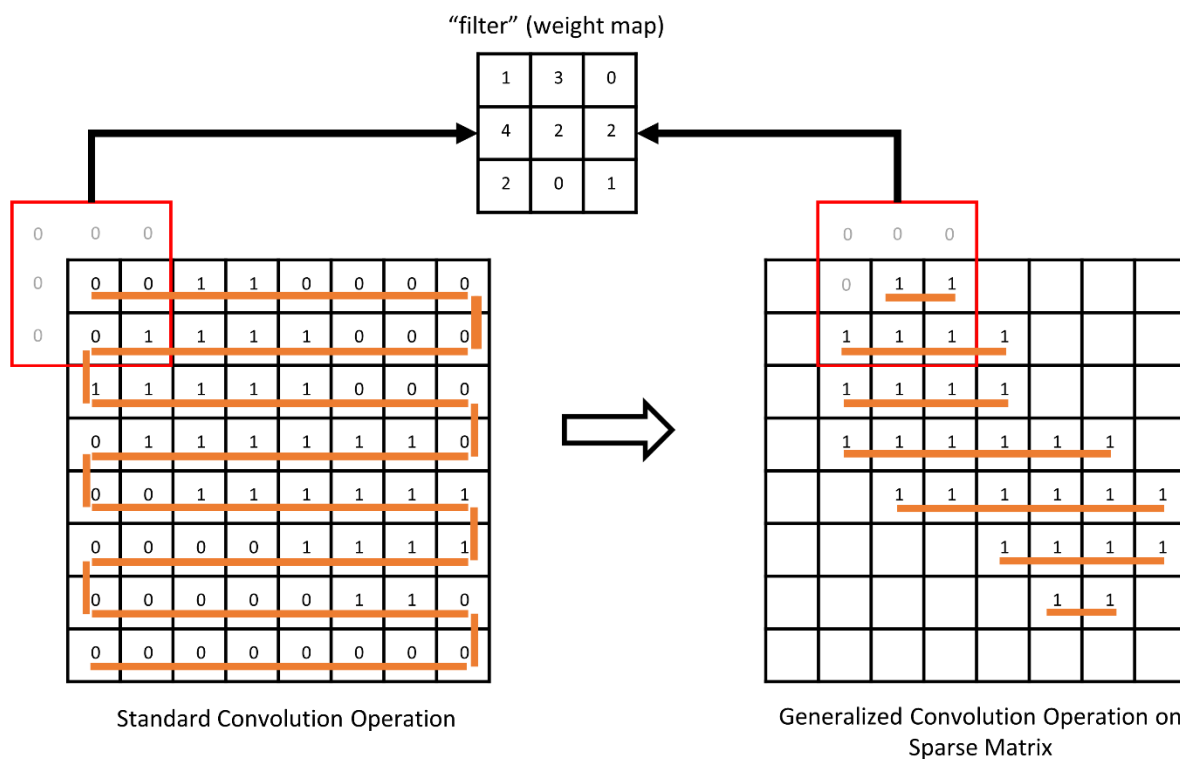


Figure 5-15: Graphical explanation of convolution on a sparse matrix

Pooling is the operation of downsampling the input variables by summarizing the presence of features in each patch [138, 139]. There are two common types of pooling operations. One is average pooling, which summarizes the average presence of the patch. The other is max pooling, which obtains the most activated presence of the input patch. Pooling for sparse data has a similar

concept to the conventional pooling operation. The difference is that the pooling for the sparse data only applies to the occupied voxels instead of the entire 3D matrix. Max pooling is used in this thesis, and it can be represented numerically as

$$O_{i,j,k} = \max I^{(n)}_{(i,j,k)}, (i,j,k) \in C \quad \text{Eq. 5-8}$$

where $O^{(n)}_{i,j,k}$ is the n-th channel of the output value of voxel (i, j, k) , and $I^{(n)}_{(i,j,k)}$ is the n-th channel of the input features of voxel (i, j, k) .

Transpose convolution on the sparse matrix has the same concept as the standard transpose convolution. It is the opposite of the convolutional operation on the sparse matrix, which is also popularly known as deconvolution [136, 137]. It operates in the backward direction of the convolution and performs a one-to-many relationship. For the convolutional operation, the output is always downsizing, but for the transpose convolution, a higher resolution output is ultimately obtained. Another new operation used in our network structure is broadcast, which was proposed by Choy [184]. It can be represented as the following equation:

$$F_u = x_2 \text{ for } u \in C^{in} \quad \text{Eq. 5-9}$$

It is the operation that copies the value x_2 for all input coordinates, and F_u is the new feature values for the input coordinate.

5.2.4. Network structure and learning parameters

Figure 5-16 shows the network structure and major-related hyperparameters for the two-class manufacturability classification. It uses a similar network structure as the voxel-based approach. As mentioned earlier, the design inputs are primarily processed using the sparse convolution operation, and the material and processing inputs pass through an FNN. The two models are integrated and pass through another two fully connected layers to make predictions of

printability. Major hyperparameters include the number of filters or neural units, activation functions, kernel size, and stride size.

Figure 5-17 shows the network structure and major-related hyperparameters for the semantic manufacturability segmentation. As mentioned earlier, the network structure was inspired by the popular ML model, 3D U-net [166]. Unlike the network structure in 3D U-net, our model has two different inputs: design aspects and material and processing aspects. The two inputs are first processed using separable ML operations and then joined to predict the printability map.

In this approach, the best learning rate is set to $1e-4$, the batch size is set to 4, and the epoch number is set to 40 to converge the loss function. These learning parameters are manually tuned to determine the best performance for the current dataset.

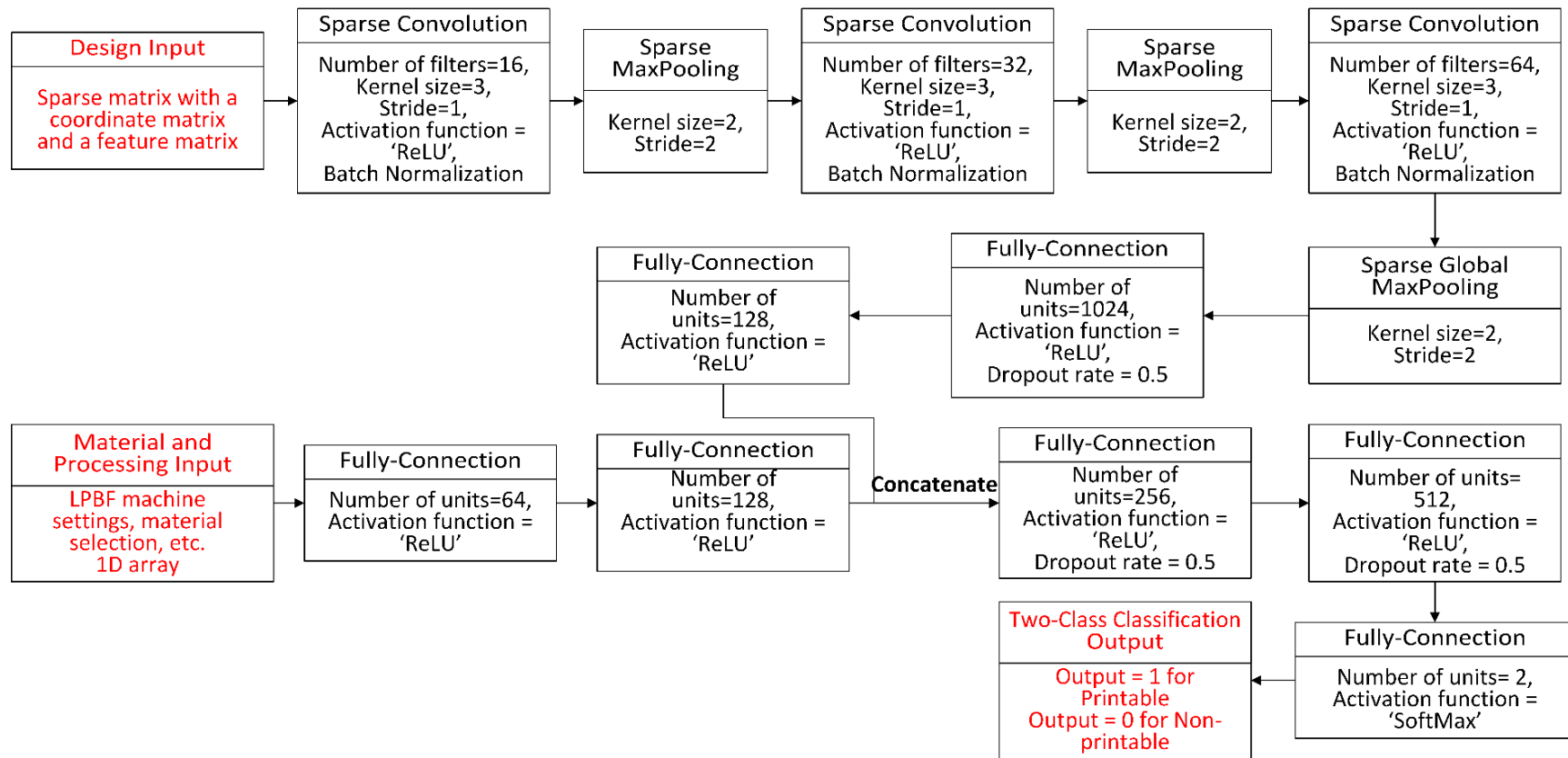


Figure 5-16: Network structure for two-class manufacturability classification

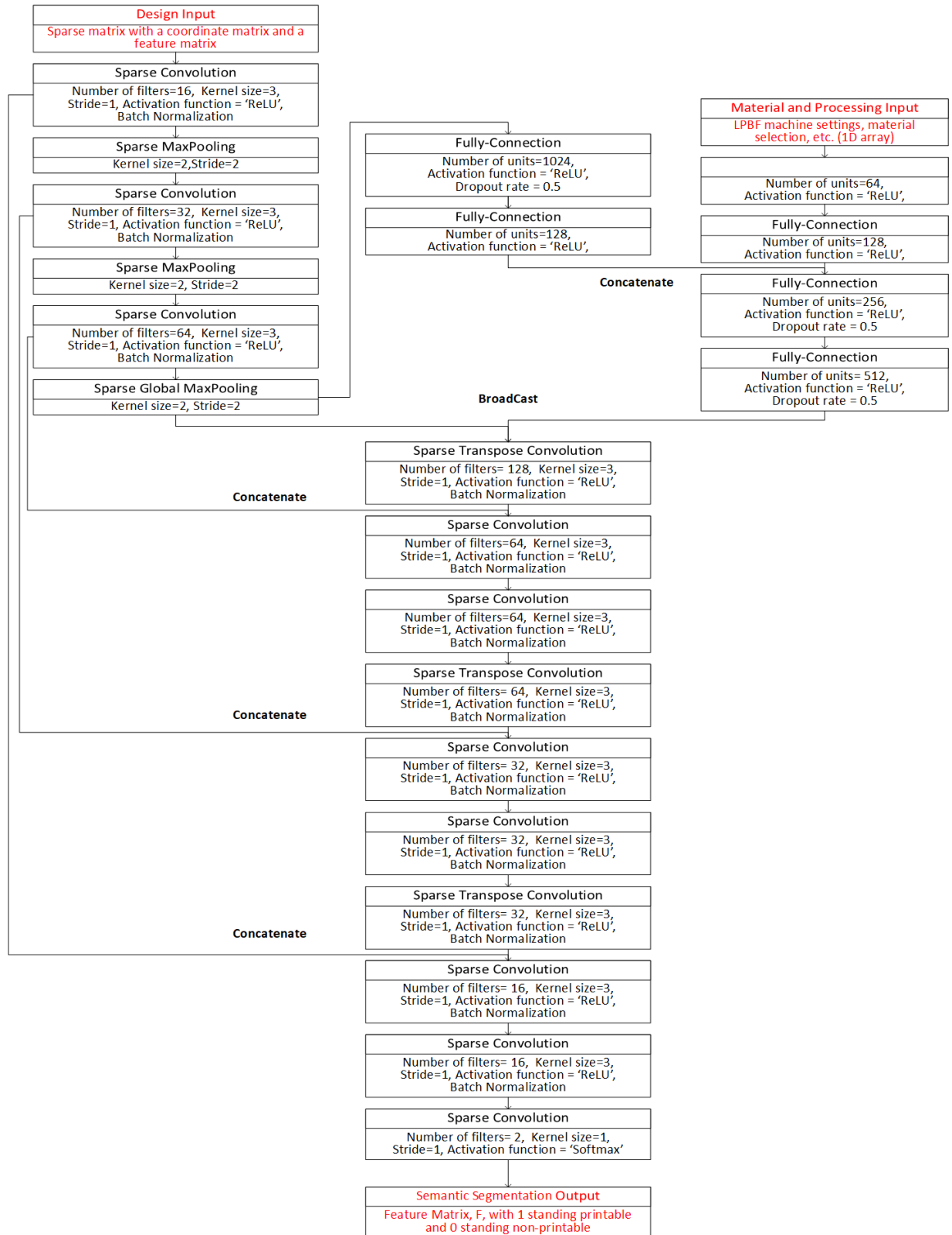


Figure 5-17: Network structure for semantic manufacturability segmentation

5.2.5. Results and discussions

The same dataset as the voxel-based approach was used, and it was split into a 4:1 ratio into training and validation datasets. The training dataset was used to train the ML model, and the validation dataset was used to validate it. Five-fold cross-validation was used for each training to avoid overfitting. The remainder of this chapter discusses the results in predicting whether the given design is printable as well as the generated printability map. It demonstrates that the developed sparse-based CNN model can accurately analyze manufacturability with better performance compared with the voxel-based approach with the same computational capability.

The developed models were implemented in Python 3.7 on an NVIDIA GeForce RTX 2080 Ti. Relevant libraries included Scikit-learn [173], PyTorch, and MinkowskiEngine [184].

5.2.5.1. Two-Class Manufacturability Classification

Table 5-5 shows the cross-validation result for the two-class manufacturability classification at the resolution of 128^3 . The model performance was evaluated on its accuracy, which is represented as $(TP + TN)/(TP + TN + FP + FN)$, where TP indicates a true positive, in which both the prediction and truth are printable. TN indicates a true negative, in which both the prediction and truth are non-printable. FP indicates a false positive, in which the prediction is printable, but the truth is non-printable. FN indicates a false negative, which depicts the opposite results of the FP . The loss function was again selected as the cross-entropy. Cross-entropy is commonly used in ML applications, and it offers the best performance in accuracy for the two-class manufacturability classification. The detailed equation is described in Section 5.1.2. After calculating the average of the cross-validation cases, the accuracy was approximately 0.9174. Compared with the voxel-based approach, which applies convolution to every element in the

matrix, the sparse matrix solution exhibited a better performance with an accuracy of 0.9174 compared with the dense matrix with an accuracy of 0.8404. Moreover, as the cross-validation indicated, the accuracy of each case did not fluctuate significantly which demonstrated the stability of the proposed model, and the model did not suffer overfitting in this dataset. As the dataset is relatively small, a maximum of 8% variations do not consider as a significant change.

Table 5-5: Cross-validation results of the two-class manufacturability classification

Cross-validation Case	Accuracy in sparse matrix	Accuracy in dense matrix
1	0.8776	/
2	0.9388	/
3	0.9592	/
4	0.8776	/
5	0.9388	/
Average	0.9174	0.8408

A memory cost comparison between the sparse and dense matrices is shown in Figure 5-18. The sparse matrix required significantly less memory than the dense matrix for all the voxelization sizes. Note that the sparse matrix could easily fit into a GPU's memory (12 GB) for the resolution of 128. In contrast, the same-size dense matrix could not fit in a single GPU. Computing in the CPU would require more running time.

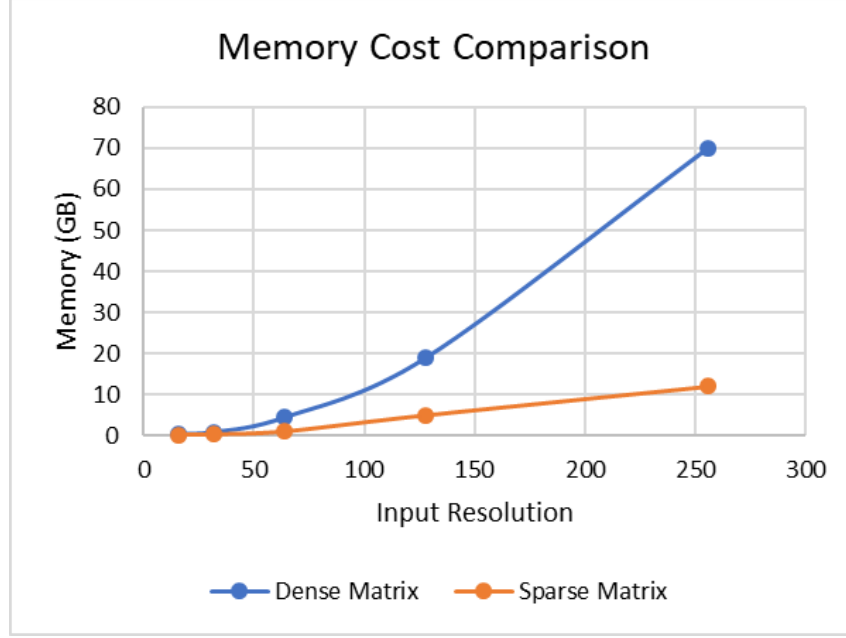


Figure 5-18: Memory cost comparison between the dense and sparse matrices

Overall, using the sparse matrix input data structures significantly decreased the computational cost and improved the model performance. By only considering the occupied voxels and removing the most useless elements which are background, the model demonstrated its capability in predicting the manufacturability of a given design.

Note that the voxel size can be applied up to 256 with a single GPU and the sparse-based approach. However, 128 is used here to compare the results with the voxel-based approach.

5.2.5.2. Semantic Manufacturability Segmentation

Cross-validations were conducted for the semantic manufacturability segmentation. For semantic manufacturability segmentation, the same evaluation metrics, IoU, and loss function, the weighted dice coefficient loss, were used. They are fully explained in Section 5.1.2. For convenience, the weighted dice coefficient is shown here again:

$$loss = \alpha DC_0 + (1 - \alpha) DC_1 \quad \text{Eq. 5-10}$$

$$DC = -\frac{2TP}{2TP + FP + FN} \quad \text{Eq. 5-11}$$

$$IoU = \frac{TP}{TP + FP + FN} \quad \text{Eq. 5-12}$$

Where DC_i is the dice coefficient for the i -th class, and α is the weight coefficient to balance the two classes. α was set to be 0.6 in this approach to emphasize the importance of the non-printable class. A set of selections for α as 0.55, 0.7, and 0.8 was also tested. The value 0.6 was selected because of the best performance. The background, which is the empty class, was not stored in the sparse matrix; hence, it was not trained in the sparse CNN. Therefore, the background was the same as the original, which was counted as 100% correct to compute the mean IoU. Table 5-6 shows the cross-validation result of IoU for each class, as well as the mean IoU, on the resolution of 128.

Table 5-6: Cross-validation results of the semantic manufacturability segmentation

Iteration	IoU_mean	IoU_empty	IoU_print	IoU_non_print
1	0.8386	1	0.7964	0.7195
2	0.8366	1	0.8217	0.6882
3	0.8359	1	0.8105	0.6972
4	0.8293	1	0.7865	0.7013
5	0.8382	1	0.8153	0.6994
Average	0.8357	1	0.8061	0.7011

Table 5-7 compares the average IoU for the voxel-based and sparse-based approaches. The sparse-based approach had a better performance than the voxel-based approach. Particularly for

the non-printable class, the sparse CNN demonstrated a better predictive result than the convolution on a dense matrix.

Table 5-7: Comparison of the dense and sparse matrices

	Average IoU_mean
Sparse Matrix	0.8357
Dense Matrix	0.7951

Qualitative results for two samples are shown in Figures 5-19 and 5-20 to demonstrate the capability of the proposed manufacturability prediction. Figure 5-19 is an example of the solid lattice hybrid structure printed using a Renishaw machine with the material selection of AlSi10Mg. The original design is depicted in Figure 5-19a. It was predicted as fully printable through the proposed sparse-based ML model (Figure 5-19b). Figure 5-19c shows the prediction from the commercial software Materialise Magics. Figure 5-19d shows the experimental result that validated the prediction of the proposed sparse-based ML model. Note that for the figure of the printed result, the support structure has been removed.

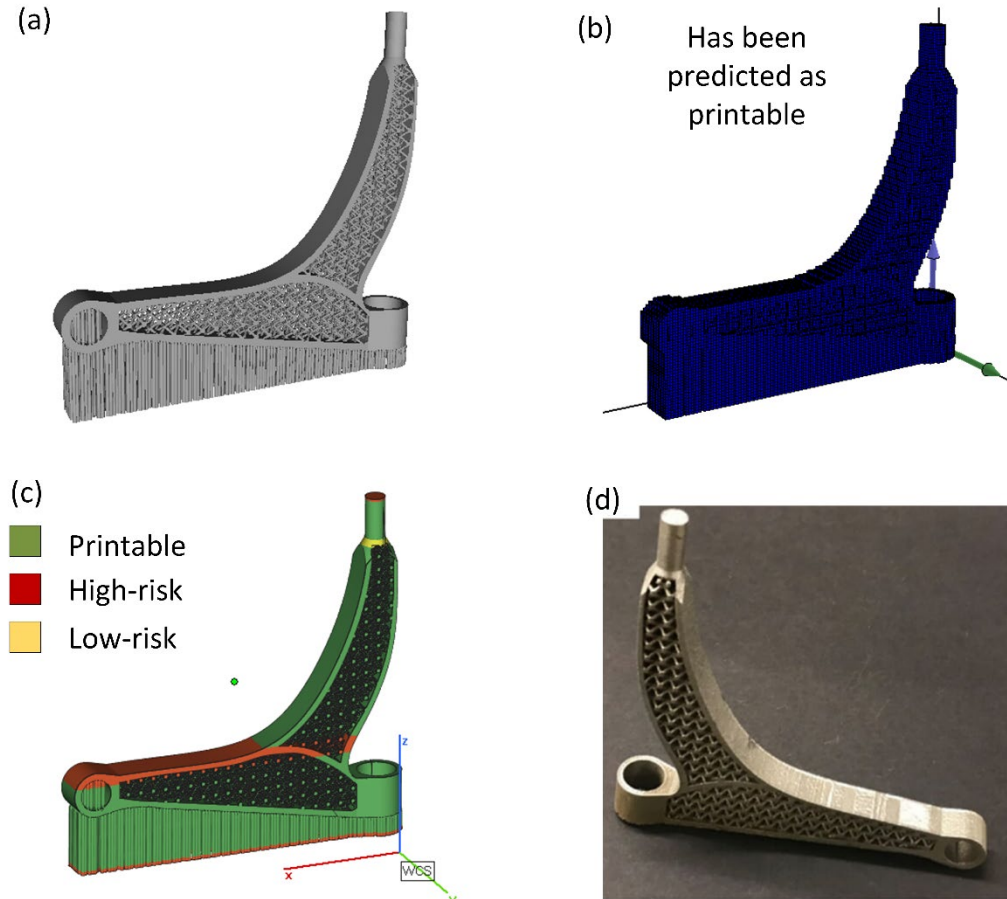


Figure 5-19: Comparison of the (a) original design model, (b) prediction from the two-class manufacturability classification, (c) prediction from the commercial software Materialise Magics, and (d) printed result [185].

Another example is shown in Figure 5-20 of a thin tensile bar printed using a Renishaw machine with the material selection of AlSi10Mg. Figure 5-20b shows the prediction of the proposed sparse-based ML model. The blue color indicates the printable area, and the red color indicates the non-printable area. The result from the commercial software is shown for comparison in Figure 5-20c. The entire tensile bar was defined as non-printable since it suffered from warping (Figure 5-20d). The prediction of the proposed sparse-based ML model was much better than the

prediction of the commercial software. Note that for the figure of the printed result, the support structure has been removed.

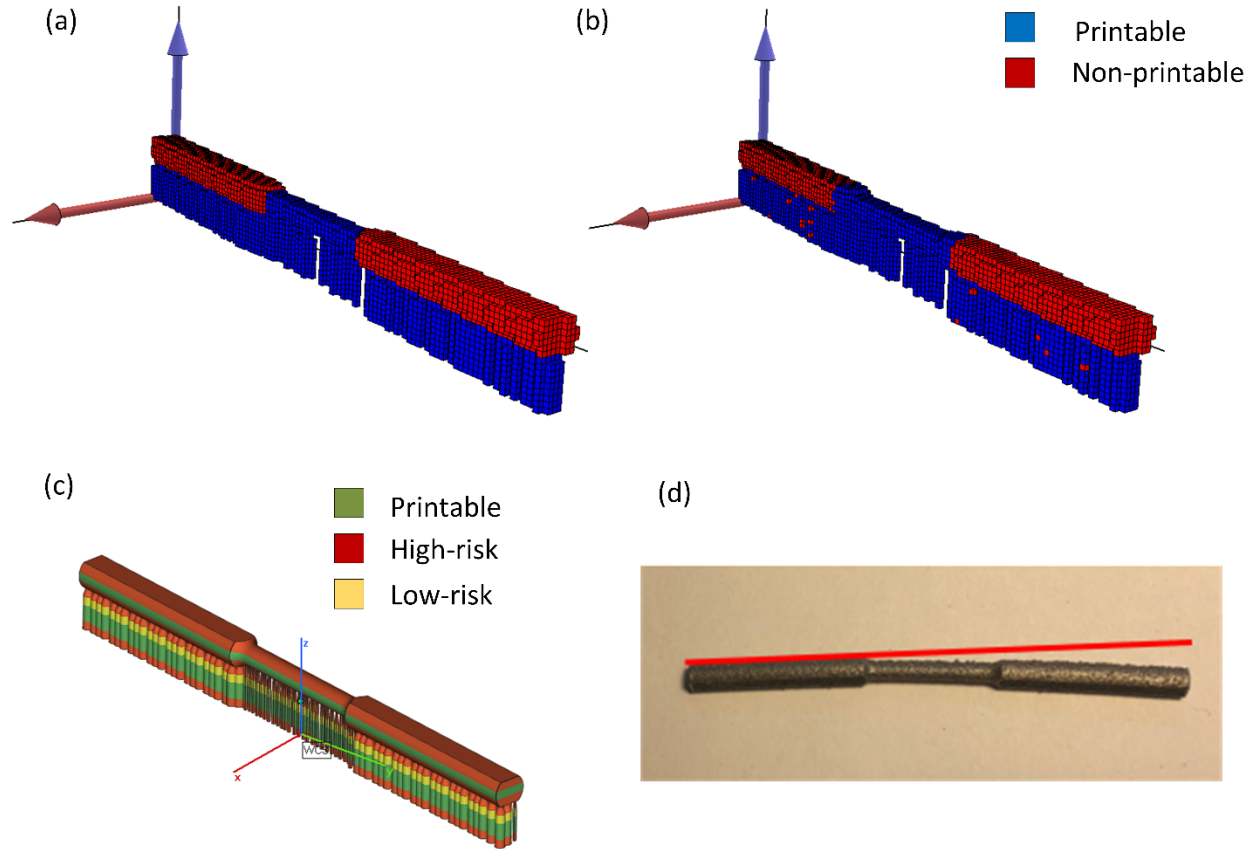


Figure 5-20: Comparison of the (a) ground truth (labeling), (b) prediction from the semantic manufacturability segmentation, (c) prediction from the commercial software Materialise Magics, and (d) printed result.

5.3. Chapter summary

This chapter presents the development of hybrid ML models using both voxel-based and sparse-based approaches as the solution for manufacturability analysis. It introduces the voxel-based approach since it is one of the most popular shape representation types for 3D geometries. A CNN model is applied to the design input and a classic FNN model is applied to the material

and processing input. The two models are merged to make the prediction of manufacturability. The result demonstrates that ML models are suitable approaches to solving manufacturability challenges in AM process. However, the limitation of the voxel-based approach is shown to be the dramatic increase in computational cost when a higher voxelized resolution is used. To solve this problem, an advanced approach using a sparse CNN model is applied in the manufacturability model. The results present a better performance and much lower computational cost than the voxel-based approach. The ML-assisted models are the key to this thesis, and they are utilized in the recommendation system, which is introduced in the next chapter.

Chapter 6. MAR-AM Recommendation system

This aims to develop a recommendation system as part of the MAR-AM to provide recommendations to assist novice AM users to obtain printable parts. In Chapter 5, the developed ML models are evaluated in the LPBF process. The network structures and learning parameters are tuned to fit the best of the current dataset. However, the framework can also be adapted to other AM techniques with simple modifications to the parameters of ML models and selections of the process parameters. For the recommendation system, instead of the LPBF process, FDM is introduced to validate the approach owing to the larger amount of valuable data. Section 6.1 explains the ML model development for FDM. Thereafter, the methodology for the recommendation system is introduced in Section 6.2. Sections 6.3 and 6.4 describe the methods to generate the potential variations in design aspects and material and processing information, respectively. Finally, this chapter is summarized.

6.1. ML-assisted manufacturability model for FDM

The hybrid sparse-based models developed in Section 5.2 are introduced here to train the FDM data with the same ML architectures as LPBF. However, as the process settings and material selection differ between FDM and LPBF, the input features for material and processing information are reselected, and example input features are shown in Table 2. Note that scale is a special factor in the table, and it is obtained from the design model. The scale parameter is also indicated as it is also considered a decisive parameter.

Table 6-1: Selected ML input features for material and processing information

Decisive parameters	Units	Source	Example # 1	Example # 2
Material type		User	PLA	ABS
Material density	g/cm ³	User	1.24	1.04
Printing speed	mm/s	User	80	60
Layer thickness	mm	User	0.15	0.15
Infill percent	%	User	20	20
Adhesion type		User	Brim	Brim
Nozzle temperature	°C	User	200	235
Bed temperature	°C	User	60	80
Scale		CAD	5.23	1

A graphical view of the general training procedure for developed ML models is presented in Figure 6-1. The entire ML-assisted manufacturability model comprises two submodels: two-class manufacturability classification and semantic manufacturability segmentation. To train the two-class manufacturability classification model, the geometric 3D model in STL format is first converted into a sparse matrix. Meanwhile, the material and processing information in tabular format is applied with a one-hot encoding method. The label with the mark of printability is turned into the number (0 or 1). Thereafter, the data with labels, the design matrix, and material and processing information array are used to train the two-class manufacturability classification model. The semantic manufacturability segmentation model operates similarly to the two-class manufacturability classification, the only difference being the data preprocessing for labels. Instead of using a single number to indicate manufacturability, the area of failure is marked in

voxels and converted into a sparse matrix. It indicates the printability map of the given design. Finally, the hyperparameters must be tuned to obtain the best performance. The accuracy for the two-class manufacturability classification model after the five-fold cross-validations in FDM data was 0.9674. The average *IoU_mean* after the five-fold cross-validations was 0.8564.

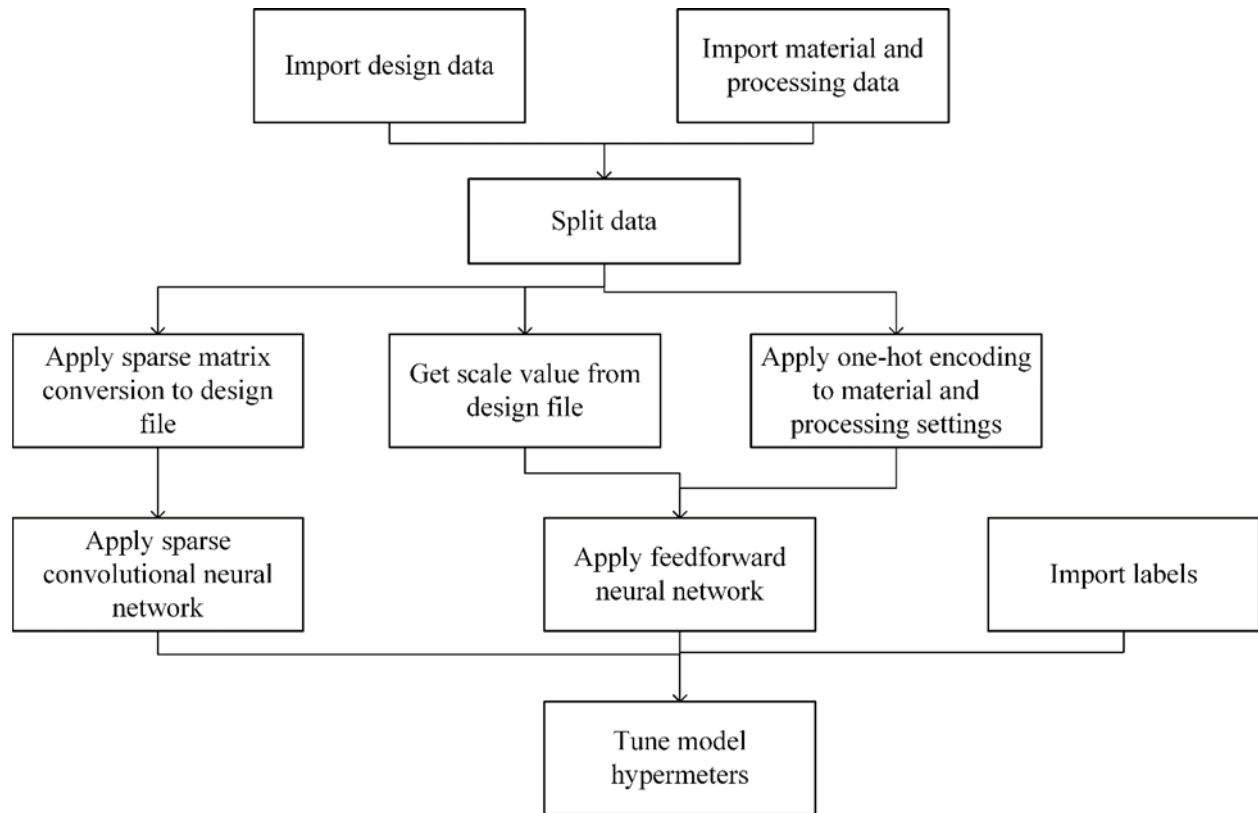


Figure 6-1: Graphical view of ML training procedure

When the two sub-ML models are trained, the models are saved and used as the manufacturability analyzer. When the new data is input, the design file is transferred to the sparse matrix and the selections of the material and processing information are transferred to an array using one-hot encoding. Thereafter, the input data is sent to the saved two-class manufacturability classification model to make the prediction. Furthermore, if the given design with the selected material and processing information is predicted as non-printable, the same input data is then sent

to the saved semantic manufacturability segmentation model to predict the printability map. The printability map is given to users to demonstrate the problematic geometric features. These saved trained ML models are the key to the recommendation system.

6.2. Proposed structure and algorithm of closed-loop recommendation system

The recommender system is expected to produce suggestions to assist users in making decisions for potential changes. In the manufacturability recommender system, when the given design passes the manufacturability analyzer, users can expect successful printing with the selected machine and material settings. However, if the assessment fails, the recommendation of potential changes to obtain a successful printing is required. With the aid of the recommender system, users are more likely to have their design successfully printed through AM process. More details on the operation of the closed-loop recommendation system are described in the following.

Figure 6-2 shows the flowchart of the recommender system. With the well-trained saved ML models, it provides predictions according to the user input. If the input of the given design and selected process settings is not printable, it will then pass through a closed-loop process to determine the first possible variation that can pass the ML prediction. The variation is served as recommendations for the user to increase their printing success rate. More than one solution may be available to make the printing successful. However, in this case, the first potential variation is provided as the recommendation since there is no optimal option, and the variation is analyzed in the order of time and cost consumption. The details on generating variations are depicted in the next sections. Moreover, the recommendation system was validated using case studies, which are described in Chapter 7.

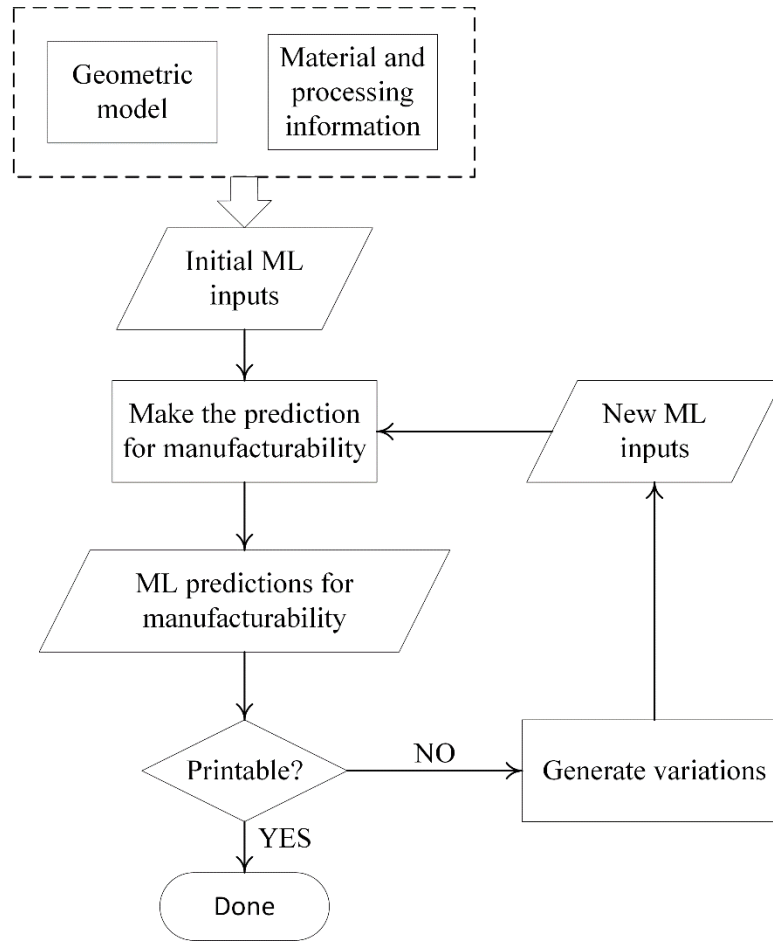


Figure 6-2: Flowchart of the recommender system

To better illustrate the systematic recommendation approach, the proposed algorithm is presented in the following with step-by-step produce. Ultimaker 3 is the only AM machine recorded for ME in the current developed database. Therefore, the factor, AM machine, is not considered in the current recommendation system. However, it can be included in future development.

Step 1. Obtain user inputs of design model and material and processing settings.

Step 2. Obtain the manufacturability prediction with the selected design model and material and processing settings

- a. if the result is not printable, obtain and printability map and go to step 3.
- b. else go to step 14.

- Step 3.** Determine the build orientation for the least overhangs, and obtain the manufacturability prediction with the new design model.
- if the result is not printable, go to step 4.
 - else store the variation made and go to step 13.
- Step 4.** Determine the build orientation for the most contacting faces to the build plate, and obtain the manufacturability prediction with the new design model.
- if the result is not printable, go to step 5.
 - else store the variation made and go to step 13.
- Step 5.** Based on the material selection, change all the material and processing settings to the default, and obtain the manufacturability prediction with new material and processing settings
- if the result is not printable, go to step 6.
 - else store the variation made and go to step 13.
- Step 6.** Vary the bed_temp from the leftmost element of the bed_temp variations, and one by one obtain the manufacturability prediction with the new bed_temp setting.
- If the prediction result is not printable, go to step 7.
 - else store the variation made and go to step 13.
- Step 7.** Vary the nozzle_temp from the leftmost element of the nozzle_temp variations, and one by one obtain the manufacturability prediction with the new nozzle_temp setting.
- If the prediction result is not printable, go to step 8.
 - else store the variation made and go to step 13.
- Step 8.** Vary the adhesion from the leftmost element of the adhesion variations, and one by one obtain the manufacturability prediction with the new adhesion setting.
- If the prediction result is not printable, go to step 9.
 - else store the variation made and go to step 13.
- Step 9.** Vary the printing_speed from the leftmost element of the printing_speed variations, and one by one obtain the manufacturability prediction with the new printing_speed setting.
- If the prediction result is not printable, go to step 10.
 - else store the variation made and go to step 13.
- Step 10.** Vary the infill_percent from the leftmost element of the infill_percent, and one by one obtain the manufacturability prediction with the new infill_percent setting.

- a. If the prediction result is not printable, go to step 11.
 - b. else store the variation made and go to step 13.
- Step 11.** Vary the layer_thick from the leftmost element of the layer_thick variations, and one by one obtain the manufacturability prediction with the new layer_thick setting.
- a. If the prediction result is not printable, go to step 12.
 - b. else store the variation made and go to step 13.
- Step 12.** Vary the mat_type from the leftmost element of the mat_type variations one by one and go back to step 5.
- Step 13.** Check if your variation is empty or not
- a. If yes, return “Your part needs some design modifications before you print it’ and the printability map
 - b. If no, return “Your part needs some modifications before you print it, and here is the recommendation:”, the printability map and variation made.
- Step 14.** Return “Congratulations! Your part is ready to print”

6.3. Potential variations in the design aspect

Potential changes can be made in either machine and material settings or specifications of the design. For the design aspect (Table 6-2), build orientation is considered as a potential change that can be made to improve the printing process. Some of the existing studies considered the build orientation as the process setting. In this thesis, the build orientation is considered a design-related factor since by changing the build orientation, the design matrix is modified in our approach. It is combined with the selected process settings as the new ML inputs. Many studies on optimizing build orientation have been conducted [122, 186, 187]. For single-objective optimization, the optimal build direction can be detected by optimizing for a single factor without considering the conflicts with the other factors. Such studies include minimizing the support volume, volumetric error, or cylindricity and flatness error, build time and maximizing the surface quality. An advanced approach with multiple objective optimizations has also been proposed. This approach considers multiple factors and expresses a weight function for each factor. For the recommendation

system in this thesis, as part of manufacturability analysis, the easiness of printing is the focus. Factors such as build time and flatness error are not considered at the current stage. Moreover, as mentioned in Section 6.2.1, there is no optimal case and only the first variation that makes the printing successful is provided. Therefore, for the current recommendation system, the build orientation with the least overhangs and the build orientation with the most contacting area to the build plate are the two potential changes. Moreover, to indicate problematic areas, the printability map predicted by the ML model is provided. Designers can make design modifications based on the indication of the potential failure areas.

Table 6-2: Potential variations for design aspects

	Variations	
Build orientations	Least overhangs	Most contacting areas to the build plate
Problematic areas	The printability map is provided.	

6.3.1. Build orientation with the least overhang

Build orientations with the least overhangs refers to minimizing the total area of the downward-facing facets. It is considered to have more impact on the object accuracy than the support volume [188, 189]. The objective function is expressed as

$$\text{Minimize } SA = \sum_i A_i |\hat{d} \cdot \hat{n}_i| \phi \quad \text{Eq. 6-1}$$

$$\text{where } \phi = \begin{cases} 1 & \text{if } \hat{d} \cdot \hat{n}_i < 0 \\ 0 & \text{if } \hat{d} \cdot \hat{n}_i > 0 \end{cases}$$

where A_i is the area of the i -th facet, \hat{d} is the unit vector of the build direction, and \hat{n}_i is the unit normal vector of the i -th facet. The build direction is obtained from the generated list of build orientations. To decrease the number of loops, the list of orientations is gathered from the area cumulation approach and death star algorithm [190]. The principle of the area cumulation is to cumulate the facet's sizes with identical orientations to identify the first several potential candidates for the optimal orientation. The death star algorithm functions as the complementary of the area cumulation algorithm when the bottom area is a circle without any resulting area.

6.3.2. Build orientation with the most contacting area to the build plate

To determine the build orientation with the most contacting area, the first step is to determine the orientated bounding box (OBB) of the given design and determine the direction with the largest contacting face between the design and the face of the OBB. The main steps of the algorithm are presented as

Algorithm: Determine the build orientation with the most contacting area to the build plate

Input: Design mesh file: **design**

Output: Build direction with the most contacting area to the build plate

```
1. function design_opt_most_contact(design)
2.     obb_design = Flat(OBB(design))
3.     scale = max bound extents(obb_design)
4.     voxels = Voxelized(obb_design, scale/64)
5.     target_list = [sum(voxels[0, :, :]), sum(voxels[-1, :, :]), sum(voxels[:, 0, :]),
        sum(voxels[:, -1, :]), sum(voxels[:, :, 0]), sum(voxels[:, :, -1])]]
6.     index = target_list.index(max(target_list))
7.     direction_list = [[0,1,0],[0,1,0],[1,0,0],[1,0,0],[1,0,0],[1,0,0]]
8.     return direction = direction_list (index)
9.     end function
```

The input of this algorithm is the design mesh file, and the output is a new build direction. The new design matrix is computed by applying the rotation matrix of both the new build direction and rotating the angle of the OBB to the original design matrix. The new design matrix is then sent to the ML models for another round of the prediction.

6.4. Potential variations in material and processing information

The potential variations in material and processing information result from the decisive parameters used in ML models. Table 6-3 presents the potential variations for material and processing information aspects. For the process aspect, the default settings are selected for the first

attempt. The default settings are recommended by the machine and material makers or AM experts. If the default values fail, the remaining potential variations are tested accordingly. All the variations differ from a certain range of the default value. The priority order is increasing from the top to the bottom, which means that the recommender considers varying the setting in the order of bed temperature, nozzle temperature, adhesion type, printing speed, layer thickness, and material type.

Table 6-3: Potential variations for process aspects

Parameters	Default	Variations			
Machine	Ultimaker 3	Only Ultimaker 3 for now. Can be expanded in the future			
Mat_Brand	Ultimaker	Only Ultimaker for now. Can be expanded in the future			
Mat_Type	PLA	[PLA, ABS, PC, nylon]			
Layer_Thickness	0.15	[0.15,0.1,0.2,0.06]			
Infill_Percent	20	[20,40,60,80,100]			
Printing_Speed	80 for PLA; 60 for ABS; 50 for PC; 70 for nylon	[80, 70, 90, 60, 100, 50, 40] for PLA	[60, 50, 70, 40, 80] for ABS	[50, 40, 60, 30, 70] for PC	[40, 50, 60, 70, 80, 90] for nylon
Adhesion	Brim for PLA, ABS, nylon; Raft with gap of 0.25 mm for PC	[Brim, Raft with a gap of 0.25 mm, None, Raft with a gap of 0.15 mm, Raft with a gap of 0.05 mm]			

Nozzle_Temp	200 for PLA; 235 for ABS; 280 for PC; 250 for nylon	[200, 205, 195, 210, 190, 215, 185, 220, 180, 225, 230] for PLA	[235, 240, 230, 245, 225, 250, 220, 215, 210] for ABS	[280, 285, 275, 290, 270, 265, 260] for PC	[250, 255, 245, 260, 240] for nylon
Bed_Temp	60 for PLA; 80 for ABS; 107 for PC; 60 for nylon	[60, 65, 55, 70, 50, 75, 45, 40] for PLA	[80, 85, 90, 95, 100, 105, 110] for ABS	[107, 110, 105, 115, 100, 120, 95, 90, 85, 80] for PC	[60, 65, 70, 75, 80, 85, 90, 95, 100] for nylon

At the current stage, variations result from the decisive parameters. As some of the key parameters have not been considered in this model, such as chamber temperature due to the limitation of the experimental setup, the potential variations related to these parameters have not been listed here. However, it is worth investigating these parameters and including them in the database. Case studies to validate the recommendation system, with the implementation of the tool and deployment, are described in the next chapter.

6.5. Chapter summary

This chapter proposes a recommendation system that aims to provide suggestions for users to increase the printing success rate. The proposed methodology is validated in the next chapter as the final delivery of this thesis. The FDM is discussed here to validate the capability of MAR-AM, and a general training procedure for the developed ML models is provided. With the ML architectures remaining the same, the developed ML models can be adapted to other AM technologies through a small number of changes in the selection of the input features and hyperparameters. The input features include geometric information and process and material

information. As the process and material information are different for each AM technique, these features are reselected based on the understanding of the FDM process. By following the proposed ML training procedure, the developed ML model for analyzing the manufacturability of FDM has good performance with satisfying accuracy. The well-trained model is then used as the manufacturability prediction model in MAR-AM.

To support the closed-loop recommendation system, the input of the design, material, and process first pass through the well-trained ML model to predict printability. If the part is not printable, the recommender searches all the potential variations in build orientations, material settings, and processing settings to determine the solution. The algorithms to generate these variations are also explained in this chapter. Moreover, if there are no possible solutions, the printability map is provided for users to make the decisions on the design modification. The next chapter describes the methodology of the recommendation system combined with the well-trained ML models being implemented into a web-based application, and case studies to validate the approach are described.

Chapter 7. Implementation and case studies

Based on the proposed core flows of the MAR-AM, a web-based tool has been developed to better assist engineers to utilize the MAR-AM. The main aim is to provide novice AM designers with an automated, easy-to-access, and comprehensive analyzer and recommender to avoid unnecessary printing failure before the real fabrication. In this chapter, the web-based implementation and deployment are fully explained. User interfaces are demonstrated to illustrate the operation of the developed MAR-AM. Finally, multiple case studies are described to demonstrate the capability of the developed MAR-AM, and the limitation is discussed based on the case studies. This chapter is concluded with a summary of the contribution and future research.

7.1. Web-based implementation and deployment

The proposed framework of MAR-AM has been implemented into a web-based application. The new user data will be collected regularly to update the ML models to provide the best performance for users. The developed tool is available on GitHub. The architecture and user interface of the MAR-AM are depicted in the following contents.

7.1.1. Architecture

The web-based application primarily consists of two parts: frontend and backend (Figure 7-1). The frontend provides a user-friendly interface, and the backend addresses business logic and data storage. In the application, the frontend was developed using JavaScript, CSS, and HTML. Three.js [191] was used as the STL viewer. It is an open-source JavaScript library used to create and display 3D computer graphics. The backend was developed using Python. Flask was also used as the web framework to connect the user interface and backend logic, including ML prediction

and closed-loop recommendation. It operates as the liaison to communicate the frontend and backend.



Figure 7-1: High-level architecture of the developed webpage

The overall framework of the developed web-based MAR-AM is presented in Figure 7-2. The application consists of three hierarchical layers: UI, logic, and data access layers. The UI layer provides an interactive layer to acquire necessary inputs from users and visualize the results. As Figure 7-2 shows, there are two main web pages for this application: the main and result pages. The main page was designed to request users to input setup information including uploading the design and defining the AM process, AM machine, material, and machine settings. All the extracted texted information is saved in a JSON file. The screen module is responsible for visualizing 3D models for both the original model and printability map to aid users to have a better concept of their design. On the result page, users are also encouraged to provide feedback based on the performance of the MAR-AM.

The logic layer provides the most critical functions for MAR-AM. Modules in this layer were developed for specific functions. As shown in Figure 7-2, this layer includes a data preprocessing module, ML prediction module, closed-loop recommendation module, build orientation module, printability map generation module, and auto ML model update module. The auto ML model update module is included only for completeness, but they are not developed in the current version. The data preprocessing module is dedicated to processing the user inputs to

the demanded ML inputs. The ML prediction module makes the prediction of the manufacturability for the given inputs. The closed-loop recommendation module generates the suggestion for users to increase the printing success rate with the aid of the build orientation module to generate the potential build orientations. The printability map generation module generates the printability map to demonstrate potential problematic areas to users.

The data access layer contains the following modules: file read and write module, AM database, and user feedback database. The file read and write module was developed to serialize and deserialize JSON and STL files (STL is the only design file format accepted in the current version). The AM database was established to train the ML models. The user feedback database is not included in the current version but is described here for completeness. It will be used to store the user feedback, which will be used to update the ML models.

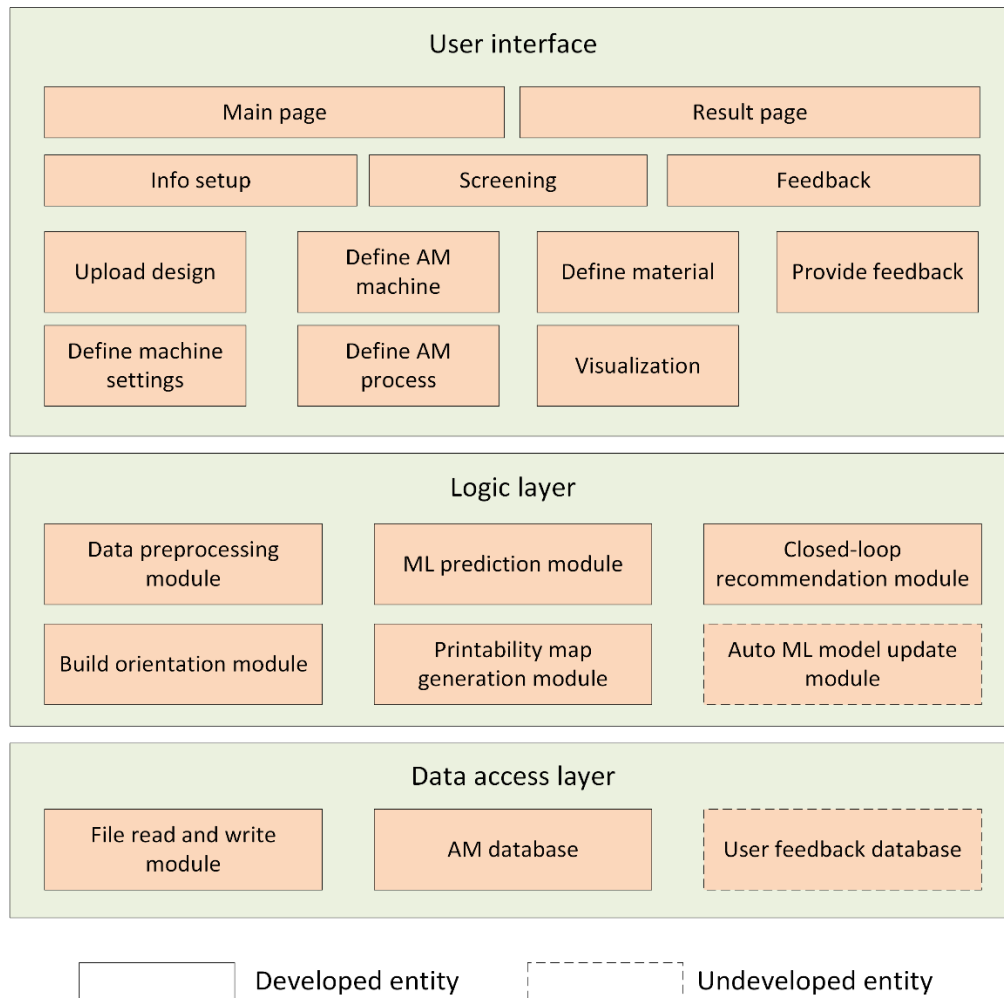


Figure 7-2: Framework of the developed web-based tool

7.1.2. User interfaces

The user interfaces consist of two major web pages: the main and result pages. As shown in Figure 7-3a, the main page was developed for users to input their selections for process settings and upload their design files in STL format. On the right panel of the webpage, the user can view their uploaded design file. When all the required fields are filled, the user can click the submit button to analyze the design (Figure 7-3b).

Manufacturability Analyzer and Recommender for Additive Manufacturing (MAR-AM)

Step1: Enter your process and material information

Type of AM technology:
Fused filament fabrication ▼

Machine Brand:
Ultimaker ▼

Machine Series:
Ultimaker 3 ▼

Material Type:
PLA ▼

Material Density (g/cm³):

Layer Thickness (mm):

Infill Percent (%):

Printing Speed (mm/s):

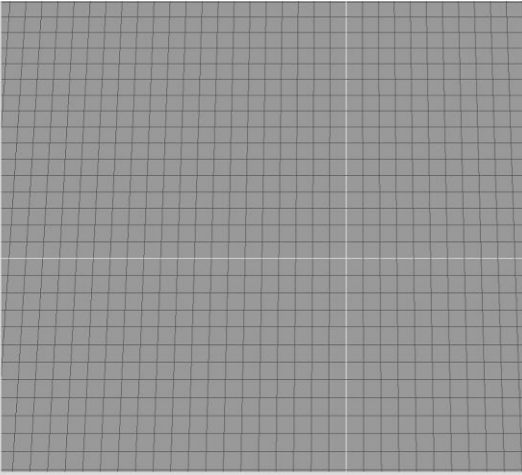
Adhesion Type:
 Brim ▼

Nozzle Temperature (°C):

Bed Temperature (°C):

Step2: Load your STL model (it should include your support)

You are all set! Please submit to see the results.



(a) Main page

Manufacturability Analyzer and Recommender for Additive Manufacturing (MAR-AM)

Step1: Enter your process and material information

Type of AM technology:
Fused filament fabrication ▼

Machine Brand:
Ultimaker ▼

Machine Series:
Ultimaker 3 ▼

Material Type:
PLA ▼

Material Density (g/cm³):

Layer Thickness (mm):

Infill Percent (%):

Printing Speed (mm/s):

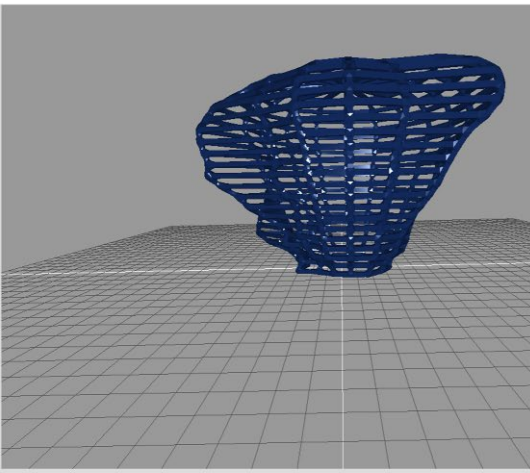
Adhesion Type:
 Brim ▼

Nozzle Temperature (°C):

Bed Temperature (°C):

Step2: Load your STL model (it should include your support)

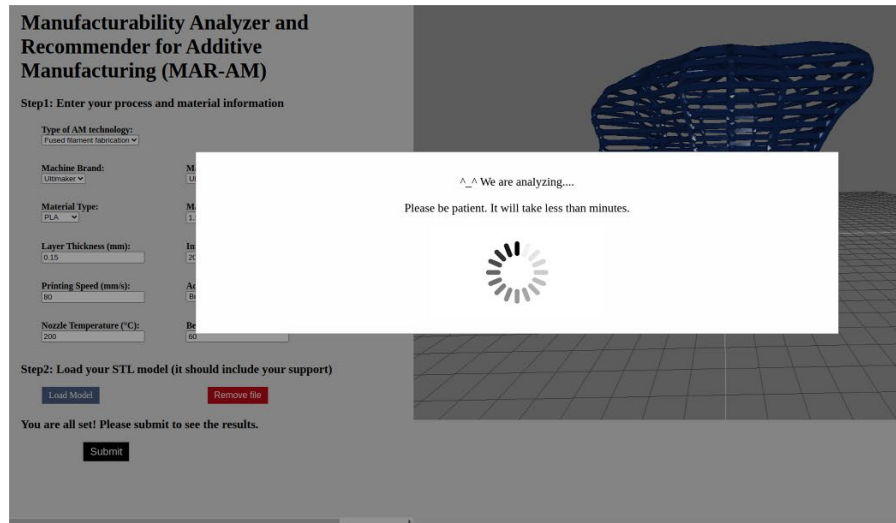
You are all set! Please submit to see the results.



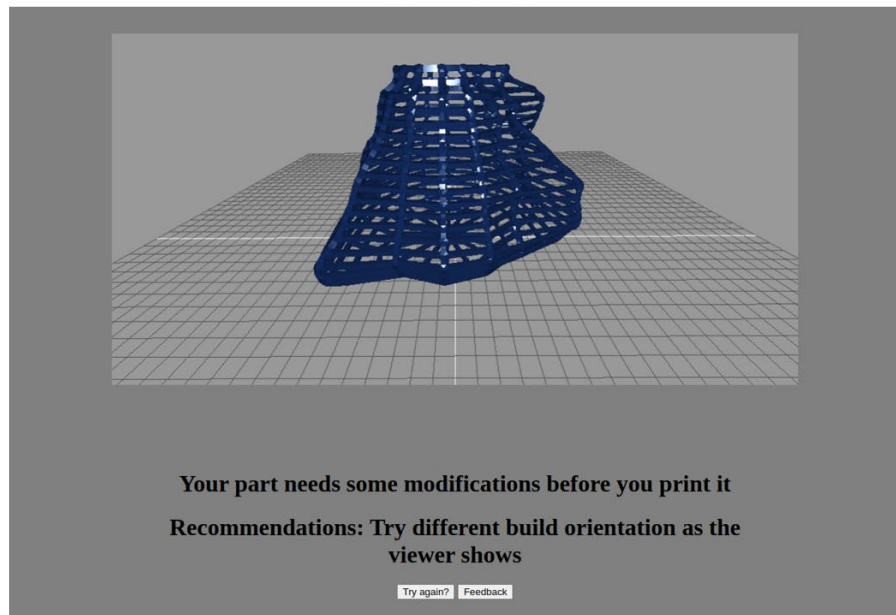
(b) Loading inputs

Figure 7-3: User interfaces of the MAR-AM: Main page

MAR-AM begins to analyze your input and the analysis is often less than a minute (Figure 7-4a). Figure 7-4b shows the result webpage. On this page, users can view the prediction results as well as recommendations for potential modifications. The visualization of the results is placed on the top of the webpage. The original design is in blue, and the potentially problematic areas are marked in red.



(a) Analyzing



(b) Result page

Figure 7-4: User interfaces of the MAR-AM: Results page

Furthermore, users are invited to provide their feedback for MAR-AM by clicking the feedback button. As shown in Figure 7-5, a simple survey appears to let users express their opinions and agreement with the prediction. Their feedback is uploaded continuously to the developer side. The trained ML model is updated based on users' agreement with the predictions regularly.

Overall, do you satisfied MAR-AM?

Do you agree with our prediction?

Have you print it to validate our analysis?

Any comments?

Recommendations: Try different build orientation as the viewer shows

Feedback page

Figure 7-5: User interfaces of the MAR-AM: Feedback page

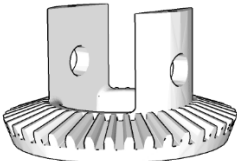
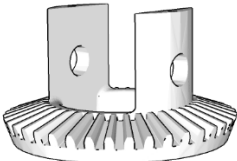
7.2. Case studies

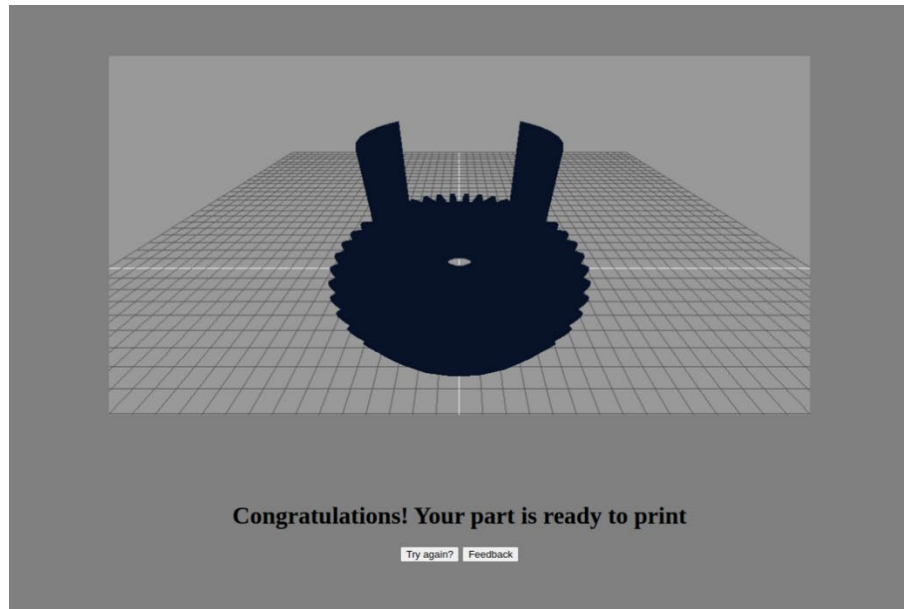
In this section, multiple case studies to validate the effectiveness of the proposed web-based MAR-AM are described. Four cases are fully explained in the following sections to demonstrate how MAR-AM works. These cases are selected to demonstrate the capability of the manufacturability prediction and the effectiveness of the recommendation in both material and machine settings and design modification. The presented material and machine selections are the original user inputs to the web-based MAR-AM.

7.2.1. Case 1: Simple customized mechanical parts

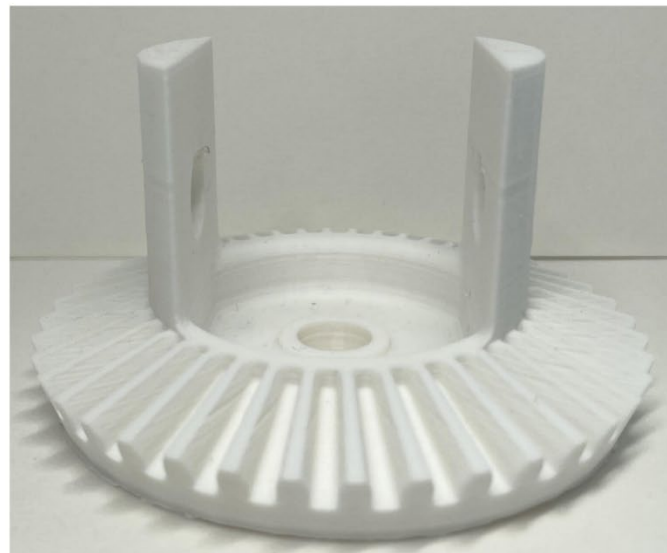
The first sample was a simple mechanical bevel gear obtained from the Thingi10K database. The detailed printing information for the gear is listed in Table 7-1. It was originally selected to be printed in ABS with default machine settings. The potential problem in this part was the two lateral holes. Large round lateral holes may need support for printing, otherwise, distortion may occur. There is a certain limitation on the hole size to avoid support structures. For the selected mechanical bevel gear, the two lateral holes were under the limit and can be printed without any support structures. The MAR-AM offered the prediction result as printable (Figure 7-6a). To validate the approach, the part with selected settings was printed, and the experimental result is presented in Figure 7-6b. The MAR-AM successfully predicted the printability of the simple mechanical bevel gear.

Table 7-1: Detailed printing information of the gear

Name	Figure of design	Machine brand Machine series	Material type Material density (g/cm ³)	Layer thickness (mm)
				Infill percent (%)
Bevel gear		Ultimaker Ultimaker 3	ABS 1.04	Printing speed (mm/s)
				Adhesion type
				Nozzle Temperature (°C)
				Bed Temperature (°C)
				0.15
				20
				60
Bevel gear		Ultimaker Ultimaker 3	ABS 1.04	Brim
				235
				80



(a)

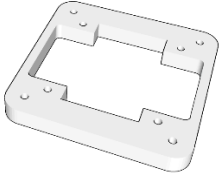

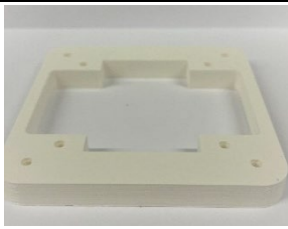
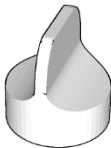
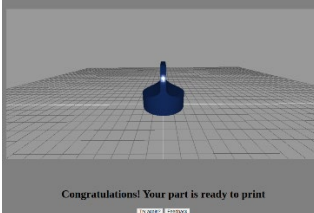
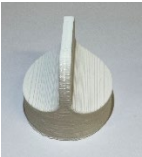

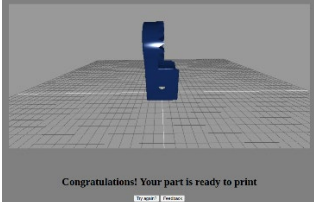
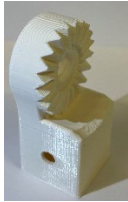
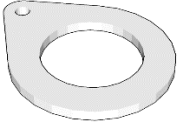




(b)

Figure 7-6: (a) Prediction of bevel gear (b) printing result of bevel gear

Several similar samples (listed in Table 7-2) were conducted to validate the proposed methodology. They were customized parts selected from some industrial applications. They were predicted as printable by the MAR-AM, and experimental results were conducted to validate the predictions.

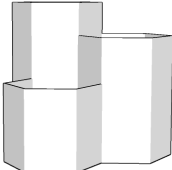
Table 7-2: More successfully printed case studies

Name	Figure of design	Machine brand Machine series	Material type Material density (g/cm ³)	Layer thickness (mm) Infill percent (%) Printing speed (mm/s) Adhesion type Nozzle Temperature (°C) Bed Temperature (°C)	MAR-AM prediction	Experimental validation
Adapter		Ultimaker Ultimaker 3	ABS 1.04	0.15 20 60 Brim 235 80		
Knob		Ultimaker Ultimaker 3	ABS 1.04	0.15 20 60 Brim 235 80		
Connector		Ultimaker Ultimaker 3	ABS 1.04	0.15 20 60 Brim 235 80		
Ring		Ultimaker Ultimaker 3	PC 1.19	0.15 20 50 Raft with gap of 0.25 mm 280 107		

7.2.2. Case 2: Material-related and process-related demo

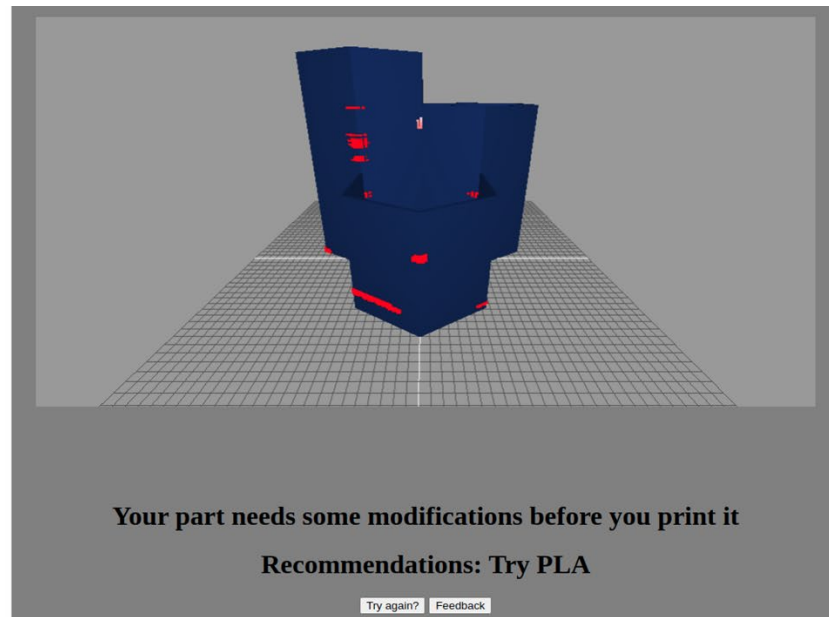
The first sample demonstrated in the second case was a hexagonal organizer provided by a fellow AM expert. It was originally selected to be printed in ABS with default machine settings (Table 7-3). As demonstrated in Figure 7-7a, the MAR-AM predicted that the part was not printable and required some modification. Moreover, it also provided the recommendation to change the material type from ABS to PLA.

Table 7-3: Detailed printing information of the organizer

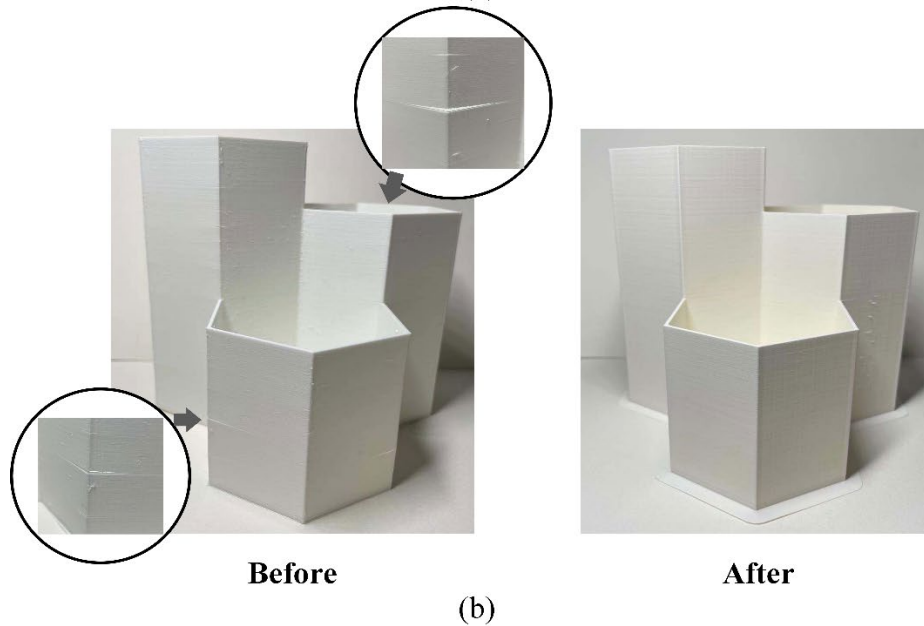
Name	Figure of design	Machine brand Machine series	Material type Material density (g/cm ³)	Layer thickness (mm) Infill percent (%) Printing speed (mm/s) Adhesion type Nozzle Temperature (°C) Bed Temperature (°C)
Hexagonal organizer		Ultimaker Ultimaker 3	ABS 1.04	0.2 20 60 Brim 235 80

To validate the prediction and recommendation, the hexagonal organizer was printed using both ABS and PLA, and the printing results are shown in Figure 7-7b. The experimental results confirmed the effectiveness of the proposed MAR-AM. The main problem with the hexagonal organizer was cracks on the wall. They were caused by the release of residual stress during the printing process. The hexagonal organizer consisted of large and thin walls, which could not endure the residual stress while printing. Thus, cracks occurred on the fabricated part. Compared with the ABS, PLA has a lower thermal expansion coefficient, which resulted in less deformation during the printing. Another solution might be available, which is to have a closed chamber with

a higher chamber temperature for printing ABS. However, the current database only contains Ultimaker 3, which is an open-chamber printer. The chamber temperature can be included as a decisive parameter in the future version of the MAR-AM.



(a)

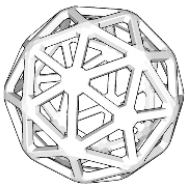


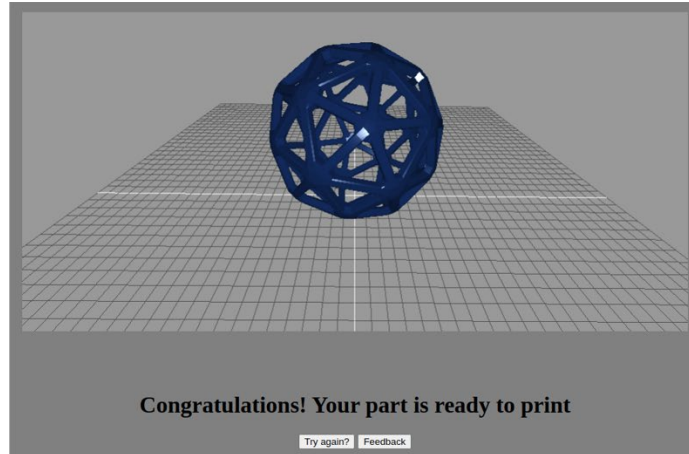
(b)

Figure 7-7: (a) Prediction of the hexagonal organizer, (b) printing results of the hexagonal organizer before implementing the suggestion, and after implementing it

Table 7-4 shows another example, which is a polyhedron model. The MAR-AM predicted that the part could be printed. However, the experimental result (Figure 7-8) shows that the part failed. This was caused by the weak adhesion between the part and build plate. The polyhedron model had a small contacting area to the build plate, which contained fewer adhesions. The part lost adhesion to the build plate in the middle of the printing process and slipped. With more experimental investigations, the part was observed to be printed successfully by increasing the bed temperatures or changing to other materials. The potential reason for the wrong prediction was the lack of data. In the current database, the geometric information has been varied and considered carefully, but for process variations, less data was collected, which motivates the future direction of this study. More printings with various process parameters must be conducted to improve the model performance.

Table 7-4: Detailed printing information of the polyhedron model

Name	Figure of design	Machine brand Machine series	Material type Material density (g/cm ³)	Layer thickness (mm)
				Infill percent (%)
Polyhedron wireframe		Ultimaker Ultimaker 3	Nylon 1.14	Printing speed (mm/s)
				Adhesion type
				Nozzle Temperature (°C)
				Bed Temperature (°C)
				0.15
				20
				70
				Brim
				250
				60



(a)



(b)


Figure 7-8: (a) Prediction of polyhedron model, (b) printing results of polyhedron model

7.2.3. Case 3: Design-related demo

The first sample in the third case was an art creative obtained from Thingi10k. Table 7-5 lists all the detailed printing information. It can be considered as a porous structure, which is challenging for the conventional manufacturing process. It was initially selected to be printed using PLA with its default setting. The MAR-AM suggested changing the original build orientation to

flip the geometry as shown in Figure 7-9a. The developed viewer is a 3D object viewer and users can rotate the viewer to identify the suggested orientation for better printing. The experiments were conducted to validate the prediction and recommendation. The problem with the original setting was the long overhang. It is not printable through the AM process without any support structures.

Table 7-5: Detailed printing information of the art creative

Name	Figure of design	Machine brand Machine series	Material type Material density (g/cm³)	Layer thickness (mm)
				Infill percent (%)
				Printing speed (mm/s)
				Adhesion type
				Nozzle Temperature (°C)
				Bed Temperature (°C)
Single tear		Ultimaker Ultimaker 3	PLA 1.24	0.15
				20
				80
				Brim
				200
				60

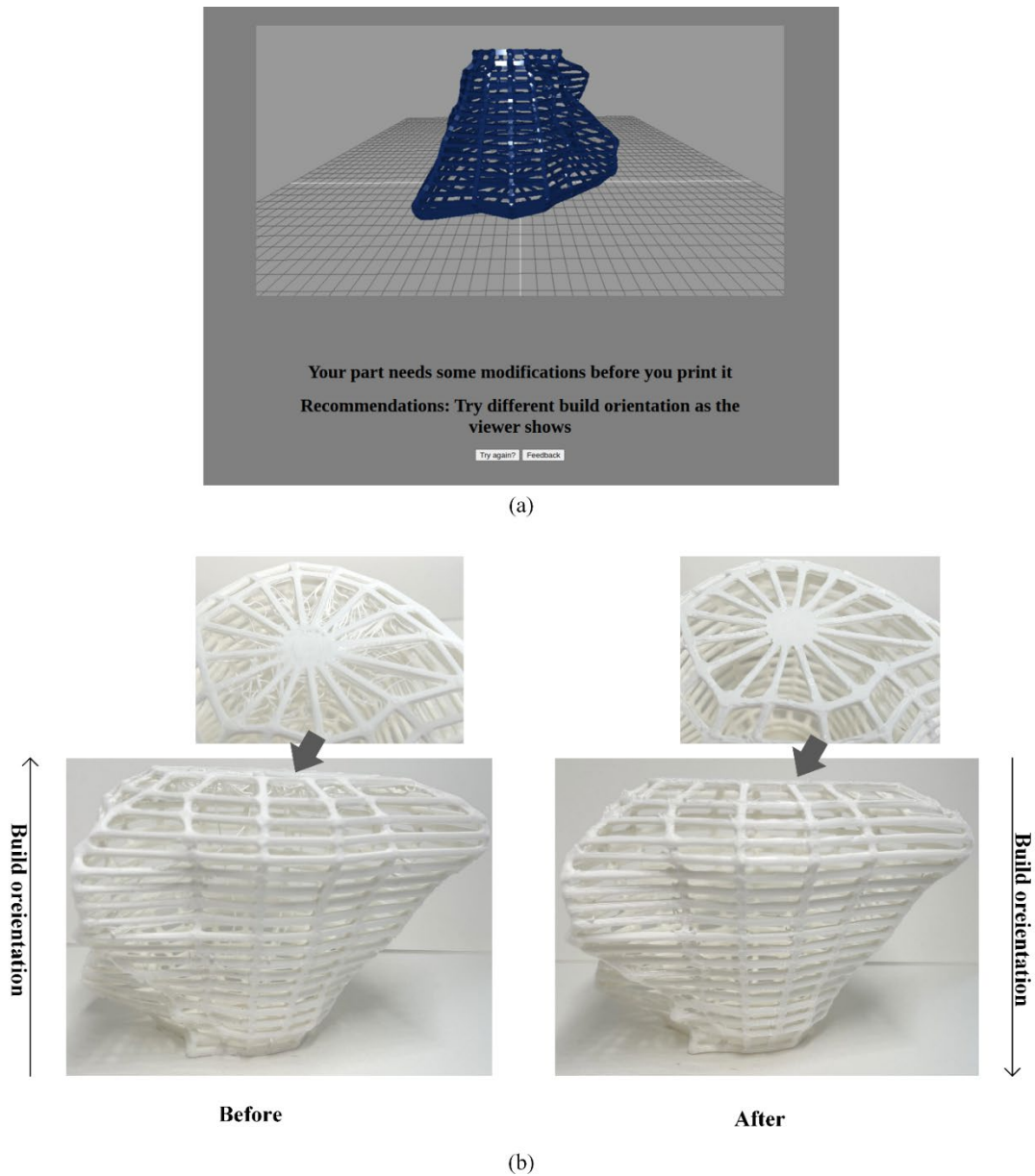



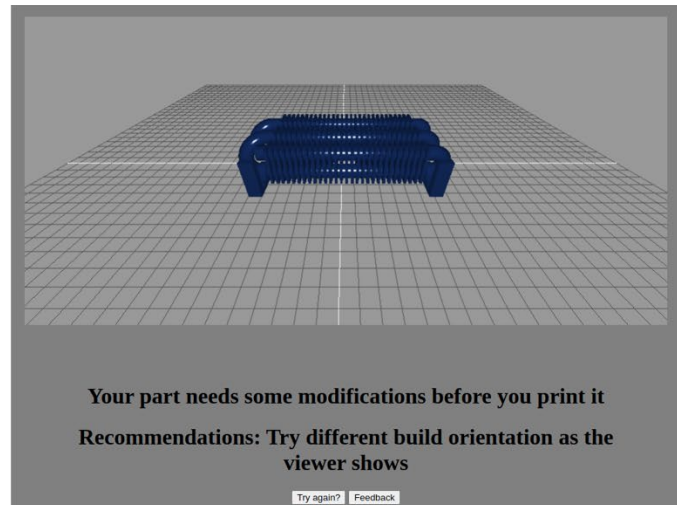
Figure 7-9: (a) Prediction of art creative, (b) printing results of art creative for both before and after the suggestion

Another example was a steam locomotive component. It was a channel-like type of geometry and was designed to be printed without any support. The design was initially selected to be printed using ABS with its default setting. The MAR-AM suggested changing the original build orientation to lay down the geometry as presented in Figure 7-10a. The experiment (Figure 7-10b)

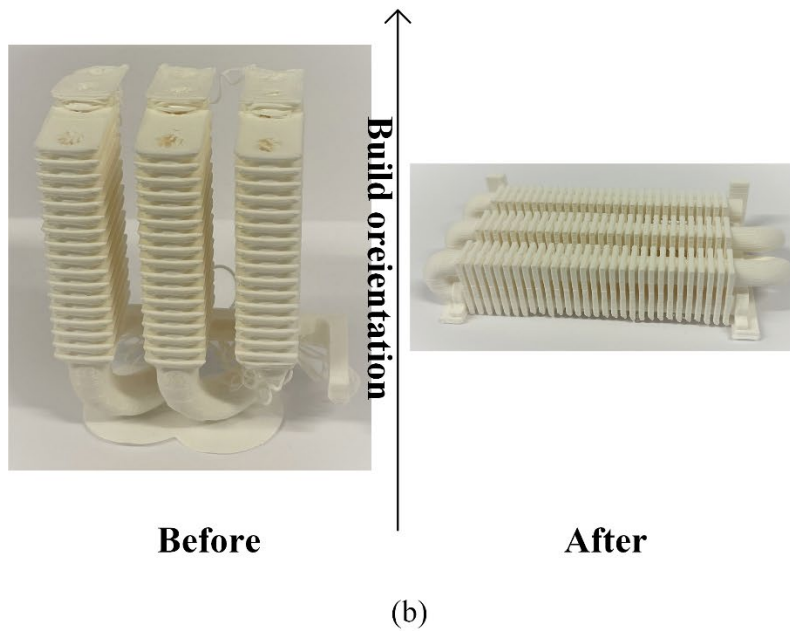
was conducted to validate the prediction and recommendation. The part with the original settings failed in the middle owing to the loss of the adhesion to the build plate. The part slipped to the side and the printing failed. This was caused by the small contacting area to the build plate that contained insufficient adhesion. It was similar to the sample of the polyhedron model demonstrated in case 2. Moreover, this part contained not only the problem of adhesion but also of suspending geometries. By changing the build orientation, the suspending geometries were avoided and the contacting areas to the build plate increased.

Table 7-6: Detailed printing information of a steam locomotive component

Name	Figure of design	Machine brand Machine series	Material type Material density (g/cm ³)	Layer thickness (mm)
				Infill percent (%)
Steam locomotive component		Ultimaker Ultimaker 3	ABS 1.04	Printing speed (mm/s)
				Adhesion type
				Nozzle Temperature (°C)
				Bed Temperature (°C)
				0.15
				20
				60
				Brim
				235
				80



(a)



(b)



Figure 7-10: (a) Prediction of the steam locomotive component, (b) printing results both before and after the suggestion

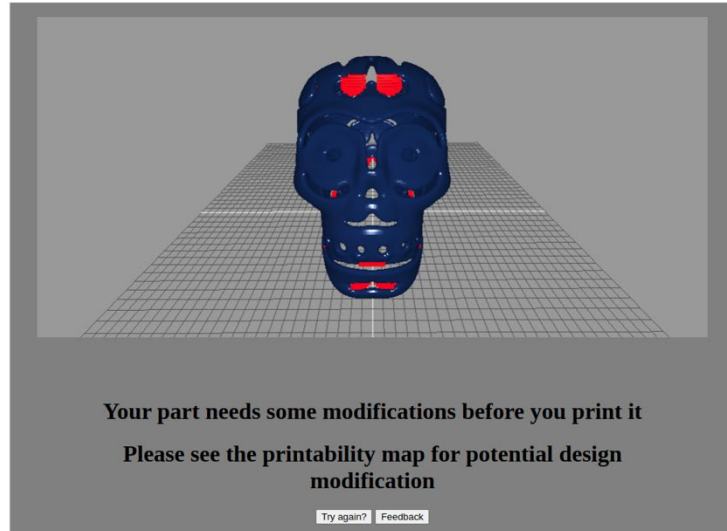
7.2.4. Case 4: Skulls

Case 4 contained two different skull models: a skull lamp cover and a skull bowl. They were initially selected to be printed using PLA with a thick layer. Although these two models had

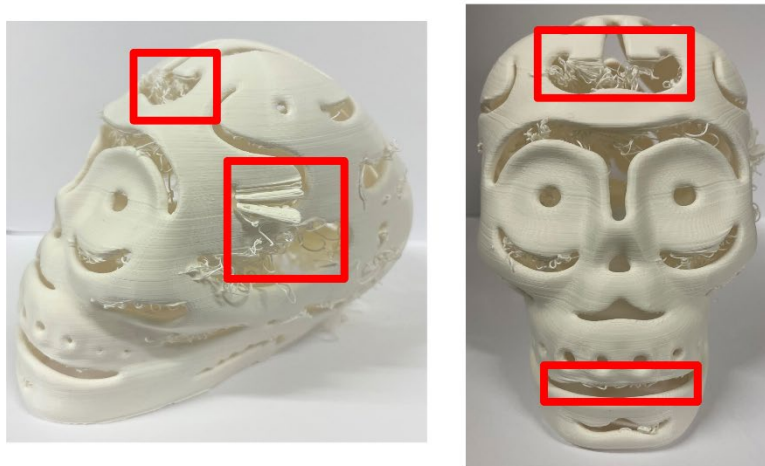
similar geometries and were set to be printed with the same materials and same machine settings, MAR-AM predicted that the skull lump cover was not printable (Figure 7-11a) and the skull bowl is printable (Figure 7-12a). For the skull lump cover, MAR-AM could not determine the potential solution by simply changing the build orientation or process parameters. It provided a printability map to support the potential design modifications. The experimental results, shown in Figures 7-11b and 7-12b validate the predictions of MAR-AM. The main problem with the skull lump cover was the suspending areas. It could not be printed without support structures. The printability map is provided to assist users to generate the proper support structures.

Table 7-7: Detailed printing information of skulls

Name	Figure of design	Machine brand Machine series	Material type Material density (g/cm ³)	Layer thickness (mm) Infill percent (%) Printing speed (mm/s) Adhesion type Nozzle Temperature (°C) Bed Temperature (°C)
Skull lump cover		Ultimaker Ultimaker 3	PLA 1.24	0.2 20 80 Brim 200 60
Skull bowl		Ultimaker Ultimaker 3	PLA 1.24	0.2 20 80 Brim 200 60

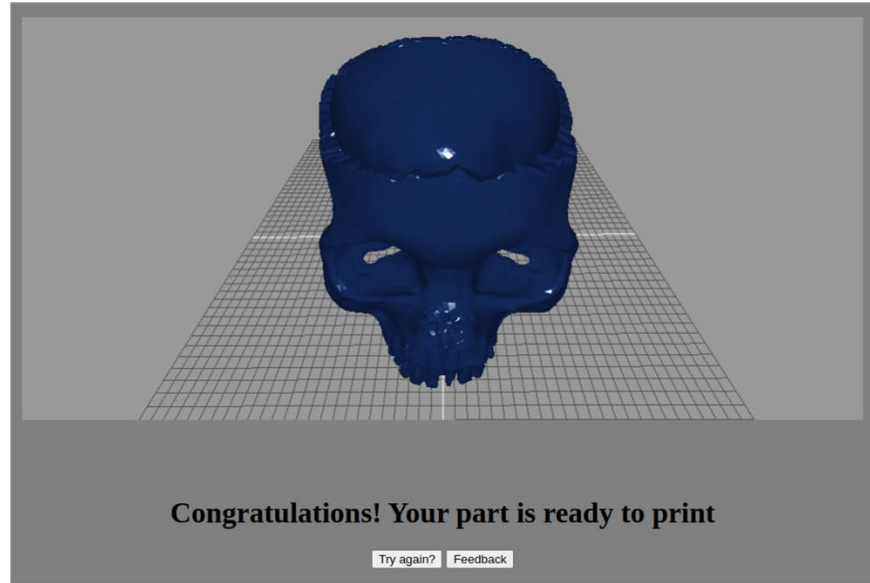


(a)



(b)

Figure 7-11: (a) Prediction of the skull lamp cover, (b) printing results of the skull lamp cover. The red boxes indicate the problematic areas



(a)



(b)

Figure 7-12: (a) Prediction of the skull bowl, (b) printing results of the skull bowl

In conclusion, these case studies demonstrated the capability of the proposed MAR-AM in both prediction and recommendation. It provides promising and satisfying performance to novice AM users at the design stage. It assists users in increasing the printing success rates and benefits from AM techniques in their product development process. Some limitations remain at the current

stage. First, the proposed MAR-AM has weaker performance on the process-related samples owing to the insufficient data in the developed AM database. However, as more data is incoming, particularly with different process settings, the performance of MAR-AM will be improved. Second, the printability map is provided to support the design modification for designers. However, the main causes of these challenges and how to modify designs to overcome them are still not clear. Certain AM knowledge is required to justify what modifications can be conducted. For future research, more investigations on guiding users on design modifications can be conducted.

7.3. Chapter summary

This chapter describes the implementation and deployment of the developed MAR-AM. It is implemented into a web-based application. With the web application, users can easily access the developed tool and share feedback with developers to improve the application. The tool was developed in Python language with a JavaScript-based viewer and Flask backend framework.

Multiple case studies are presented in this chapter to validate the recommendation system and the entire flow of the proposed MAR-AM. These case studies validate the performance of the proposed MAR-AM on both prediction and recommendation. Only one sample in the discussed eleven case studies had the incorrect prediction, which motivates more data gathering on process variations.

The current MAR-AM is still at the beta version. Thus, some additional features and functions can be added to increase its functionality. These future developments are summarized as follows.

- 1) The developed web application can join the AM data port together to offer a better environment for users to use the applications and contribute their efforts.

- 2) The model is expected to perform better with a more extensive database, particularly for the process-related samples. More data must be collected to mature the methodology and developed applications.
- 3) The current database is stored locally. It will be better to upload it online. Moreover, filtering and utilizing the user feedback to improve the developed model must be investigated.
- 4) The use of the given printability map to support the design modification can be further investigated. The current printability map still requires some AM knowledge to justify the potential challenges. It will be better to categorize these problematic challenges into groups to provide designers with a better concept of how to modify their designs for a successful print.

Chapter 8. Conclusions and future research

8.1. Conclusions

At the current stage, the AM process still has a very high threshold for novice users to fully utilize its capabilities in fabricating complex parts. It has a large number of selections on materials, machines, and even parameter settings. It requires designers to have extensive knowledge of the AM process to make the design manufacturable. Even for an advanced commercial AM machine, printing may fail owing to many factors such as build orientations, support structures, and minimum features. There are still limitations on printable geometrical features. The relationships of geometric information, material information, process information, and final part qualities are closely coupled. Identifying whether a given design is printable and what modifications are possible to make the design more suitable for AM is one of the major challenges limiting the wide adoption of AM in the industry. Therefore, an automated, easy-to-access, and comprehensive manufacturability analysis before fabrication is significantly important to stimulate the application of AM technology. There are seven different types of AM techniques, and each technique has a different manufacturing process. This thesis focuses on two AM techniques: LPBF and FDM. They were selected owing to their wide applications and popularity. To develop the desired manufacturability model, this thesis answers three research questions: 1) how to define the manufacturability of the given design in AM, particularly for LPBF and FDM processes; 2) based on the definition, how to predict what geometries with corresponding material and process information is not printable; 3) if the given design is not printable, what modification can be conducted to make the design printable. To solve the above challenges, the following efforts are performed in this thesis.

At the beginning of the thesis, a comprehensive literature review is conducted over the topics of manufacturability analysis for both AM and SM. Existing methodologies of manufacturability analysis on SM are provided to understand how manufacturability analysis is conducted for the traditional processes, and they are compared to motivate the manufacturability analysis on AM process. Thereafter, the major effects on evaluating manufacturability are reviewed and summarized. Without the understanding of these factors, the manufacturability model of AM cannot be fully developed. In the past, similar to the conventional manufacturing process, design guidelines or checklists are the most common methods to aid designers in evaluating the manufacturability of their designs. It provides a manufacturable range of geometrical design features including minimum thickness, part orientation, surface roughness, chamfers and radius, holes, and overhang. Designers are expected to follow these guidelines in their product design process. However, this approach is limited, as the relationships among the process settings, materials, and quality of parts are not considered. Moreover, it requires manual scanning through the checklist, and designers are expected to have certain AM knowledge. To assist non-AM experts in better determining whether their designs are printable through AM processes, a few methods such as heuristic and computational approaches are reported. These approaches consider either only the process aspect or the design aspect. None of the previous studies simultaneously considered the effects of design and process. The relationships among the process, design and printing qualities of the parts are highly coupled and difficult to model. The literature review also indicates that there is no proper definition of the manufacturability of AM. Moreover, previous methods on manufacturability analysis offer limited evaluation at the design stage in terms of efficiency, effectiveness, and comprehensiveness, and lack of recommendation to users. No well-defined, automated, and easy-to-access manufacturability analysis is available

in the literature. To comprehensively model the manufacturability model of AM with the coupled relationships among process, material, design, and final product qualities, the ML approach is developed in this thesis as the potential solution owing to its capability in solving complex problems.

To solve the problems summarized in the literature review, this thesis first defines the manufacturability of AM. The manufacturability analysis is differentiated from the engineering analysis to ensure that a part is properly fabricated with the given design, material, and manufacturing process. Based on that definition, three manufacturability levels are introduced. Level 1 checks visual defects of the printed part to ensure geometric completeness. Level 2 evaluates the micro-level structure to ensure the printed part is dense without any significant pores or cracks. Finally, Level 3 ensures the geometric resolution in terms of dimensional accuracy, surface roughness, etc. These levels are expected to be achieved in a step-by-step manner to guarantee the manufacturability of a given design. This thesis focuses on Manufacturability Level 1, which is to detect the visual defects to ensure geometric completeness at the design stage with given designs under the selected material and process settings. Subsequently, a methodological framework of MAR-AM enabling the manufacturability analysis on Level 1 is proposed. This framework is comprised of three main parts: data establishment, ML-assisted manufacturability model development, and a manufacturability recommendation system. Experimental data was designed and collected to train the ML model. With the gathered data, ML models were developed to analyze manufacturability in terms of printability value and the printability map. With the trained ML-assisted manufacturability model, when the design and corresponding settings are given, the ML model will make a prediction on the printability of the given design. If the part is predicted as non-printable, the geometric, material, and process information are then sent to the

recommendation system to determine the potential solutions to avoid printing failure. As the support of the potential design modification, a printability map is also provided.

In the use of ML, data is extremely important as it can directly affect the performance of the ML models. In this study, both FDM and LPBF data were collected to train the ML models. The experiments were designed to create a rich and comprehensive dataset. The critical geometrical consideration and material and process considerations are summarized based on the literature reviews. The dataset was set to include all the variations on both design and process aspects. Moreover, to better manage these data, a well-organized relational database was developed. All the data is stored in the developed database. With the well-defined data organization structure, the data can be easily extracted and used. Furthermore, an AM data port was developed to increase the data sharing and popularize ML approaches in AM applications. Data can be extremely expensive in AM studies. However, with the AM data port, users are encouraged to share their experimental data. AM researchers can reuse, reunion, and reorganize data contributions from other users. They are expected to fully utilize the existing experimental results in their own studies.

The initial approach to developing the ML-assisted manufacturability model is to use voxel-based geometrical information combined with the material and process settings to make the prediction of the Manufacturability Level 1—visual defects. The design model is represented as voxels and applied using a CNN model. The material and process aspects are applied using an FNN model. The two models are then combined to predict the manufacturability of a given design in the selected AM process settings. The specific loss function is developed for model training to avoid challenges resulting from the imbalanced class. The hyperparameters of the ML models are tuned to determine the best performance. The results verified that the developed model can

accurately predict the manufacturability of the specific design. However, the voxel-based model is restricted by the available computational capability and only lower resolution was performed. A low resolution is insufficient for precisely analyzing the AM manufacturing process. Some detailed features may be omitted through the voxelization process. To solve this problem, this thesis establishes a more efficient CNN. Design data is stored in a sparse matrix such that only the occupied voxels are trained by CNN operations. It joins with the process data, which is trained using an FNN model to make the prediction of manufacturability. By performing the generalized convolutions, the computational costs decrease significantly compared with the voxel-based model, which offers the advantage of performing with high resolutions. The approach was validated in terms of effectiveness and efficiency on the manufacturability prediction.

To guarantee a successful print, novice AM users also seek recommendations on their designs and selections of material and process settings to avoid potential printing failure before the actual fabrications. Therefore, a recommendation system is developed in this thesis. The user inputs of design and selections of material and process are first analyzed by the trained ML models to make the prediction of printability. If the given input is not printable, the recommendation system determines the potential variations in either design or process aspects. The entire process repeats until all the variations have been attempted. If there is no printable solution, the printability map is generated for users to modify their designs. The printability map indicates the problematic area, which can aid users in modifying their designs.

To validate the proposed MAR-AM and recommendation system, a web-based application was developed and presented at the end of this thesis. The web-based application provides a rapid, automated, and easy-to-access tool for novice AM designers to evaluate their designs before the real fabrication. Moreover, it provides a friendly user interface and enables users to provide their

feedback. The feedback is sent to the developed database to update the ML model. With continuous updates, the ML models can be improved and provide better and more mature performance. Finally, multiple case studies are discussed as validation of the effectiveness of the proposed methodology.

In conclusion, the proposed MAR-AM fills the research gap in the manufacturability analysis of the AM process. The MAR-AM provides the prediction of printability with the consideration of both the given design and selected material and process information. More importantly, it can provide promising suggestions for users to avoid printing failures before the actual fabrication, and these were validated using multiple case studies. The MAR-AM can serve as a first-level evaluation of designs for novice AM users such as designers to reduce the waste of time and cost in AM fabrications. Moreover, the MAR-AM is easily accessible and useable as a web application. While training an ML model can take a few hours, the prediction only takes seconds. This thesis provides insightful and useful methods and tools to lower the threshold of AM processes and support wider AM applications in the future.

8.2. Future research

This research had some limitations. For instance, this thesis only focuses on Manufacturability Level 1, which is the visual defects. Manufacturability Levels 2 and 3 are not investigated. To overcome these limitations, future research is planned in the following areas:

- 1) The current database should be expanded. The number of instances in the current database is still under expectation, particularly for the process-related samples. More data must be collected to mature the methodology and developed applications. Moreover, with more data, a recommendation system can be developed for LPBF.

- 2) The current data labeling process requires a large amount of manual work, particularly to create the data to train the ML model to predict the printability map. A potential automated annotation tool should be developed to reduce the amount of manual work.
- 3) More ML algorithms can be investigated such as recurrent neural networks (RNN). RNNs facilitate temporal dynamic behaviours as AM manufacturing processes. The parts are printed layer by layer in AM processes, particularly for LPBF and FDM. The consequence from the previous layers can be fed as the input to the current layer, which can be conducted in an RNN.
- 4) The current recommendation system searches for all the potential variations in the design, material, and process aspects. However, there are still some limitations. First, to generate variations, only a single feature is varied. The current recommendation system does not consider varying multiple settings simultaneously. Second, for the build orientation, current variations may not be the optimal build orientations. More investigations can be conducted in future research. Finally, although the printability map is provided to support the design modification, more specific design solutions can be investigated and provided as the next step. The reasons for the printing failure of each problematic area can be categorized and offered to users, which can further aid designers in making modifications.

References

1. Aboulkhair, N.T., et al., *Reducing porosity in AlSi10Mg parts processed by selective laser melting*. Additive Manufacturing, 2014. **1**: p. 77-86.
2. Sufiiarov, V.S., et al., *The effect of layer thickness at selective laser melting*. Procedia engineering, 2017. **174**: p. 126-134.
3. Pegues, J., et al. *Effect of Specimen Surface Area Size on Fatigue Strength of Additively Manufactured Ti-Al-4V Parts*. in *28th International Solid Freeform Fabrication Symposium*. 2017.
4. Pegues, J., et al. *Effect of process parameter variation on microstructure and mechanical properties of additively manufactured Ti-6Al-4V*. in *Solid freeform fabrication 2017*. 2017.
5. Krauss, H. and M. Zaeh, *Investigations on manufacturability and process reliability of selective laser melting*. Physics Procedia, 2013. **41**: p. 815-822.
6. Kruth, J., et al., *Benchmarking of different SLS/SLM processes as rapid manufacturing techniques*. Laser, 2005. **1**: p. 3D.
7. Adam, G.A. and D. Zimmer, *On design for additive manufacturing: evaluating geometrical limitations*. Rapid Prototyping Journal, 2015. **21**(6): p. 662-670.
8. Thomas, D., *The development of design rules for selective laser melting*. 2009, University of Wales.
9. ISO, A., *Standard Terminology for Additive Manufacturing—General Principles—Terminology*. 2015.
10. Leary, M., et al., *Selective laser melting (SLM) of AlSi12Mg lattice structures*. Materials & Design, 2016. **98**: p. 344-357.
11. Sun, S., M. Brandt, and M. Easton, *2 - Powder bed fusion processes: An overview*, in *Laser Additive Manufacturing*. 2017, Woodhead Publishing. p. 55-77.
12. Redwood, B. *Additive Manufacturing Technologies: An Overview*. 2018; Available from: <https://www.3dhubs.com/knowledge-base/additive-manufacturing-technologies-overview#/powder-bed-fusion>.
13. Bhavar, V., et al. *A review on powder bed fusion technology of metal additive manufacturing*. in *4th International Conference and Exhibition on Additive Manufacturing Technologies-AM-2014, September*. 2014.
14. Beaman, J.J., et al., *SLS Process Modeling and Control*, in *Solid Freeform Fabrication: A New Direction in Manufacturing: with Research and Applications in Thermal Laser Processing*. 1997, Springer US: Boston, MA. p. 167-243.
15. Kruth, J.-P., et al., *Binding mechanisms in selective laser sintering and selective laser melting*. Rapid prototyping journal, 2005. **11**(1): p. 26-36.
16. Frazier, W.E., *Metal Additive Manufacturing: A Review*. Journal of Materials Engineering and Performance, 2014. **23**(6): p. 1917-1928.
17. Wohlers, T., *Wohlers report*. Wohlers Associates Inc, 2014.
18. King, W., et al., *Laser powder bed fusion additive manufacturing of metals; physics, computational, and materials challenges*. Applied Physics Reviews, 2015. **2**(4): p. 041304.
19. Mullen, L., et al., *Selective Laser Melting: A regular unit cell approach for the manufacture of porous, titanium, bone in -growth constructs, suitable for orthopedic applications*. Journal of Biomedical Materials Research Part B: Applied Biomaterials: An Official Journal of The Society for Biomaterials, The Japanese Society for Biomaterials, and The

- Australian Society for Biomaterials and the Korean Society for Biomaterials, 2009. **89**(2): p. 325-334.
20. Arabnejad, S., et al., *High-strength porous biomaterials for bone replacement: A strategy to assess the interplay between cell morphology, mechanical properties, bone ingrowth and manufacturing constraints*. Acta biomaterialia, 2016. **30**: p. 345-356.
 21. Uriondo, A., M. Esperon-Miguez, and S. Perinpanayagam, *The present and future of additive manufacturing in the aerospace sector: A review of important aspects*. Proceedings of the Institution of Mechanical Engineers, Part G: Journal of Aerospace Engineering, 2015. **229**(11): p. 2132-2147.
 22. Santos, E.C., et al., *Rapid manufacturing of metal components by laser forming*. International Journal of Machine Tools and Manufacture, 2006. **46**(12-13): p. 1459-1468.
 23. Louvis, E., P. Fox, and C.J. Sutcliffe, *Selective laser melting of aluminium components*. Journal of Materials Processing Technology, 2011. **211**(2): p. 275-284.
 24. Brandl, E., et al., *Additive manufactured AlSi10Mg samples using Selective Laser Melting (SLM): Microstructure, high cycle fatigue, and fracture behavior*. Materials & Design, 2012. **34**: p. 159-169.
 25. Castells, R. *DMLS vs SLM 3D Printing for Metal Manufacturing*. 2016; Available from: <https://www.element.com/nucleus/2016/06/29/dmls-vs-slm-3d-printing-for-metal-manufacturing>.
 26. Thompson, M.K., et al., *Design for Additive Manufacturing: Trends, opportunities, considerations, and constraints*. CIRP annals, 2016. **65**(2): p. 737-760.
 27. EOS. *EOS Metal Materials for Additive Manufacturing*. Available from: www.eos.info.
 28. Ning, F., et al., *Additive manufacturing of carbon fiber reinforced thermoplastic composites using fused deposition modeling*. Composites Part B: Engineering, 2015. **80**: p. 369-378.
 29. Ziemke, M.C. and M.S. Spann, *Concurrent engineering's roots in the World War II era*, in *Concurrent Engineering*. 1993, Springer. p. 24-41.
 30. Gupta, S.K. and D.S. Nau, *Systematic approach to analysing the manufacturability of machined parts*. Computer-Aided Design, 1995. **27**(5): p. 323-342.
 31. Manfredi, D., et al., *From powders to dense metal parts: Characterization of a commercial AlSiMg alloy processed through direct metal laser sintering*. Materials, 2013. **6**(3): p. 856-869.
 32. Mani, M., P. Witherell, and H. Jee, *Design Rules for Additive Manufacturing: A Categorization*. 2017(58110): p. V001T02A035.
 33. Hauser, J.R. and D. Clausing, *The house of quality*. 1988.
 34. Park, T. and K.-J. Kim, *Determination of an optimal set of design requirements using house of quality*. Journal of operations management, 1998. **16**(5): p. 569-581.
 35. Akao, Y., *Quality function deployment*. 2004.
 36. Carbonell, J.G., R.S. Michalski, and T.M. Mitchell, *1 - AN OVERVIEW OF MACHINE LEARNING*, in *Machine Learning*, R.S. Michalski, J.G. Carbonell, and T.M. Mitchell, Editors. 1983, Morgan Kaufmann: San Francisco (CA). p. 3-23.
 37. Hoefer, M., N. Chen, and M. Frank. *Automated Manufacturability Analysis for Conceptual Design in New Product Development*. in *IIE Annual Conference. Proceedings*. 2017. Institute of Industrial and Systems Engineers (IISE).
 38. Kerbrat, O., P. Mognol, and J.-Y. Hascoët, *A new DFM approach to combine machining and additive manufacturing*. Computers in Industry, 2011. **62**(7): p. 684-692.

39. Jang, D., K. Kim, and J. Jung, *Voxel-based virtual multi-axis machining*. The International Journal of Advanced Manufacturing Technology, 2000. **16**(10): p. 709-713.
40. Das, S. and A. Kanchanapiboon, *A multi-criteria model for evaluating design for manufacturability*. International Journal of Production Research, 2011. **49**(4): p. 1197-1217.
41. Shukor, S.A. and D.A. Axinte, *Manufacturability analysis system: issues and future trends*. International Journal of Production Research, 2009. **47**(5): p. 1369-1390.
42. Han, J., M. Pratt, and W.C. Regli, *Manufacturing feature recognition from solid models: a status report*. IEEE transactions on robotics and automation, 2000. **16**(6): p. 782-796.
43. Li, Y. and M.C. Frank, *Machinability analysis for 3-axis flat end milling*. 2006.
44. Joshi, S. and T.-C. Chang, *Graph-based heuristics for recognition of machined features from a 3D solid model*. Computer-Aided Design, 1988. **20**(2): p. 58-66.
45. Kailash, S., Y. Zhang, and J.Y. Fuh, *A volume decomposition approach to machining feature extraction of casting and forging components*. Computer-Aided Design, 2001. **33**(8): p. 605-617.
46. Kim, Y.S., *Convex decomposition and solid geometric modeling*. 1990.
47. Kim, Y.S., *Recognition of form features using convex decomposition*. Computer-Aided Design, 1992. **24**(9): p. 461-476.
48. Sakurai, H. and P. Dave, *Volume decomposition and feature recognition, Part II: curved objects*. Computer-Aided Design, 1996. **28**(6-7): p. 519-537.
49. Sakurai, H. and C.-W. Chin, *Definition and recognition of volume features for process planning*, in *Manufacturing Research and Technology*. 1994, Elsevier. p. 65-80.
50. Regli III, W.C., *Geometric algorithms for recognition of features from solid models*. 1995.
51. Han, J. and A.A. Requicha, *Integration of feature based design and feature recognition*. Computer-Aided Design, 1997. **29**(5): p. 393-403.
52. Brooks, S.L., et al., *Using STEP to integrate design features with manufacturing features*. 1995, Allied-Signal Aerospace Co., Kansas City, MO (United States). Kansas City Div.
53. Vandenbrande, J.H. and A.A. Requicha, *Spatial reasoning for the automatic recognition of machinable features in solid models*. IEEE Transactions on Pattern Analysis and Machine Intelligence, 1993. **15**(12): p. 1269-1285.
54. Materialise. *materialise design guidelines*. 2018; Available from: <https://www.materialise.com/en/manufacturing/materials/design-guidelines>.
55. Materialise. *Design guidelines - steel*. 2018; Available from: <https://www.materialise.com/en/manufacturing/materials/stainless-steel/design-guidelines>.
56. Stratasys. *Design Guidelines*. 2018; Available from: <https://www.stratasysdirect.com/resources/design-guidelines?resources={43022F6B-C24F-4BEC-A37B-7205C8BC6C27}>.
57. Rehme, O. and C. Emmelmann, *Reproducibility for properties of selective laser melting*, in *Third International WLT-Conference in Laser Manufacturing*. 2005: Munich.
58. Averyanova, M., P. Bertrand, and B. Verquin, *Studying the influence of initial powder characteristics on the properties of final parts manufactured by the selective laser melting technology: a detailed study on the influence of the initial properties of various martensitic stainless steel powders on the final microstructures and mechanical properties of parts manufactured using an optimized SLM process is reported in this paper*. Virtual and Physical Prototyping, 2011. **6**(4): p. 215-223.

59. Hanzl, P., et al., *The influence of processing parameters on the mechanical properties of SLM parts*. Procedia Engineering, 2015. **100**: p. 1405-1413.
60. Uddin, S.Z., et al. *Laser powder bed fusion fabrication and characterization of crack-free aluminum alloy 6061 using in-process powder bed induction heating*. in *Solid Freeform Fabrication 2017*. 2017.
61. Ponnusamy, P., et al. *Mechanical performance of selective laser melted 17-4 PH stainless steel under compressive loading*. in *Solid Freeform Fabrication 2017*. 2017.
62. Qi, T., et al. *Porosity Development and Cracking Behavior of Al-Zn-Mg-Cu Alloys Fabricated by Selective Laser Melting*. in *Solid Freeform Fabrication 2017*. 2017.
63. Peng, A.H. and Z.M. Wang. *Researches into influence of process parameters on FDM parts precision*. in *Applied Mechanics and Materials*. 2010. Trans Tech Publ.
64. Popescu, D., et al., *FDM process parameters influence over the mechanical properties of polymer specimens: A review*. Polymer Testing, 2018. **69**: p. 157-166.
65. Ameta, G., et al., *Investigating the role of geometric dimensioning and tolerancing in additive manufacturing*. Journal of Mechanical Design, 2015. **137**(11): p. 111401.
66. Meisel, N. and C. Williams, *An investigation of key design for additive manufacturing constraints in multimaterial three-dimensional printing*. Journal of Mechanical Design, 2015. **137**(11): p. 111406.
67. Booth, J.W., et al., *The design for additive manufacturing worksheet*. Journal of Mechanical Design, 2017. **139**(10): p. 100904.
68. Grasso, M. and B.M. Colosimo, *Process defects and in situ monitoring methods in metal powder bed fusion: a review*. Measurement Science and Technology, 2017. **28**(4): p. 044005.
69. Tapia, G. and A. Elwany, *A review on process monitoring and control in metal-based additive manufacturing*. Journal of Manufacturing Science and Engineering, 2014. **136**(6): p. 060801.
70. Mani, M., et al., *Measurement science needs for real-time control of additive manufacturing powder bed fusion processes*. 2015: US Department of Commerce, National Institute of Standards and Technology.
71. Everton, S.K., et al., *Review of in-situ process monitoring and in-situ metrology for metal additive manufacturing*. Materials & Design, 2016. **95**: p. 431-445.
72. Sames, W.J., et al., *The metallurgy and processing science of metal additive manufacturing*. International Materials Reviews, 2016. **61**(5): p. 315-360.
73. Spears, T.G. and S.A. Gold, *In-process sensing in selective laser melting (SLM) additive manufacturing*. Integrating Materials and Manufacturing Innovation, 2016. **5**(1): p. 2.
74. Sharratt, B.M., *Non-destructive techniques and technologies for qualification of additive manufactured parts and processes*. Sharratt Research and Consulting Inc., Victoria, BC, Technical Report No. DRDC-RDDC-2015-C035. http://cradpdf.drdc-rddc.gc.ca/PDFS/unc200/p801800_A1b.pdf, 2015.
75. Okaro, I.A., et al., *Automatic fault detection for laser powder-bed fusion using semi-supervised machine learning*. Additive Manufacturing, 2019. **27**: p. 42-53.
76. Yuan, B., et al. *Semi-supervised convolutional neural networks for in-situ video monitoring of selective laser melting*. in *Proceedings - 2019 IEEE Winter Conference on Applications of Computer Vision, WACV 2019*. 2019.
77. Yuan, B., et al., *Machine-Learning-Based Monitoring of Laser Powder Bed Fusion*. Advanced Materials Technologies, 2018. **3**(12).

78. Wasmer, K., et al., *In Situ Quality Monitoring in AM Using Acoustic Emission: A Reinforcement Learning Approach*. Journal of Materials Engineering and Performance, 2019. **28**(2): p. 666-672.
79. Scime, L. and J. Beuth, *A multi-scale convolutional neural network for autonomous anomaly detection and classification in a laser powder bed fusion additive manufacturing process*. Additive Manufacturing, 2018. **24**: p. 273-286.
80. Scime, L. and J. Beuth, *Using machine learning to identify in-situ melt pool signatures indicative of flaw formation in a laser powder bed fusion additive manufacturing process*. Additive Manufacturing, 2019. **25**: p. 151-165.
81. Imani, F., et al., *Process mapping and in-process monitoring of porosity in laser powder bed fusion using layerwise optical imaging*. Journal of Manufacturing Science and Engineering, Transactions of the ASME, 2018. **140**(10).
82. Gobert, C., et al., *Application of supervised machine learning for defect detection during metallic powder bed fusion additive manufacturing using high resolution imaging*. Additive Manufacturing, 2018. **21**: p. 517-528.
83. Zhang, Y. and A. Bernard. *AM feature and knowledge based process planning for additive manufacturing in multiple parts production context*. in *Proceedings of 25th Annual International Solid Freeform Fabrication Symposium*. 2014.
84. Shi, Y., et al., *Manufacturability analysis for additive manufacturing using a novel feature recognition technique*. Computer-Aided Design and Applications, 2018. **15**(6): p. 941-952.
85. Kerbrat, O., P. Mognol, and J.Y. Hascoet, *Manufacturability analysis to combine additive and subtractive processes*. Rapid Prototyping Journal, 2010. **16**(1): p. 63-72.
86. Tedia, S. and C.B. Williams. *Manufacturability analysis tool for additive manufacturing using voxel-based geometric modeling*. in *27th Annual International Solid Freeform Fabrication (SFF) Symposium*. 2016.
87. Telea, A. and A. Jalba. *Voxel-based assessment of printability of 3D shapes*. in *International Symposium on Mathematical Morphology and Its Applications to Signal and Image Processing*. 2011. Springer.
88. Nelaturi, S., W. Kim, and T. Kurtoglu, *Manufacturability feedback and model correction for additive manufacturing*. Journal of Manufacturing Science and Engineering, 2015. **137**(2): p. 021015.
89. Schmitt, W., et al. *A 3D shape descriptor based on depth complexity and thickness histograms*. in *2015 28th SIBGRAPI Conference on Graphics, Patterns and Images*. 2015. IEEE.
90. Ulu, E., et al., *Manufacturability Oriented Model Correction and Build Direction Optimization for Additive Manufacturing*. Journal of mechanical Design, 2019(In process).
91. Lu, T. *Towards a fully automated 3D printability checker*. in *2016 IEEE International Conference on Industrial Technology (ICIT)*. 2016. IEEE.
92. Kim, S., et al., *A Design for Additive Manufacturing Ontology to Support Manufacturability Analysis*. 2019. 1.
93. Chen, Y. and X. Xu. *Manufacturability analysis of infeasible features in polygonal models for web-based rapid prototyping*. in *2010 International Conference on Manufacturing Automation*. 2010. IEEE.
94. Cabiddu, D. and M. Attene, *Epsilon-shapes: characterizing, detecting and thickening thin features in geometric models*. 2017.

95. Wang, Y., et al., *A Knowledge Management System to Support Design for Additive Manufacturing Using Bayesian Networks*. Journal of Mechanical Design, 2018. **140**(5): p. 051701.
96. Mokhtarian, H., et al., *A conceptual design and modeling framework for integrated additive manufacturing*. Journal of Mechanical Design, 2018. **140**(8).
97. Kim, S., et al., *A design for additive manufacturing ontology to support manufacturability analysis*. 2019. **19**(4).
98. Jin, Z., et al., *Precise localization and semantic segmentation detection of printing conditions in fused filament fabrication technologies using machine learning*. 2021. **37**: p. 101696.
99. Li, Z., et al., *Prediction of surface roughness in extrusion-based additive manufacturing with machine learning*. 2019. **57**: p. 488-495.
100. Snow, Z., et al., *Toward in-situ flaw detection in laser powder bed fusion additive manufacturing through layerwise imagery and machine learning*. Journal of Manufacturing Systems, 2021. **59**: p. 12-26.
101. Yazdi, R.M., F. Imani, and H.J.J.o.M.S. Yang, *A hybrid deep learning model of process-build interactions in additive manufacturing*. Journal of Manufacturing Systems, 2020. **57**: p. 460-468.
102. Liu, C., et al., *Image analysis-based closed loop quality control for additive manufacturing with fused filament fabrication*. Journal of Manufacturing Systems, 2019. **51**: p. 75-86.
103. Li, Z., et al., *Prediction of surface roughness in extrusion-based additive manufacturing with machine learning*. Robotics and Computer-Integrated Manufacturing, 2019. **57**: p. 488-495.
104. Cerda-Avila, S.N., H.I. Medellín-Castillo, and T. Lim, *An experimental methodology to analyse the structural behaviour of FDM parts with variable process parameters*. Rapid Prototyping Journal, 2020.
105. Guo, Y., W.F. Lu, and J.Y.H. Fuh, *Semi-supervised deep learning based framework for assessing manufacturability of cellular structures in direct metal laser sintering process*. Journal of Intelligent Manufacturing, 2020: p. 1-13.
106. Mycroft, W., et al., *A data-driven approach for predicting printability in metal additive manufacturing processes*. Journal of Intelligent Manufacturing, 2020: p. 1-13.
107. Hassanin, H., et al., *Controlling the properties of additively manufactured cellular structures using machine learning approaches*. Advanced Engineering Materials, 2020. **22**(3): p. 1901338.
108. Sing, S.L., F.E. Wiria, and W.Y. Yeong, *Selective laser melting of lattice structures: A statistical approach to manufacturability and mechanical behavior*. Robotics and Computer-Integrated Manufacturing, 2018. **49**: p. 170-180.
109. Norton, R.L., *Cam design and manufacturing handbook*. 2009: Industrial Press Inc.
110. Yang, S. and Y.F. Zhao, *Additive manufacturing-enabled design theory and methodology: a critical review*. The International Journal of Advanced Manufacturing Technology, 2015. **80**(1-4): p. 327-342.
111. Sutton, A.T., et al., *Powder characterisation techniques and effects of powder characteristics on part properties in powder-bed fusion processes*. Virtual and Physical Prototyping, 2017. **12**(1): p. 3-29.

112. Yan, C., et al., *Evaluation of light-weight AlSi10Mg periodic cellular lattice structures fabricated via direct metal laser sintering*. Journal of Materials Processing Technology, 2014. **214**(4): p. 856-864.
113. Brown, B., W. Everhart, and J. Dinardo, *Characterization of bulk to thin wall mechanical response transition in powder bed AM*. Rapid Prototyping Journal, 2016. **22**(5): p. 801-809.
114. Zeng, K., *Optimization of support structures for selective laser melting*. 2015.
115. Gibson, I., D. Rosen, and B. Stucker, *Additive Manufacturing Technologies*. Vol. 17. 2014, New York: Springer.
116. Calignano, F., *Design optimization of supports for overhanging structures in aluminum and titanium alloys by selective laser melting*. Materials & Design, 2014. **64**: p. 203-213.
117. Adam, G.A. and D. Zimmer, *Design for Additive Manufacturing—Element transitions and aggregated structures*. CIRP Journal of Manufacturing Science and Technology, 2014. **7**(1): p. 20-28.
118. Hague, R., I. Campbell, and P. Dickens, *Implications on design of rapid manufacturing*. Proceedings of the Institution of Mechanical Engineers, Part C: Journal of Mechanical Engineering Science, 2003. **217**(1): p. 25-30.
119. Prüß, H. and T. Vietor, *Design for fiber-reinforced additive manufacturing*. Journal of Mechanical Design, 2015. **137**(11): p. 111409.
120. Diegel, O., et al., *Tools for sustainable product design: additive manufacturing*. 2010.
121. Das, P., et al., *Selection of build orientation for optimal support structures and minimum part errors in additive manufacturing*. Computer-Aided Design and Applications, 2017. **14**(sup1): p. 1-13.
122. Zhang, Y., et al., *Build orientation optimization for multi-part production in additive manufacturing*. Journal of Intelligent Manufacturing, 2017. **28**(6): p. 1393-1407.
123. Panesar, A., et al., *Design framework for multifunctional additive manufacturing: Placement and routing of three-dimensional printed circuit volumes*. Journal of Mechanical Design, 2015. **137**(11): p. 111414.
124. Alharbi, N., R. Osman, and D. Wismeijer, *Effects of build direction on the mechanical properties of 3D-printed complete coverage interim dental restorations*. The Journal of Prosthetic Dentistry, 2016. **115**(6): p. 760-767.
125. Gorguluarslan, R.M., et al., *A multilevel upscaling method for material characterization of additively manufactured part under uncertainties*. Journal of Mechanical Design, 2015. **137**(11): p. 111408.
126. Zhao, D., M. Li, and Y. Liu, *Self-supporting Topology Optimization for Additive Manufacturing*. arXiv preprint arXiv:1708.07364, 2017.
127. Gaynor, A.T., *Topology optimization algorithms for additive manufacturing*. 2015.
128. Gaynor, A.T. and J.K. Guest, *Topology optimization considering overhang constraints: Eliminating sacrificial support material in additive manufacturing through design*. Structural and Multidisciplinary Optimization, 2016. **54**(5): p. 1157-1172.
129. Patterson, A.E., S.L. Messimer, and P.A. Farrington, *Overhanging features and the SLM/DMLS residual stresses problem: Review and future research need*. Technologies, 2017. **5**(2): p. 15.
130. Bertolini, M., et al., *Machine Learning for industrial applications: a comprehensive literature review*. Expert Systems with Applications, 2021: p. 114820.

131. Yoo, S. and N. Kang, *Explainable Artificial Intelligence for Manufacturing Cost Estimation and Machining Feature Visualization*. Expert Systems with Applications, 2021: p. 115430.
132. Dogan, A. and D. Birant, *Machine learning and data mining in manufacturing*. Expert Systems with Applications, 2020: p. 114060.
133. Saluja, A., J. Xie, and K.J.J.o.M.P. Fayazbakhsh, *A closed-loop in-process warping detection system for fused filament fabrication using convolutional neural networks*. 2020. **58**: p. 407-415.
134. Shalev-Shwartz, S. and S. Ben-David, *Understanding machine learning: From theory to algorithms*. 2014: Cambridge university press.
135. Rojas, R., *Neural networks: a systematic introduction*. 2013: Springer Science & Business Media.
136. Dumoulin, V. and F. Visin, *A guide to convolution arithmetic for deep learning*. arXiv preprint arXiv:1603.07285, 2016.
137. Xu, L., et al. *Deep convolutional neural network for image deconvolution*. in *Advances in neural information processing systems*. 2014.
138. Graham, B., *Fractional max-pooling*. arXiv preprint arXiv:1412.6071, 2014.
139. LeCun, Y., Y. Bengio, and G. Hinton, *Deep learning*. nature, 2015. **521**(7553): p. 436-444.
140. Srivastava, N., et al., *Dropout: a simple way to prevent neural networks from overfitting*. The journal of machine learning research, 2014. **15**(1): p. 1929-1958.
141. Suri, R., *A new perspective on manufacturing systems analysis*. Design and analysis of integrated manufacturing systems, 1988: p. 118-133.
142. Chua, C.K., C.H. Wong, and W.Y. Yeong, *Chapter Eight - Benchmarking for Additive Manufacturing*, in *Standards, Quality Control, and Measurement Sciences in 3D Printing and Additive Manufacturing*, C.K. Chua, C.H. Wong, and W.Y. Yeong, Editors. 2017, Academic Press. p. 181-212.
143. Hudson, J., E. Liu, and S. Crampin, *The mechanical properties of materials with interconnected cracks and pores*. Geophysical Journal International, 1996. **124**(1): p. 105-112.
144. Chawla, N. and X. Deng, *Microstructure and mechanical behavior of porous sintered steels*. Materials Science and Engineering: A, 2005. **390**(1): p. 98-112.
145. Gupta, S.K., et al., *Automated manufacturability analysis: A survey*. Research in Engineering Design, 1997. **9**(3): p. 168-190.
146. Aboulkhair, N.T., et al., *3D printing of Aluminium alloys: Additive Manufacturing of Aluminium alloys using selective laser melting*. Progress in Materials Science, 2019. **106**: p. 100578.
147. Pragana, J.P., et al., *Influence of processing parameters on the density of 316L stainless steel parts manufactured through laser powder bed fusion*. Proceedings of the Institution of Mechanical Engineers, Part B: Journal of Engineering Manufacture, 2020. **234**(9): p. 1246-1257.
148. Lietaert, K., et al., *Mechanical properties and cytocompatibility of dense and porous Zn produced by laser powder bed fusion for biodegradable implant applications*. Acta biomaterialia, 2020. **110**: p. 289-302.
149. Rausch, A.M., et al., *Predictive simulation of process windows for powder bed fusion additive manufacturing: influence of the powder bulk density*. Materials, 2017. **10**(10): p. 1117.

150. Dong, G., J. Marleau-Finley, and Y.F. Zhao, *Investigation of electrochemical post-processing procedure for Ti-6Al-4V lattice structure manufactured by direct metal laser sintering (DMLS)*. The International Journal of Advanced Manufacturing Technology, 2019. **104**(9): p. 3401-3417.
151. Zhou, Q. and A.J.a.p.a. Jacobson, *Thingi10k: A dataset of 10,000 3d-printing models*. 2016.
152. Çiçek, Ö., et al. *3D U-Net: learning dense volumetric segmentation from sparse annotation*. in *International conference on medical image computing and computer-assisted intervention*. 2016. Springer.
153. Ronneberger, O., P. Fischer, and T. Brox. *U-net: Convolutional networks for biomedical image segmentation*. in *International Conference on Medical image computing and computer-assisted intervention*. 2015. Springer.
154. Bui, T.D., J. Shin, and T. Moon, *3D densely convolutional networks for volumetric segmentation*. arXiv preprint arXiv:1709.03199, 2017.
155. Zhong, Z., et al. *3D fully convolutional networks for co-segmentation of tumors on PET-CT images*. in *2018 IEEE 15th International Symposium on Biomedical Imaging (ISBI 2018)*. 2018. IEEE.
156. Leng, B., et al., *3D object understanding with 3D convolutional neural networks*. Information sciences, 2016. **366**: p. 188-201.
157. Maturana, D. and S. Scherer. *Voxnet: A 3d convolutional neural network for real-time object recognition*. in *2015 IEEE/RSJ International Conference on Intelligent Robots and Systems (IROS)*. 2015. IEEE.
158. Milletari, F., N. Navab, and S.-A. Ahmadi. *V-net: Fully convolutional neural networks for volumetric medical image segmentation*. in *2016 Fourth International Conference on 3D Vision (3DV)*. 2016. IEEE.
159. Yang, S., et al., *Towards an automated decision support system for the identification of additive manufacturing part candidates*. Journal of Intelligent Manufacturing, 2020: p. 1-17.
160. Khadilkar, A., J. Wang, and R. Rai, *Deep learning-based stress prediction for bottom-up SLA 3D printing process*. The International Journal of Advanced Manufacturing Technology, 2019. **102**(5): p. 2555-2569.
161. Ayeb, M., M. Frija, and R. Fathallah, *Prediction of residual stress profile and optimization of surface conditions induced by laser shock peening process using artificial neural networks*. The International Journal of Advanced Manufacturing Technology, 2019. **100**(9): p. 2455-2471.
162. White, D.A., et al., *Multiscale topology optimization using neural network surrogate models*. Computer Methods in Applied Mechanics and Engineering, 2019. **346**: p. 1118-1135.
163. Zhang, J., P. Wang, and R.X. Gao, *Deep learning-based tensile strength prediction in fused deposition modeling*. Computers in industry, 2019. **107**: p. 11-21.
164. Usama, M., et al., *Unsupervised machine learning for networking: Techniques, applications and research challenges*. IEEE Access, 2019. **7**: p. 65579-65615.
165. Arulkumaran, K., et al., *Deep reinforcement learning: A brief survey*. IEEE Signal Processing Magazine, 2017. **34**(6): p. 26-38.
166. Simonyan, K. and A. Zisserman, *Very deep convolutional networks for large-scale image recognition*. arXiv preprint arXiv:1409.1556, 2014.

167. Tustison, N. and J. Gee, *Introducing Dice, Jaccard, and other label overlap measures to ITK*. Insight J, 2009. **2**.
168. Zhou, Z., et al., *Unet++: A nested u-net architecture for medical image segmentation*, in *Deep Learning in Medical Image Analysis and Multimodal Learning for Clinical Decision Support*. 2018, Springer. p. 3-11.
169. Dahl, G.E., T.N. Sainath, and G.E. Hinton. *Improving deep neural networks for LVCSR using rectified linear units and dropout*. in *2013 IEEE international conference on acoustics, speech and signal processing*. 2013. IEEE.
170. Agarap, A.F., *Deep learning using rectified linear units (relu)*. arXiv preprint arXiv:1803.08375, 2018.
171. Min, P., *Binvox 3D mesh voxelizer*. Available on: <http://www.cs.princeton.edu/~min/binvox>, 2004.
172. Hiller, J. and H. Lipson, *Dynamic simulation of soft multimaterial 3d-printed objects*. Soft robotics, 2014. **1**(1): p. 88-101.
173. Pedregosa, F., et al., *Scikit-learn: Machine learning in Python*. the Journal of machine Learning research, 2011. **12**: p. 2825-2830.
174. Qi, X., et al., *Applying Neural-Network-Based Machine Learning to Additive Manufacturing: Current Applications, Challenges, and Future Perspectives*. Engineering, 2019. **5**(4): p. 721-729.
175. Scime, L., et al., *Layer-wise anomaly detection and classification for powder bed additive manufacturing processes: A machine-agnostic algorithm for real-time pixel-wise semantic segmentation*. Additive Manufacturing, 2020. **36**: p. 101453.
176. Alwosheel, A., S. van Cranenburgh, and C.G. Chorus, *Is your dataset big enough? Sample size requirements when using artificial neural networks for discrete choice analysis*. Journal of choice modelling, 2018. **28**: p. 167-182.
177. Cho, J., et al., *How much data is needed to train a medical image deep learning system to achieve necessary high accuracy?* arXiv preprint arXiv:1511.06348, 2015.
178. Kavzoglu, T. and P. Mather, *The use of backpropagating artificial neural networks in land cover classification*. International journal of remote sensing, 2003. **24**(23): p. 4907-4938.
179. Jain, A.K. and B. Chandrasekaran, *39 Dimensionality and sample size considerations in pattern recognition practice*. Handbook of statistics, 1982. **2**: p. 835-855.
180. Abu-Mostafa, Y.S., *Hints*. Neural Computation, 1995. **7**(4): p. 639-671.
181. Haykin, S., *Neural networks and learning machines*, 3/E. 2010: Pearson Education India.
182. Fox, J.C., S.P. Moylan, and B.M. Lane, *Effect of process parameters on the surface roughness of overhanging structures in laser powder bed fusion additive manufacturing*. Procedia Cirp, 2016. **45**: p. 131-134.
183. Gaynor, A.T., et al. *Topology optimization for additive manufacturing: considering maximum overhang constraint*. in *15th AIAA/ISSMO multidisciplinary analysis and optimization conference*. 2014.
184. Choy, C., J. Gwak, and S. Savarese. *4d spatio-temporal convnets: Minkowski convolutional neural networks*. in *Proceedings of the IEEE Conference on Computer Vision and Pattern Recognition*. 2019.
185. Dong, G., et al., *Design and optimization of solid lattice hybrid structures fabricated by additive manufacturing*. Additive Manufacturing, 2020. **33**: p. 101116.

186. Di Angelo, L., et al., *A reliable build orientation optimization method in additive manufacturing: the application to FDM technology*. International Journal of Advanced Manufacturing Technology, 2020. **108**.
187. Brika, S.E., et al., *Multi-objective build orientation optimization for powder bed fusion by laser*. Journal of Manufacturing Science and Engineering, 2017. **139**(11).
188. Jibin, Z. *Determination of optimal build orientation based on satisfactory degree theory for RPT*. in *Ninth International Conference on Computer Aided Design and Computer Graphics (CAD-CG'05)*. 2005. IEEE.
189. Rocha, A.M.A., A.I. Pereira, and A.I.F. Vaz. *Build orientation optimization problem in additive manufacturing*. in *International conference on computational science and its applications*. 2018. Springer.
190. Schranz, C., *Tweaker-Auto Rotation Module for FDM 3D Printing*. 2016.
191. Danchilla, B., *Three.js framework*, in *Beginning WebGL for HTML5*. 2012, Springer. p. 173-203.
192. Torries, B., N. Shamsaei, and S.M. Thompson. *Effects of build orientation on fatigue performance of Ti-6Al-4V parts fabricated via laser-based powder bed fusion*. in *28th International Solid Freeform Fabrication Symposium-An Additive Manufacturing Conference*. 2017.
193. Jia, Q. and D. Gu, *Selective laser melting additive manufacturing of Inconel 718 superalloy parts: Densification, microstructure and properties*. Journal of Alloys and Compounds, 2014. **585**: p. 713-721.
194. Wang, X., X. Gong, and K. Chou, *Review on powder-bed laser additive manufacturing of Inconel 718 parts*. Proceedings of the Institution of Mechanical Engineers, Part B: Journal of Engineering Manufacture, 2017. **231**(11): p. 1890-1903.
195. Shrestha, R., et al. *Effect of Build Orientation on the Fatigue Behavior of Stainless Steel 316L Manufactured Via A Laser-Powder Bed Fusion Process*. in *27th Annual Solid Freeform Fabrication Symposium Proceedings*. 2016.
196. Riemer, A., et al., *On the fatigue crack growth behavior in 316L stainless steel manufactured by selective laser melting*. Engineering Fracture Mechanics, 2014. **120**: p. 15-25.
197. Zhang, B., L. Dembinski, and C. Coddet, *The study of the laser parameters and environment variables effect on mechanical properties of high compact parts elaborated by selective laser melting 316L powder*. Materials Science and Engineering: A, 2013. **584**: p. 21-31.
198. Uddin, S.Z., et al., *Laser powder bed fusion fabrication and characterization of crack-free aluminum alloy 6061 using in-process powder bed induction heating*.
199. Ponnusamy, P., et al., *Mechanical performance of selective laser melted 17-4 PH stainless steel under compressive loading*.
200. Mahmoudi, M., et al., *Mechanical properties and microstructural characterization of selective laser melted 17-4 PH stainless steel*. Rapid Prototyping Journal, 2017. **23**(2): p. 280-294.
201. Yadollahi, A., et al. *Mechanical and microstructural properties of selective laser melted 17-4 PH stainless steel*. in *ASME 2015 International Mechanical Engineering Congress and Exposition*. 2015. American Society of Mechanical Engineers.
202. Yadollahi, A., et al., *Mechanical and Microstructural Properties of Selective Laser Melted 17-4 PH Stainless Steel*. 2015(57359): p. V02AT02A014.

203. Wang, P., et al., *Selective laser melting of Al-Zn-Mg-Cu: Heat treatment, microstructure and mechanical properties*. Journal of Alloys and Compounds, 2017. **707**: p. 287-290.
204. Qi, T., et al. *Porosity development and cracking behavior of Al-Zn-Mg-Cu alloys fabricated by selective laser melting*. in *2017 International Solid Freeform Fabrication Symposium*. 2017. University of Texas at Austin.
205. Zhang, H., et al., *Effect of Zirconium addition on crack, microstructure and mechanical behavior of selective laser melted Al-Cu-Mg alloy*. Scripta Materialia, 2017. **134**: p. 6-10.
206. Zhang, H., et al. *Fabrication and heat treatment of high strength Al-Cu-Mg alloy processed using selective laser melting*. in *SPIE LASE*. 2016. SPIE.
207. Zhang, H., et al., *Selective laser melting of high strength Al-Cu-Mg alloys: Processing, microstructure and mechanical properties*. Materials Science and Engineering: A, 2016. **656**: p. 47-54.
208. Kempen, K., et al., *Processing AlSi10Mg by selective laser melting: parameter optimisation and material characterisation*. Materials Science and Technology, 2015. **31**(8): p. 917-923.
209. Tradowsky, U., et al., *Selective laser melting of AlSi10Mg: influence of post-processing on the microstructural and tensile properties development*. Materials & Design, 2016. **105**: p. 212-222.
210. Yadroitsev, I. and I. Smurov, *Surface Morphology in Selective Laser Melting of Metal Powders*. Physics Procedia, 2011. **12**: p. 264-270.
211. Mumtaz, K. and N. Hopkinson, *Top surface and side roughness of Inconel 625 parts processed using selective laser melting*. Rapid Prototyping Journal, 2009. **15**(2): p. 96-103.
212. Mumtaz, K. and N. Hopkinson, *Selective laser melting of Inconel 625 using pulse shaping*. Rapid Prototyping Journal, 2010. **16**(4): p. 248-257.

APPENDIX I: Investigations of effects on varying processing parameters

Major investigated parameters	Materials	Key findings	Reference
Laser power; Scan speed; Hatch distance; Build orientation	Ti-6Al-4V	<p>Scan velocity has the most significant effect on mechanical properties.</p> <p>Laser power has some effect on ductility, but not as significantly as scan velocity.</p> <p>Hatch distance exhibits relatively no effect on the ductility of the AM parts.</p> <p>Orientation does not have a significant effect on fatigue behaviour</p>	[3, 4, 192]
Layer thickness; Laser beam power; Speed hatch distance; Building direction	Inconel 718 alloy	For a larger layer thickness, it has lower strength properties and higher plasticity.	[2, 193, 194]
Laser power; Scan speed; Thickness of layer; Overlap rate; Building direction	Steel	<p>The samples of steel produced by AM method has better tensile test result than ANSI samples.</p> <p>Laser power stings and scanning speeds have the most significant effects on mechanical properties.</p> <p>The deterioration in mechanical and geometrical properties occurs when the building angle is less than 45 °.</p>	[59, 195-197]

		The layer thickness has more effects on surface roughness than the mechanical properties.	
Powder bed temperature	Aluminum alloy 6061	Optimized parameters are recommended based on the author's machine and printed materials. Preheating of the powder bed is very useful in producing crack-free parts.	[198]
Laser power; Build Orientation; Layer Thickness; Defocus Distance	17-4 PH stainless steel	Optimized laser power, orientation, layer thickness and defocus distance are observed based on microhardness and ultimate compressive strength. Machine and material are fixed. Building orientation exhibits a noticeable effect on the mechanical properties	[199-202]
Scanning speed	Al-Zn-Mg-Cu alloys	The effect of scanning speed on porosity development and crack behaviour is investigated. The best scanning velocity is observed with fixed material and machine.	[203, 204]
Scanning speed; Heat treatment; Laser energy density;	Al-Cu-Mg alloy	Scanning speed and laser energy density are observed to influence the products' qualities. Heat treatment was proved to increase the mechanical properties.	[205-207]

Scanning speed; hatch spacing; Scanning strategy; Build orientation; Thermal post- processing	AlSi10Mg	The best parameters and scan strategies are observed for AlSi10Mg using the printer SLM-50 The influence of post-processing on the microstructural and tensile properties is investigated.	[1, 208, 209]
Hatch distance; Layer thickness	Stainless steel grade 904L	Morphology of the first layer and surface structure of the thin walls is studied.	[210]
Scan speed; Pulse width; Pulse energy; Repetition rate	Inconel 625	Higher peak power has a better top and side surface. Increased repetition rate and decreased scan speed have better top surface roughness but worse side roughness.	[211, 212]

APPENDIX II: Lists of related publications

Published journal papers

1. Zhang, Ying, and Yaoyao Fiona Zhao. "Hybrid sparse convolutional neural networks for predicting manufacturability of visual defects of laser powder bed fusion processes." *Journal of Manufacturing Systems* (2021).
2. Zhang, Ying, Sheng Yang, Guoying Dong, and Yaoyao Fiona Zhao. "Predictive Manufacturability Assessment System for Laser Powder Bed Fusion Based on a Hybrid Machine Learning Model." *Additive Manufacturing* (2021): 101946.
3. Zhang, Ying, Sheng Yang, and Yaoyao Fiona Zhao. "Manufacturability analysis of metal laser-based powder bed fusion additive manufacturing—a survey." *The International Journal of Advanced Manufacturing Technology* 110, no. 1 (2020): 57-78.
4. Zhang, Ying, and Yaoyao Fiona Zhao. "A Web-based automated manufacturability analyzer and recommender for additive manufacturing (MAR-AM) via a hybrid Machine learning model." *Expert Systems with Applications* 199 (2022): 117189.

Journal papers under review or revision

1. Zhang, Ying, Safdar, Mutahar, Xie, Jiarui, Li, Jinghao, Sage, Manuel, Yaoyao Fiona Zhao. "The current status of additive manufacturing data for machine learning applications: A systematic review. " (Submitted to *Journal of Intelligent Manufacturing*)

Peer-reviewed conference papers

1. Zhang, Ying, Guoying Dong, Sheng Yang, and Yaoyao Fiona Zhao. "Machine Learning Assisted Prediction Of The Manufacturability Of Laser-based Powder Bed Fusion Process." ASME 2019 International Design Engineering Technical Conferences and Computers and Information in Engineering Conference. American Society of Mechanical Engineers, 2019.

APPENDIX III: Abstract of major journal publications

Journal publication D1

The International Journal of Advanced Manufacturing Technology (2020) 110:57–78
<https://doi.org/10.1007/s00170-020-05825-6>

ORIGINAL ARTICLE



Manufacturability analysis of metal laser-based powder bed fusion additive manufacturing—a survey

Ying Zhang¹ · Sheng Yang¹ · Yaoyao Fiona Zhao¹

Received: 19 March 2020 / Accepted: 23 July 2020 / Published online: 9 August 2020
© Springer-Verlag London Ltd., part of Springer Nature 2020

Abstract

The laser-based powder bed fusion (LPBF) process is able to produce complex part geometries. The fast development of the LPBF process offers new opportunities for the industries. Most research done to date has focused on the modeling of the process, which shows that both part geometries and process parameters play an essential role in the result of end-product quality. The definition of the manufacturability of the LPBF is vague. In this review, the focus is set on the manufacturability of the metal-LPBF process. What manufacturability is in the LPBF process and how it is investigated so far are discussed. All process parameters and design constraints for LPBF processes are introduced. The relationship between process parameters and design constraints and how they affect the manufacturability are discussed as well. A detailed discussion on how other researchers evaluate manufacturability analysis of LPBF is conducted. Finally, the manufacturability of LPBF is defined, and future prospects on filling the research gaps on the manufacturability analysis of the LPBF are presented.

Keywords Manufacturability · Laser-based powder bed fusion · Additive manufacturing

1 Introduction and background

Laser-based powder bed fusion, referred to as LPBF is a type of additive manufacturing (AM) process. In the metal-LPBF process, a laser beam as a power source will melt and fuse the metal powder according to the given pattern on each layer. After one layer is done, the next layer of metal powder will be applied, and the laser is projected. The process continues layer by layer until the products are completely built [1–4]. The schematic of the LPBF process is shown in Fig. 1. The LPBF process is ultimately about the successful control of heat transferred from an intense laser beam to a powder bed with poor heat conductivity to produce the geometrically precise localized fusion of powder [5]. The fusion mechanisms can be grouped into four groups, which are solid-state

sintering, chemically induced binding, liquid-phase sintering (LPS), and full melting [6]. When metal is used, LPS and full melting are two conventional approaches to solidify metal powder.

Because of its relatively high resolution, numerous material choices, and potentials on manufacturing virtually any shape, the process is widely used and studied in both academics and industries [4, 7–9]. The application of LPBF can be found in medical and dental, aerospace, automotive, energy, and tooling industries [7, 9–14]. Compared with conventional manufacturing (CM), the LPBF process is more suitable for prototyping and low production volumes of high complexity parts due to its advantages on the cost, production time, and machinability [8]. Opposite to subtractive manufacturing methodologies, it provides more design freedom with the layer upon layer material addition approach [4]. As no tooling is needed in the LPBF process, designers could consider more complex geometries that are not achievable by CM processes. The growing market demand on the LPBF process boosts increasing research efforts in academia [7, 15, 16].

Over the past 20 years, significant research has been carried out in the field of LPBF. Process, materials, designs, applications, and constraints related to LPBF have been investigated extensively and summarized in a recent survey paper [17]. With the rapid iterative deployment of LPBF equipment, the

✉ Yaoyao Fiona Zhao
yaoyao.zhao@mcgill.ca

Ying Zhang
ying.zhang8@mail.mcgill.ca

Sheng Yang
sheng.yang@mail.mcgill.ca

¹ Department of Mechanical Engineering, McGill University,
Montreal, Quebec H3A 0G4, Canada



Research Paper

Predictive manufacturability assessment system for laser powder bed fusion based on a hybrid machine learning model

Ying Zhang, Sheng Yang, Guoying Dong, Yaoyao Fiona Zhao^{*}

Department of Mechanical Engineering, McGill University, Montreal, Quebec H3A0G4, Canada



ARTICLE INFO

Keywords:

Laser powder bed fusion
Hybrid machine learning model
Voxelization
3D object printing

ABSTRACT

Laser powder bed fusion (LPBF) is an additive manufacturing (AM) process widely adopted in multiple industries for various purposes. When LPBF is used for part fabrication, determining the manufacturability of a specific design is a challenge. Therefore, this study aimed to identify a printable design using a novel approach to predict the potential printing failures of a given design via the LPBF process. A voxel-based convolutional neural network (CNN) model is developed for analyzing the design aspect, and a neural network (NN) model is applied to the process aspect. The two models are then combined to predict the manufacturability of the given design in the selected LPBF process settings. The validation samples were selected randomly, and the results verified that the developed model can accurately predict the manufacturability of the specific design. However, the proposed model is restricted by the computational power and the number of training datasets and therefore requires further investigation in this regard.

1. Introduction

Laser powder bed fusion (LPBF) is a commonly used additive manufacturing (AM) process to develop three-dimensional (3D) objects and affords more freedom in terms of hierarchical and shape complexities than the conventional manufacturing processes [1]. In the LPBF process, a power source melts and fuses the powdered material spread on a layer based on a specific pattern. The process is repeated on each layer until the entire part is completely fabricated [2–5]. Various industries, such as automotive, energy, aerospace, tooling, medical, and dental industries, widely utilize the LPBF technique to fabricate numerous components [6]. Although the LPBF process has several advantages, certain limitations exist during its application. For instance, the LPBF process requires an extremely high threshold, and the designers must possess extensive knowledge of the entire process to ensure fabricable designs. The manufacturing process can fail even when an advanced commercial LPBF machine is used owing to the minimum features, support structures, orientation of builds, and other factors. Hence, a manufacturability assessment is critical at the early stage to evaluate the design before the actual fabrication. To identify the manufacturability of a specific design, the printability of the design in the desired shape using the selected LPBF process must be determined [7].

Therefore, this study aimed to predict the completeness of the shape in the printing parts before examining the mechanical performances, as the investigation of mechanical properties becomes futile if the part fails to be printed completely.

The process parameters of the LPBF, material selection, and design characteristics are the three primary aspects that significantly affect manufacturability [7]. To verify the manufacturability of the given design using the LPBF process, it is essential to identify the relationship between these three aspects and the quality of the final product. To this end, numerous studies have investigated the influence of each aspect [8–15]. In terms of manufacturability analysis, the reported techniques include the design guidelines [14–19], knowledge management system [20], real-time monitoring [21–23], and offline automated manufacturability checker [24,25]. However, these approaches do not provide automatic manufacturability assessment at the early design stage. Moreover, most studies consider the influence of either the design or the process aspect individually to analyze the manufacturability. Therefore, we propose a machine learning (ML) assisted manufacturability prediction of a specific design in the LPBF process, combining the design and process aspects to fill the gaps in the literature.

In the proposed method, a voxel-based convolutional neural network (CNN) model is used for design analysis, while a neural network (NN)

^{*} Corresponding author.E-mail addresses: ying.zhang8@mail.mcgill.ca (Y. Zhang), sheng.yang@mail.mcgill.ca (S. Yang), guoying.dong@mail.mcgill.ca (G. Dong), yaoyao.zhao@mcgill.ca (Y.F. Zhao).<https://doi.org/10.1016/j.addma.2021.101946>

Received 29 June 2020; Received in revised form 6 March 2021; Accepted 6 March 2021

Available online 18 March 2021

2214-8604/© 2021 Elsevier B.V. All rights reserved.



Hybrid sparse convolutional neural networks for predicting manufacturability of visual defects of laser powder bed fusion processes

Ying Zhang, Yaoyao Fiona Zhao *

Department of Mechanical Engineering, McGill University, Montreal, Quebec, H3A0G4, Canada

ARTICLE INFO

Keywords:
Manufacturability
Machine learning
Additive manufacturing
Laser powder bed fusion

ABSTRACT

This paper presents a novel solution to predict the visual defects, one of the major criteria for analyzing manufacturability for the Laser-based Powder Bed Fusion (LPBF) process. For the existing manufacturability investigations, the key challenge is how to model the complex interrelationships among the design, process, and final quality. The recent research proposed machine learning methods to model the manufacturability analysis. Voxel-based Convolutional Neural Network (CNN) has been investigated as one potential solution for design shape analysis. Those approaches are limited by the computational capability available and only lower resolution was performed. However, low resolution is not enough for analyzing the LPBF manufacturing process precisely. Some detailed features may be omitted through the voxelization process. To solve this issue, a more efficient CNN is proposed in this paper. Design data is stored in a sparse matrix so that only the occupied voxels are trained by CNN operations. It joins with the process data, which is trained by a Neural Network (NN) model to make the prediction of manufacturability. By performing the generalized convolutions, the computational costs decrease sharply compared to voxel-based CNN, which offers the advantage of performing with high resolutions. The approach is validated in terms of effectiveness and efficiency on the manufacturability prediction for the LPBF process.

1. Introduction

In the past decade years, Additive Manufacturing (AM) has rapidly expanded in various areas such as aerospace, automotive, tooling, medicals, etc. [1–3]. It opens new opportunities in both design and manufacturing by removing the constraints imposed by conventional manufacturing (CM) such as machining or casting. However, not all designs can be fabricated by AM. There are still some limitations that need to be considered before fabrication to be carried out. These constraints include but are not limited to the narrow printable material selections, poor surface roughness, pores, and unfeasible features (e.g., overhangs) [4–11]. Failure in identifying the design features or printing process parameter setups often leads to printing failure, which eventually leads to increased manufacturing costs and a slower product development process. To solve this issue, manufacturability analysis research has been conducted to develop methods or tools to ensure the design could be successfully printed at the early design stage. In this paper, the manufacturability for the Laser Powder Bed Fusion (LPBF) process - one of the AM techniques - is the focus. LPBF process has

demonstrated its capability of producing metal or polymer parts for a wide range of applications. The manufacturing failures this research aims to detect are visual defects such as geometric incompleteness, cracking, and warping.

Existing main strategies for analyzing manufacturability in the LPBF process have been identified as design guidelines, real-time process monitoring, manufacturing feature recognitions, and integrated modeling [12]. These approaches provide some basic functions of quality check, reparation of STL meshes, slicing, support structure generation, and limited functionality of overhang and thin feature detection. However, none of them offers an automated and well-modeled manufacturability analysis for a given design to be fabricated via the LPBF process. There has been an increasing demand for automated computational applications for LPBF, on which the tool helps to visualize the troublesome areas and give feedbacks for modification. Recently, a new approach of applying the Machine Learning (ML) method to analyze manufacturability has been widely investigated [13]. Comparing to conventional methods, ML has several advantages in solving manufacturability issues. When evaluating manufacturability,

* Corresponding author.

E-mail addresses: ying.zhang8@mail.mcgill.ca (Y. Zhang), yaoyao.zhao@mcgill.ca (Y.F. Zhao).

<https://doi.org/10.1016/j.jmansys.2021.07.002>

Received 27 August 2020; Received in revised form 31 May 2021; Accepted 3 July 2021

0278-6125/© 2021 The Society of Manufacturing Engineers. Published by Elsevier Ltd. All rights reserved.



Contents lists available at ScienceDirect

Expert Systems With Applications

journal homepage: www.elsevier.com/locate/eswa

A Web-based automated manufacturability analyzer and recommender for additive manufacturing (MAR-AM) via a hybrid Machine learning model

Ying Zhang, Yaoyao Fiona Zhao^{*}

Department of Mechanical Engineering, McGill University, Montreal, Quebec H3A0G4, Canada

ARTICLE INFO

Keywords:
Machine learning application
Manufacturability
Recommendation system
Additive manufacturing

ABSTRACT

Additive manufacturing (AM) offers the potential to fabricate complex design and functional assembly which opens up new opportunities for product design. One of the current challenges for novice AM users is the difficulty to guarantee their design to be manufacturable through the selected AM printer. To address this issue, this paper presents a web-based automated manufacturability analyzer and recommender for additive manufacturing (MAR-AM) assisted by a hybrid machine learning (ML) model. This tool provides a quick, automated, easy-to-access and comprehensive manufacturability analysis on a given design with the selected machine and material settings for novice AM users at the design stage. Moreover, to ensure users get a successful print, a recommender system is developed to provide appropriate changes as recommendations for a successful fabrication. Finally, the effectiveness of MAR-AM is demonstrated using a number of case studies. MAR-AM demonstrates the capability of predicting the printability of a given design with selected material and process parameters. The recommendations provided by MAR-AM reduce the potential failures before the real fabrication. At the current stage, MAR-AM is still limited at the initial stage of testing. The performance is weaker in the process-related samples. Moreover, in this research, the approach is only applied to material extrusion and only Ultimaker is utilized. More data needs to be gathered to train the ML model for other types of AM processes and process settings. With more data obtained, the approach can be applied to different AM techniques.

1. Introduction

Additive manufacturing (AM), which is also well-known as 3D printing, is a new trend of the manufacturing process in recent years. It builds parts following a generated 3D model by adding layers of materials and fusing them together. As introduced by ISO/ASTM standards (ISO, 2015), AM techniques can be divided into seven categories: binder jetting, directed energy deposition, powder bed fusion (PBF), sheet lamination, material extrusion (ME), material jetting, and vat photopolymerization. The first four have the ability to produce metal products, and the rest mainly focus on polymers. The main advantage of AM is the ability to allow customization and the ability to fabricate complex geometries such as lattice structures which are extremely hard to be manufactured in the subtractive manufacturing process. Though AM has been employed in many industrial applications, it still has a very high threshold for beginning users. It requires users to have a deep understanding on the AM techniques in order to take full advantage of this technology. The printing may fail due to many factors such as the poor selection of the build orientation (Yicha Zhang, Bernard, Harik, &

Karunakaran, 2017; Zwier & Wits, 2016), materials (Popovich & Sufiarov, 2016; Zielinski, Vervoort, Mindt, & Megahed, 2017), layer thickness (Nguyen et al., 2018; Sufiarov et al., 2017), process settings (Chen & Zhao, 2016; H. Kim, Lin, & Tseng, 2018; Pegues et al., 2017), and insufficient support (Jiang, Xu, & Stringer, 2018; Stringer, Xu, Zheng, & Jiang, 2018). It is hard for non-AM experts to determine whether their designs are printable through the selected AM process, and it is even more difficult for them to make proper modifications alone before the fabrication.

Identifying whether the given design is printable or not and what modification can be done to make the design more suitable for AM is one of the major challenges for AM to be widely adopted in the industry. In the past, similar to the conventional manufacturing process, design guidelines (Greer et al., 2019; Mani, Witherell, & Jee, 2017; Materialise, 2018; Stratasys, 2018) or checklists (Booth et al., 2017) are the most common methods to help designers to evaluate the manufacturability of their designs. It provides a manufacturable range of geometrical design features including minimum thickness, part orientation, surface roughness, chamfers and radius, holes, overhang, etc. Designers are expected

^{*} Corresponding author.

E-mail addresses: ying.zhang@mail.mcgill.ca (Y. Zhang), yaoyao.zhao@mcgill.ca (Y. Fiona Zhao).

<https://doi.org/10.1016/j.eswa.2022.117189>

Received 15 September 2021; Received in revised form 29 March 2022; Accepted 2 April 2022

Available online 6 April 2022

0957-4174/© 2022 Elsevier Ltd. All rights reserved.